Louisiana State University
LSU Digital Commons

LSU Doctoral Dissertations | Graduate School

2007

Lanthanide complexes as fluorescent indicators for neutral sugars and cancer biomarkers

Onur Alpturk
Louisiana State University and Agricultural and Mechanical College, oalptu1@lsu.edu

Follow this and additional works at: https://digitalcommons.lsu.edu/gradschool_dissertations

 Part of the Chemistry Commons

Recommended Citation
Alpturk, Onur, "Lanthanide complexes as fluorescent indicators for neutral sugars and cancer biomarkers" (2007). *LSU Doctoral Dissertations*. 469.
https://digitalcommons.lsu.edu/gradschool_dissertations/469

This Dissertation is brought to you for free and open access by the Graduate School at LSU Digital Commons. It has been accepted for inclusion in LSU Doctoral Dissertations by an authorized graduate school editor of LSU Digital Commons. For more information, please contactgradetd@lsu.edu.

LANTHANIDE COMPLEXES AS FLUORESCENT INDICATORS FOR NEUTRAL SUGARS AND CANCER BIOMARKERS

A Dissertation

Submitted to the Graduate Faculty of the
Louisiana State University and
Agricultural and Mechanical College
in partial fulfillment of the
requirements for the degree of
Doctor of Philosophy

In

The Department of Chemistry

By
Onur Alptürk
B.S., Middle East Technical University, 1998, Ankara
M.S., Middle East Technical University, 2001, Ankara
May, 2007

DEDICATION

To my grandmother and my aunt Nursel,

Wish you were here

ACKNOWLEDGMENTS

I would like to deeply thank Dr. Robert M. Strongin. This Ph.D. has been quite a journey to me. Thank you very much for your endless support, guidance and more importantly for your sense of humor throughout these years (*I am in a meeting too*).

Many thanks Dr. Laurent Brard and Dr. Isiah M. Warner. I have learnt so much from my collaborations with your groups. Thanks for giving me this opportunity.

To Dr. William E. Crowe and Dr. Robin L. McCarley, many thanks for your support and your care for me.

I would like to thank to my friends Veronica Holmes, Steve Lawrence, Maria Appeaning, Cupcake Tesfia, Corin Schowalter, Lakia Champagne, Alicia Williams, Mark Lowry and Sayo Fakayode. To be honest, I would not be able to finish this Ph.D. without you guys.

Thanks my group-mates, Dr. Oleksandr Rusin, Dr. Jorge Escobedo, Charles, Sam, Wang, George and Susan. Thank you all for friendship and help.

Also, I would like to thank to my friends in Turkey. Thanks for still being part my life.

My thanks to Dr. Carol M. Taylor Dr. David A. Spivak and Dr. Ilya Vekhter for being on my research committee and giving me invaluable advice on my studies.

TABLE OF CONTENTS

LIST OF TABLES

LIST OF FIGURES

LIST OF SCHEMES

LIST OF ABBREVIATIONS

LPA	Lysophosphatidic acid
PC	Phosphatidylcholine
SM	Sphingomyelin
TLC	Thin-layer chromatography
Neu5Ac	N-Acetylneuraminic acid
HEPES	N-(2-hydroxyethyl)-piperazine-N'-2-ethanesulfonic acid
NMR	Nuclear Magnetic Resonance
DMF	Dimethyl Formamide
PA	3-*sn*-phosphatidic acid, Na salt
MeOH	Methyl Alcohol

ABSTRACT

Simple water soluble lanthanum and europium complexes are effective at detecting neutral sugars as well as glyco- and phospholipids. In solutions at physiologically relevant pH the fluorescent lanthanum complex binds neutral sugars with apparent binding constants comparable to those of arylboronic acids. Interference from commonly occurring anions is minimal. The europium complex detects sialic acid-containing gangliosides at pH 7.0 over an asialoganglioside. This selectivity is attributed, in large part, to the cooperative complexation of the oligosaccharide and sialic acid residues to the metal center, based on analogous prior studies. In MeOH, lysophosphatidic acid (LPA), a biomarker for several pathological conditions including ovarian cancer, is selectively detected by the europium complex. LPA is also detected via a fluorescence increase in human plasma samples. The 2-*sn*-OH moiety of LPA plays a key role in promoting binding to the metal center. Other molecules found in common brain ganglioside and phospholipid extracts do not interfere in the ganglioside or LPA fluorescence assays.

CHAPTER 1
INTRODUCTION

1.1. Lanthanide Complexes in Supramolecular Chemistry

Lanthanides complexes have gained significant attention due to their unique chemical and physical properties.[1.1] The prime interest towards such complexes originate from so-called "ligand-field extension". Unlike transition metal complexes wherein the ligand complexation is of both covalent and ionic character, lanthanide coordination is largely ionic. Consequently, lanthanides, even if in electrically neutral form, can bind to additional neutral or ionic ligands whereby they can achieve coordination numbers up to 12.

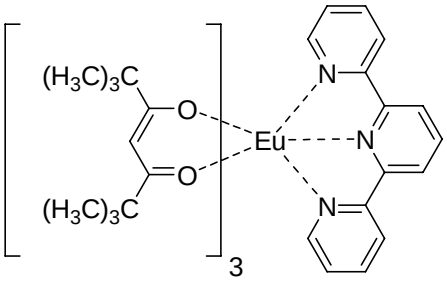

Figure 1.1. Europium tris(2,2,6,6-tetramethyl-3,5-heptadionate) and highly coordinated complexation with terpryridine.

Consequently, the use of such complexes have been widely reported in: **(a)** light converters, **(b)** Nuclear Magnetic Resonance and **(c)** catalysts in both chemical and biological systems. The field of application of lanthanides have also strecthed out to molecular recognition, especially recognition of biomolecules such as amino acids, nucleic acids, charged carbohydrates.

Although such biomolecules have been known to participate to several physiological conditions, their *in vivo* functions are not fully understood. Hence, their

quantification in physiological states by simple spectroscopic methods are of paramount importance. Hence, we have turned our attention to the design and synthesis of lanthanide-based chemosensors to quantify neutral carbohydrates and certain cancer biomarkers such as lysophosphatidic acid (LPA) and gangliosides.

1.2. Selective Detection of Lysophosphatidic Acid for Early Diagnosis of Ovarian Cancer

Ovarian cancer is a devastating health problem. Nearly 10 million women in the US are at high risk for ovarian cancer. There are 26,000 new US cases per year.[1.2] The lack of effective methods for the early diagnosis of ovarian cancer is a serious health problem. Ovarian cancer is a deadly gynecological disease.

Survival rates increase dramatically with early diagnosis. Ovarian cancer is extremely difficult to detect early enough to allow for effective treatment. To quote from a recent assessment: "Ovarian cancer is an insidious disease that kills more than 15,000 Americans each year.[1.3] The lethality of this disease stems from our inability to diagnose it easily and early; this is because its symptoms — such as nausea, loss of appetite and abdominal discomfort — are common to many disorders. Consequently, most women are diagnosed with ovarian cancer in the late stage of the disease, for which the five-year survival rate is less than 30%. Yet, survival rates soar to over 90% if the disease is discovered when cancer is still localized to the ovaries."[1.2,1.3] There are significant barriers to the diagnosis of early stage ovarian cancer.

Current methods used to identify ovarian cancer include transvaginal ultrasound, laparoscopy, or positive emission tomography. While transvaginal sonography shows promise for early detection, it is too expensive to be widely used for routine screening.[1.4]

The correlation of altered levels of serum biomarkers to ovarian cancer have been the subject of many studies. The protein CA-125 is currently the main biomarker of choice. However, other physiological conditions also promote increased CA-125 levels. CA-125 is less specific in premenopausal women. The well-known low accuracy of CA-125, even in combination with other methods, has led to intensive efforts to find better biomarkers. For instance, detailed computer analyses of the mass spectrometric data obtained from ovarian cancer and non-cancer subjects afforded nearly 100% accuracy of detection.[1.5] This exciting report indicates that the early detection of ovarian cancer may be possible; however, this method is expensive, not point-of-care, and different analyses of the same data suggest different biomarker molecules. For a detailed discussion of the drawbacks and complexity of this method, see references 1.2 and 1.6.

It is generally agreed that LPA monitoring is a useful biomarker for early detection. LPA (oleoyl-L-α-lysophosphatidic acid) is a bioactive phospholipid with mitogenic and growth factor-like activities, an "oncolipid," which stimulates the proliferation of cancer cells, and, as concluded in a recent review, "ovarian cancer appears to be driven through the production and action of LPA."[1.8] There is general agreement in the biomedical literature that monitoring plasma LPA levels is potentially a highly promising way to detect ovarian cancer in its early stages.[1.2,1.7,1.8] Findings in this area came from the lab of Xu *et al*., who found that plasma LPA levels afford a more sensitive diagnostic compared to CA-125.

LPA's use as a biomarker is limited due to current problems with its monitoring. Large-scale population studies with the capability of yielding more-precise estimates of the sensitivity and specificity of LPA, both alone and in combination with other markers, for both screening and detection of recurrence, are necessary, as stated in a recent paper

of Sutphen *et al*.[1.7] Currently, there are no methods that allow for very efficient monitoring of elevated LPA. For example, using analytical HPLC, researchers could not separate some LPAs from lysophosphatidyl inositols (LPIs). In a recent article, scientists from Sloan-Kettering state that LPA is a potentially useful ovarian cancer biomarker; "however, the current method of measuring LPA, which involves lipid extraction followed by gas chromatography, may limit its utility."[1.9]

Additionally, controversy regarding the reliability of LPA as an early-stage ovarian cancer marker exists due to problems with LPA isolation and handling: "…differences in the results from the groups likely arise from challenges in the collection and handling of plasma to prevent post collection production, metabolism or loss of LPA. A very significant complication is that during sample incubation prior to many analyses, significant enzyme generated elevation in serum LPA levels occurs (i.e., non-tumor-related), greatly hindering diagnosis of ovarian cancer."[1.8]

A summary of specific current problems with LPA detection*:*

(a) It is difficult to extract and quantify LPAs in the presence of other lipids [e.g., phosphatidylcholine, (PC) and sphingomyelin (SM)], which are present at much higher concentrations (in addition to LPI).[1.10]

(b) Routine laboratory analysis demands minimum sample preparation. The LPA extraction process is complex and time-consuming, due in part to the structure of the LPAs. Ideally, direct LPA detection from blood without any sample preparation is required.[1.7,1.10]

(c) Studies have revealed that plasma LPA levels can be misleading. If the sample is incubated, LPA levels increase via biosynthesis via lysophospholipase activity, rather than originating from tumors! Hence, LPA detection in plasma will be misleading as long as non-tumorogenic biosynthesis is not blocked.

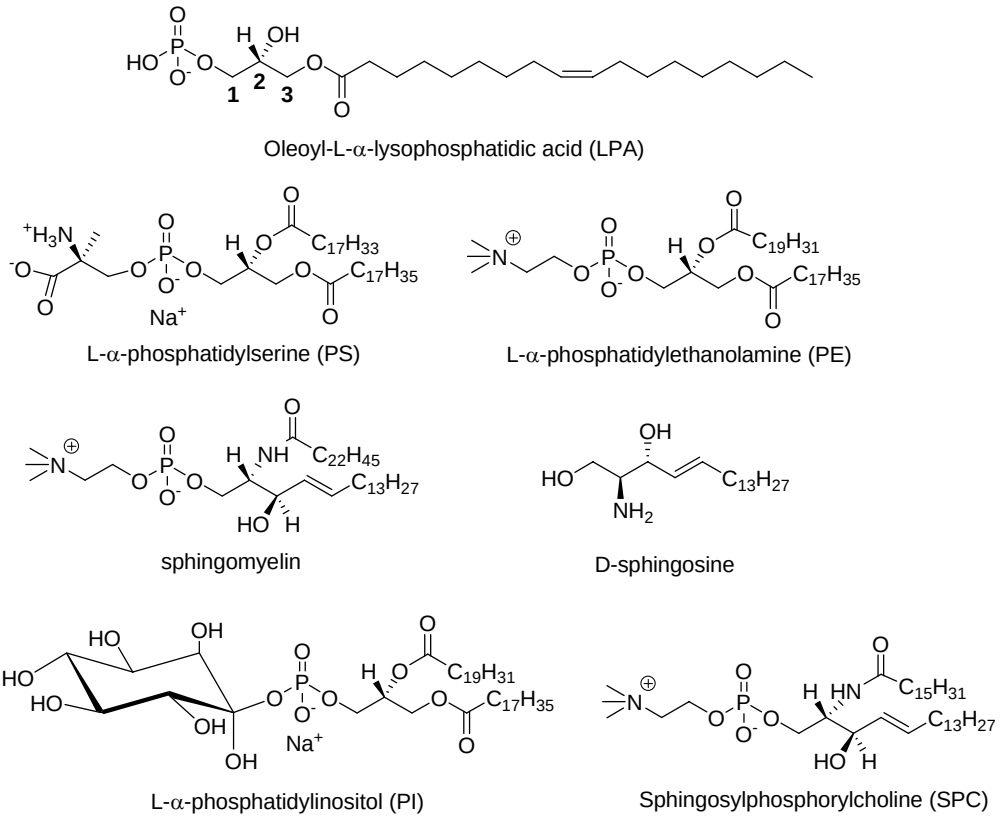

Figure 1.2. The structures of LPA and other phospholipids.

To date, several methodologies have been used to address the selective and sensitive detection of LPA. These include HPLC[1.10], tandem mass spectroscopy[1.6], thin-layer chromatography (TLC)[1.11], capillary electrophoresis with indirect ultraviolet detection,[1.12] radio-enzymatic assays[1.13] and voltage clamped Xenopus oocytes.[1.14] These

approaches involve expensive, sophisticated devices and complicated procedures unsuited for point-of care applications; for example,

(i) GC analysis necessitates esterification of the lipids prior to analysis. Although techniques such as HPLC or GC and mass spectroscopy may achieve selectivity and sensitivity, simpler methods allowing routine diagnosis of LPA are more desirable.

(ii) The problems related to LPA separation via 2D-TLC are complicated by the fact that the same LPA salts with differing counter ions (e.g., calcium and sodium) exhibit different mobilities, regardless of the nature of stationary phase material.

(iii) Colorimetric and fluorometric techniques are generally preferred, due to their simplicity. The only colorimetric LPA detection reported uses an enzymatic cycling method.[1.15] In general, enzymes have relatively limited shelf life and stability and are relatively expensive, compared to synthetic materials. In the particular case of this aforementioned of the enzyme cycling method, indirect detection (peroxide) is used to determine LPA levels. However, this methodology has to date never been cited since its publication (2003) in the context of its embodying a feasible method for LPA detection.

(iv) Direct chromatographic detection with absorption spectroscopy is feasible but at wavelengths below 215 nm. Unfortunately, this region is where solvent and solvent trace impurity absorption becomes substantial.[1.10]

1.3. Non-hydrolytic Detection of Gangliosides

Glycosphingolipids (GSLs) are complex lipid molecules that are components of eukaryotic cell membranes.[1.16] The structures of some sphingolipids are shown in Figure **1.1**. Typically, they consist of at least one monosaccharide that is glycosidically linked to hydrophobic lipid residues such as sphingosine or ceramide. The nature of these lipids

depends on the cell type; sphingosine is mostly found in mammalian cells whereas phytosphingosine is encountered in yeast and plant cells. Modifications of the lipid backbone that range from phosphorylation to gluco- and galactosylation generate large structural diversity. Indeed, more than 300 biomolecules are currently known as glycosphingolipids. They are an integral part of the eukaryotic cell membrane with their sugar residues residing on the outer layer of the membrane. The orientation of the sugar residues renders these glycolipids critical in numerous intercellular processes including cellular protection against both mechanical and chemical damage, proliferation, differentiation, cell-cell recognition and cell development. They moreover function as receptors for lectins, selectins, toxins and viruses. However, their in vivo functions are not fully understood.[1.16]

Their metabolism is linked to the synthesis of several biomolecules. Glycosphingolipids are synthesized in the endoplasmic reticulum and Golgi apparatus while being catabolized in lysosomes. The condensation of palmitoyl-CoA and serine is a common step in all glycosphingolipid syntheses which initiate the individual biosynthetic pathways. Whereas the anabolism of glycosphingolipids allows access to several metabolic products (for instance, sphingomyelin can be synthesized from ceramide simply via the addition of a phosphorylcholine residue), their catabolism is mostly essential for biomolecular recycling purposes. This recycling route commences with the import of macromolecules into lysosomes by several mechanisms such as endocytosis, pinocytosis, phagocytosis and autophagocytosis. Therein, macromolecules are cleaved by acidic hydrolytic enzymes and some accessory proteins that are utilized for sequential degradation. Thereafter, the hydrolytic products are carried back to the cytoplasm for reutilization. This process is also essential since it constitutes the first step

of the synthesis of some key molecules such as ceramide which is vital in signal transduction.[1.16]

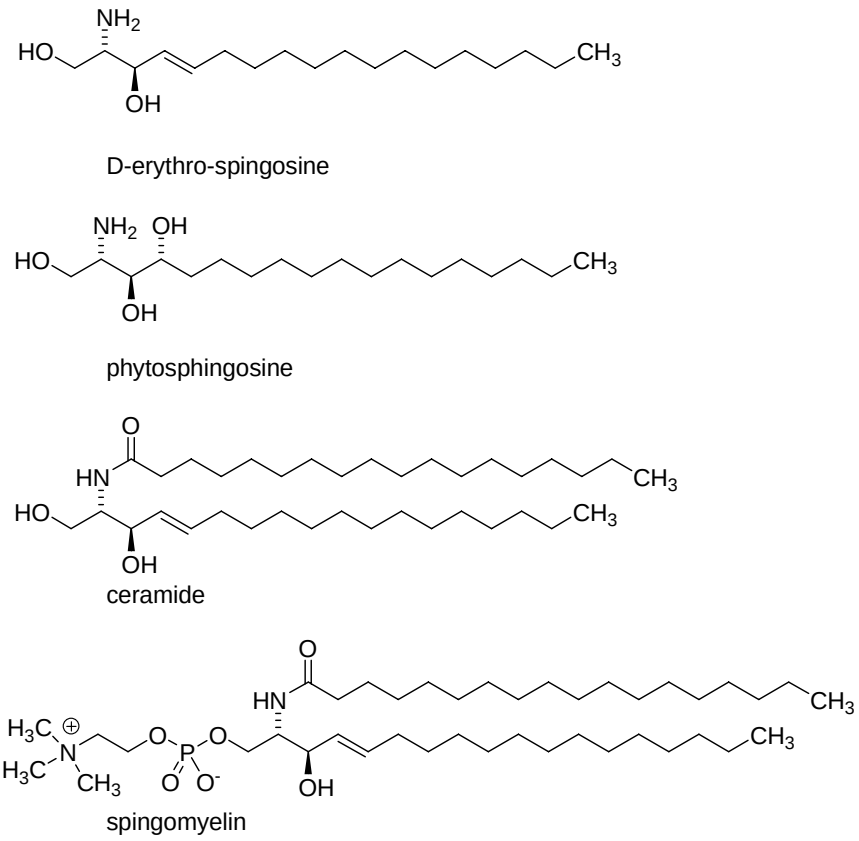

Figure 1.3. The structures of selected sphingolipids.

Defects in GSL metabolism can potentially have severe consequences that result in metabolic disorders. Interestingly, these disorders are related to their catabolism, not their biosynthesis. There is no disease known to originate from defects in glycosphingolipid synthesis. Conversely, failure in their catabolism results in their extensive accumulation in tissues, which leads to physiological conditions also known as lysosomal storage diseases. To date, more than 40 different types of lysosomal storage diseases are known. Although the frequency of each lysosomal storage disease is relatively rare, their cumulative effect can be significant.[1.16]

The deficiency of the corresponding hydrolytic enzymes in lysosomes is the origin of the storage diseases. The reason for this deficiency is defects in genes that encode the enzymes. Studies toward the underlying mechanism of these defects have revealed that the expressed enzymes possess relatively low or no activity. Accordingly, it was found that mutations in genes cause alterations in nucleotide bases that are in close proximity to the active site. These mutations include base substitution, insertion or deletion and partial gene deletion. Relatively mild mutations, on the other hand, may alter the stability of both mRNA and the enzymes. The severity of the disease is determined by the extent of the mutations. Although regarded as indirect effects, mechanisms such as deficiency in lysosomal enzyme transport or localization are also known. The lack of enzymes and the associated lysosomal storage diseases are summarized in Table **1.1**.[1.16-1.18]

Gangliosides (Figures **1.2** and **1.3**) are the sialic acid-containing glycosphingolipids. They exhibit the greatest structural variation and complexity of the GSLs. Gangliosides are characterized by a high amount of stearic acid (C18, about 80%) in their hydrophobic region, as well as C16, C20 and C22. Changing the fatty acid component to α-linoleic acid alters biological activity dramatically in vitro. However, it is the carbohydrate moiety that is of primary importance in determining distinctive ganglioside properties. In any given cell type, the number of different gangliosides may be relatively small, but their nature and compositions may be characteristic and highly relevant to the functioning of the cell.[1.16-1.18]

Table 1.1. Sphingolipid, glycosphingolipid and lysosomal storage diseases (adapted from reference **1.16d**).

Disease	Enzymatic defect	GSL storage material
Gaucher	*β*-glucosidase, saposin C activator	Glucosylceramide, GM1, GM2, GM3, GD3, Glucosylsphingosine
Sphingolipid activator deficiency	Sphingolipid activator protein	Glycolipids
GM1 gangliosidosis	GM1 gangliosidosis	GM1, GM2, GM3, GD1A
Tay Sachs	*β*-Hexosaminidase A	GM2, other glycolipids
Sandhoff	*β*-Hexosaminidase A and B	GM2, other glycolipids
GM2 activator deficiency	GM2 activator protein	GM2, other glycolipids
Krabbe	*β*-Galactosidase	Galactosylceramide
Fabry	*α*-Galactosidase A	Globotriaosylceramide and blood group B substances
Metachromatic leukodystrophy	Arylsulfatase A, saposin B activator	Sulphated glycoproteins and glycolipids, and GM2
Farber	Ceramidase	Ceramide, GM3
Niemann-Pick A & B	Sphingomyelinase	Sphingomyelin, GM2, GM3
Fucosidosis	*α*-Fucosidase	Fucosides and glycolipids
Mucolipidosis II & III	GlcNac transferase	Oligosaccharides, mucopolysaccharides, lipids, GM1
Mucopolysacharidosis I, II, III, VII	Various enzymes	GM2 and GM3
Alpha mannosidosis	*A*-mannosidase	GM2, GM3
Galactosialidosis	Protective protein cathepsin A	GM1, GM2, GM3

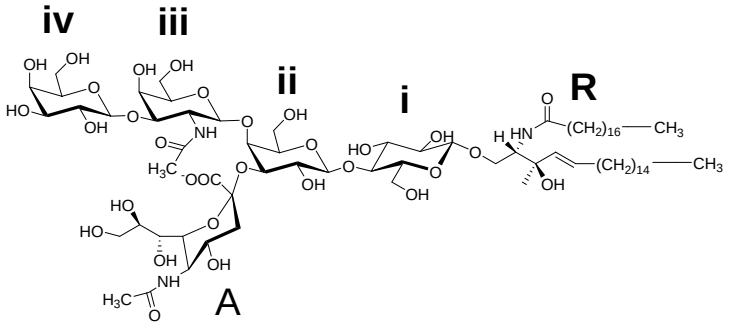

Figure 1.4. Structures and symbolism for gangliosides and their asialo derivatives, glucosylceramide, and N-acetyl-α-neuraminic acid: (GlcCer): R, i; (GalCer): R, ii; (LacCer): R, i, ii; (GA_2): R, i, ii, iii; (GA1): R, i, ii, iii, iv; (GM4): R, ii, A; (GM_3): R, i, ii, A; (GM_2): R, i, ii, iii, A; (GM_1): R, i, ii, iii, iv, A; (NeuAc): A (adapted from ref. **1.19**).

As the brain develops, the content of gangliosides and the degree of sialylation increases. Numerous biological properties of gangliosides related to cellular and molecular recognition have been attributed to the sialic acid residues. They are involved in the binding and the transport of positively charged molecules as well as the attraction and repulsion of the cells. Due to their terminal position on glycolipids, sialic acids mostly function as receptors for a large variety of molecules such as hormones, toxins, viruses, cells and bacteria. In addition, they behave as ligands for lectins and selectins during a number of cell-cell and cell-matrix processes. Interestingly, they are known to shield the recognition sites whereby the activation of the immune system is inhibited. Accordingly, oversialylation of the cell surface results in the protection of malignant cells. For these reasons, it is clear that sialic acids play roles in tumor biology. In fact, imbalances in sialic acid levels can have clinical manifestations such as alterations in cell adhesion, a condition implicated in some cancers, and graft rejection. An increase in the levels of both soluble and cellular sialic acid can thus be a marker for cancer.[1.17] However, since the levels of sialic acids can also be altered by non-pathological factors (e.g., smoking, pregnancy and age), altered levels do not solely indicate the presence of cancer and must be viewed in conjunction with other markers for diagnostic purposes.[1.2]

N-Acetylneuraminic acid (Neu5Ac) is the most abundant form in humans. As a part of glycosphingolipids (i.e., the gangliosides) or glycoproteins, they typically occupy the terminal position of the glycan chain. An interesting aspect of sialic acid chemistry is that the anomeric configuration is determined by whether sialic acid is in a free or conjugated form. In solution, the anormeric equilibrium between the α- and β- favors the

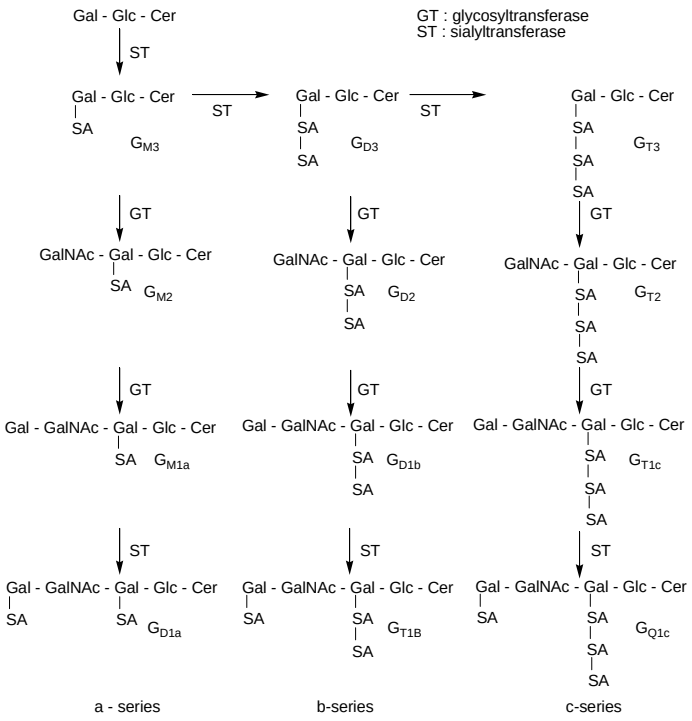

Scheme. **1.1.** Pathways for the biosynthesis of the common series of gangliosides involving sequential activities of sialyltransferases and glycosyltransferases.

latter. However, sialic acids, when conjugated to biomolecules, are predominantly in the α-anomer form.[1.17]

- **Major Biochemical Properties of Gangliosides.** Gangliosides are ligands for myelin stability and aid in nerve regeneration by binding a myelin-associated glycoprotein. They can act as cell-type specific antigens controlling cell growth and differentiation and intercellular interactions. They play key roles in the immune systems and serve as biomarkers of cancerous tissue. They regulate cell signaling, serving as receptors for interferon, epidermal growth factor, nerve growth factor and insulin. Gangliosides bind to bacterial toxins and mediate interactions between microbes and host cells during infections. Genetic defects in catabolism lead to ganglioside accumulation. In generalized gangliosidosis, excess GM_1 in the nervous system results in mental

retardation and liver enlargement. In Tay-Sachs syndrome, GM_2 accumulation in the brain leads to mental retardation and blindness.[1.16-1.18]

Table 1.2. Selected examples of studies using total ganglioside determination for research on various cancers.

Disease	Levels	Matrix	Reference
Colorectal Cancer	15.6 – 58.6 mg/dL	Serum	1.4
Pancreatic Adenocarcinoma	16.6 – 34.6 mg/dL	Serum	1.5
Advanced Ovarian Cancer	2.7 – 4.8 mg/mL/105 cells/24 h	Tumor Cells	1.6
	14 – 40 mg/mL	Peritoneal Fluid	
	18 – 57 mg/mL	Plasma	

- **The Significance of Total Ganglioside Determination for Modern Biomedical Research.** Gangliosides account for 6 % of brain tissue. The main gangliosides found in the human brain are GM_1, GD_{1a}, GD_{1b} and GT_1. GM_3 is mainly localized in extraneural tissues. The overall composition of the gangliosides can be influenced by environmental factors as well as by nerve stimulation or drug administration. The determination of total ganglioside content is highly useful in studying storage diseases (Table **1.1**) and in the investigation of specific cancers (Table **1.2**).[1.20-1.24] Recent investigations show that serum total ganglioside (STG) levels have shown promise as a potential tool for assessing the response to immunotherapy in melanoma patients.[1.23] Additionally, in a recent example, total ganglioside content was recently shown to increase by 20-fold in studies involving the links between lipid metabolism and Alzheimer's disease.[1.24a]

This represents a relatively small subset of many recent investigations. Ganglioside detection is a major challenge. Because biological media contain a high content of other lipids, extensive purification of gangliosides by methods such as reversed-phase chromatography and DEAE-Sephadex columns are often required prior to

analysis. Table **1.3** summarizes the most commonly used current methods for ganglioside detection. Simple and rapid, reliable and user-friendly techniques are needed:

According to Tsui *et al*.,[1.24b] "conventional strategies for profiling gangliosides suffer from poor reproducibility, low sensitivity, and low throughput capacity. Prior separation of gangliosides by thin-layer chromatography and/or high-performance liquid chromatography not only was tedious and laborious but also could introduce uneven losses of molecular species." These researchers prove that it is necessary to separate phospholipids from gangliosides to obtain satisfactory MS data. In fact the method ultimately used required partitioning of gangliosides into an aqueous phase to obtain enrichment. Aqueous phase partitioning requires purification via gel filtration to remove low molecular weight contaminants such as salts and peptides. Percent recovery in the aqueous phase was not described; however, others have described moderate sample losses during sample handling prior to analysis.

In another recent representative example, Sato *et al*.[1.24a] used the following procedure prior to analyzing total ganglioside content in embryonal carcinoma cells: lipids were extracted from cells successively in $CHCl_3$/MeOH, total lipid extract was next "further purified", then separated by TLC using $CHCl_3$/MeOH/0.2 % $CaCl_2$ (55:45:10), detected with orcinol sulfuric acid reagent and quantified with a dual-wavelength flying spot scanner in reflectance mode at 500 nm. This method also partitions and detects other "acidic glycolipids". Therein, potential interferences/co-elution was not described. More importantly, the orcinol reagent is non-selective and reacts with reducing sugars.

Sample pre-treatment procedures may be written in a somewhat simplified manner in experimental sections. For example, in a recent volume of Methods in

Enzymology (*vide infra*), an initial "total lipid extraction" step can entail lyophilization, pulverization, re-suspension in solvent, sonication, 18 h re-extraction, centrifugation, re-extraction, clarification, extract combination, concentration, centrifugation, partitioning and drying. This is all done prior to the partitioning of gangliosides from other lipids. The ensuing partitioning step involves addition of mixed alcohol solvents to the extract, vortexing, sonication, addition of saline solution, alternating vortexing and sonication, centrifugation, removal of the organic solvent and repartioning the aqueous layer. Alternating vortexing and sonication is again repeated, and organic solvent is removed followed by lyophilization. The sample is then loaded onto a Sephadex G-50 column using very precise specifications. Recoveries from the individual steps are reported to be 93 % or higher.

It is, in other words, relatively tedious to purify the gangliosides and prepare them for analysis. We thus propose an extensive study aimed at developing highly selective receptors. Our goal is to provide simple and enabling new methods for ganglioside research and ultimately for the early and efficient screening of ganglioside-related diseases. We envision that the detailed spectroscopic work planned will guide the near future development of reagents not just for detecting gangliosides, but also neutral glycolipids. For example, future targets would include the smaller glycosphingolipids glucosylceramide and lactosylceramide, for which there aren't good reagents available.

Table 1.3. Major current techniques used for ganglioside detection and their associated challenges (summarized from the introduction in reference **1.9b**).

Technique	**Main Challenge**
Antibodies	Cross-react with multiple gangliosides and/or glycoprotein species with similar carbohydrate epitopes.
TLC	Low resolution does not adequately resolve heterogeneity of gangliosides

Table 1.3. Continued

HPLC	Laborious purification, and requiring derivatization with chromogens/fluorogens
MS/TLC or MS/HPLC	Tedious purifications/derivatizations
Tandem MS/MS	Ganglioside ionization is significantly suppressed by samples containing other biomolecules such as phospholipids

1.4. References

1.1. For a review, see: Tsukube, H.; Shinoda, S. *Chem. Rev*. **2002**, 102, 2389.

1.2. a) Cancer Facts & Figures. 2005 Am. Cancer Soc. Available on-line at http//:www.cancer.org/docroot/STT/stt_0.asp .Last accessed Feb. 13, 2005. b) Li, C., Ovarian Cancer: New Frontiers in Detection Technology. Pharmaceutical Discovery, 2005.

1.3. http://lcgcmag.mediwire.com/main/Default.aspx?P=Content&ArticleID=154148

1.4. Taylor, K. J.; Schwartz, P. E. *Radiology*, **1994**, 192, 1.

1.5. Petricoin-III, E. F.; Ardekani, A. M.; Hitt, B. A.; Levine, P. J.; Fusaro, V. A.; Steinberg, S. M.; Mills, G. B.; Simone, C.; Fishman, D. A.; Kohn, E. C.; Liotta, L. A. *Lancet*, **2002**, **7**, 572.

1.6. Kim, H.; Yoon, H.-R.; Pyo, D. *Bull. Korean Chem. Soc*., **2002**, 23, 1139.

1.7. Sutphen, R.; Xu, Y.; Wilbanks, G. D.; Fiorica, J.; Grendys, E. C. Jr.; LaPolla, J. P.; Arango, H.; Hoffman, M. S.; Martino, M.; Wakeley, K.; Griffin, D.; Blanco, R. W.; Cantor, A. B.; Xiao, Y.-J.; Krischer, J. P. *Cancer Epidem. Biomar*., **2004**, 13, 1185.

1.8. Umezu-Goto, M.; Tanyi, J.; Lahad, J.; Liu, S.; Yu, S.; Lapushin, R.; Hasegawa, Y.; Lu, Y.; Trost, R.; Bevers, T.; Jonasch, E.; Aldape, K.; Liu, J.; James, R. D.; Ferguson, C. G.; Xu, Y.; Prestwich, G. D.; Mills, G. B. *J. Cell. Biochem.*, **2004**, 92, 1115.

1.8. Dupont, J.; Tanwar, M. K.; Thaler, H. T.; Fleisher, M.; Kauff, N.; Hensley, M. L.; Sabbatini, P.; Anderson, S.; Aghajanian, C.; Holland, E. C.; Spriggs, D. R. *J. Clin. Oncol.*, **2004**, 22, 3330.

1.9. Holland, W. L.; Stauter, E. C.; Stith, B. J. *J. Lipid Res.,* **2003**, 44, 854.

1.10. Shen, Z., Wu, M.; Elson, P.; Kennedy, A. W.; Belinson, J.; Casey, G.; Xu, Y. *Gynecol. Oncol.*, **2001**, 83, 25.

1.11. Chen, Y.-L.; Xu, Y. *J. Chromatogr. B,* **2001**, 753**,** 355.

1.12. Saulnier-Blache, J. S.; Girard, A.; Simon, M.-F.; Lafontan, M.; Valet, P. *J. Lipid Res.,* **2000**, 41**,** 1947.

1.13. Tigyi, G.; Miledi, R. *J. Biol. Chem.,* **1992**, 267, 21360.

1.14. Tigyi, G.; Hong, L.; Yakubu, M.; Parfenova, H.; Shibata, M.; Leffler, C. W. *Am. J. Physiol.,* **1995**, 286, H2048.

1.15. Kishimoto, T.; Matsuoka, T.; Imamura, S.; Mizuno, K. *Clin Chim Acta.* **2003**, 333, 59.

1.16. (a) Merrill, A. H.; Sandhoff, K. Sphingolipids: metabolism and cell signaling. In: Biochemistry of lipids. Lipoproteins and Membranes (4th Edition). pp. 373-407, Vance, D. E. and Vance, J., eds., Elsevier, Amsterdam, 2002. Reviews: (b) Huwiler, A.; Kolter, T.; Pfeilschifter, J.; Sandhoff, K. *Biochim. Biophys. Acta* **2000**, 1485, 63. (c) Zhang, X. B.; Kiechle, F. L. *Ann. Clin. Lab. Sci.* **2004**, 34, 3. (d) Raas-Rothschild, A.; Pankova-Kholmyansky, I.; Kacher, Y.; Futerman, A. H. *Glycoconjugate J.* **2004**, 21, 295. (e) Ledeen, R. W.; Wu, G. S. *Biochim. Biophys. Acta-Molecular and Cell Biology of Lipids*, **2006**, 1761, 588.

1.17. Reviews: (a) Schutter, E. M.; Visser, J. J.; van Kamp, G. J.; Mensdorff-Pouilly, S.; van Dijk, W.; Hilgers, J.; Kenemans, P. *Tumor Biol*. **1992**, 13, 121. (b) Roth, J. *Histochem. J.* **1993**, 25, 687. (c) Kobata, A. *Acc. Chem. Res.* **1993**, 26, 319. (d) Schauer, R.; Kelm, S.; Rerter, G.; Roggentin, P.; Shaw, L. in Biology of the Sialic Acids, Rosenberg, A., Ed. Plenum, N. Y., 1995, p. 7. (d) Nagai, Y.; Iwamori, M. in Biology of the Sialic Acids, Rosenberg, A., Ed. Plenum, N. Y., 1995, p. 197. (e) Reuter, G.; Gabius, H.-J. *Biol. Chem. H-S* **1996**, 377, 325. (f) Furuhata, K. *Trends Glycosci. Glycotechnol.* **2004**, 16, 143.

1.18. Review: Tettamanti, G. *Glycoconjugate J*. **2003**, 20, 3001.

1.19. Koerner, T. A. Jr; Prestegard. J. H.; Demou, P. C.; Yu, R. K. *Biochemistry*, **1983**, 22, 2676.

1.20. Perez, C. A.; Ravindranath, M. H.; Gupta, R. K.; Tollenaar, R. A. E. M.; van de Velde, C. J.; Wood, T. F.; Soh, D.; Morton, D. L.; Bilchik, A. J. *Cancer J.* **2002**, 8, 55.

1.21. Chu, K. U.; Ravindranath, M. H.; Gonzalez, A.; Nishimoto, K.; Tam, W. Y.; Soh, D.; Bilchik, A. J.; Katopodis, N.; Morton, D. L. *Cancer*, **2000**, 88, 1828.

1.22. Santin, A. D.; Ravindranath, M. H.; Bellone, S.; Muthugounder, S.; Palmieri. M.; O'Brien, T. J.; Roman, J.; Cannon, M. J.; Pecorelli, S. *BJOG*, **2004**, 111, 613.

1.23. Ravindranath M. H.; Hsueh, E. C.; Verma, M.; Ye, W.; Morton, D. L. S. *J. Immunother*. **2003**, 26, 277.

1.24. (a) Sato, T.; Zakaria, A. M.; Uemura, S.; Ishii, A.; Ohno-Iwashita, Y.; Igaraski, Y.; Inokuschi, J.-I. *Glycobiology* **2005**, *15*, 687. (b) Tsui, Z.-C.; Chen, Q.-R.; Thomas, M. J.; Samuel, M.; Cui, Z. *Anal. Biochem*. **2005**, 341, 251.

CHAPTER 2

LANTHANIDE COMPLEXES AS FLUORESCENT INDICATORS FOR NEUTRAL SUGARS AND CANCER BIOMARKERS*

2.1. Introduction

Nature uses tools such as lectins for the molecular recognition of saccharides. An important mode of lectin binding involves the coordination of a carbohydrate ligand to a metal center. C-type lectins recognize saccharides in a calcium-dependent manner.[2.1] The similar properties of lanthanides and calcium render trivalent lanthanides ions useful substitutes for Ca^{2+} in studying proteins.[2.2] Herein, we describe the utility of water soluble salophene[2.3]-lanthanide complexes (Figure **2.1**) towards addressing three current challenges: (**i**) the detection of neutral carbohydrates at physiologically-relevant pH, (**ii**) the selective detection of gangliosides and (**iii**) the selective detection of lysophosphatidic acid (LPA).

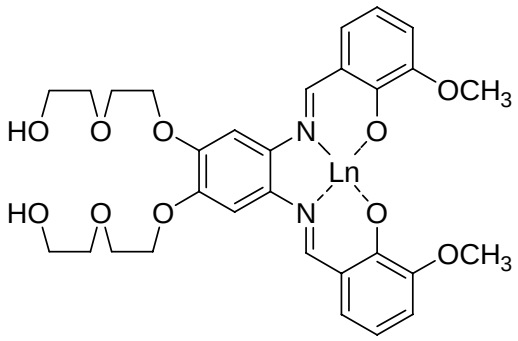

2.1 Ln = La^{3+}
2.2 Ln = Eu^{3+}

Figure 2.1. Salophene-lanthanide complexes.

*Reprinted in part with permission from *Proceedings of the National Academy of Sciences of the United States of America*, 2006, Volume 103, pages 9756-9760; Onur Alpturk, Oleksandr Rusin, Sayo O. Fakayode, Weihua Wang, Joege O. Escobedo, Isiah M. Warner, Williams E. Crowe, Vladimir Kral, Jeff M. Pruet, and Robert M. Strongin, Lanthanide Complexes as Fluorescent Indicators for Neutral Sugars and Cancer Biomarkers. Copyright 2006 National Academy of Sciences, U.S.A.

2.2 Results and Discussion

2.2.1. Detection of Neutral Sugars at Physiological pH.

A main problem in the detection of neutral sugars with artificial receptors is competitive binding by bulk water. Elevated solution pH is therefore typically required to attain a useful degree of coordination and signal transduction in the most innovative new metal-based detection methods.[2.4] There is an unmet demand for biomimetic sugar sensing agents that function in neutral buffer solution.[2.4] Since La^{3+} and Ca^{2+} exhibit relatively strong affinity for saccharides as compared to most other metal ions,[2.5] we hypothesize that **2.1** may be useful for detecting sugars in neutral aqueous media. Interestingly, lanthanides can extend their ligand coordination number by the addition of either neutral or charged ligands through ligand-sphere extension, leading to highly coordinated complexes.[1.1]

Addition of saccharides (1.1×10^{-3} M) to a solution of **2.1** (5.53×10^{-6} M, 0.1 M HEPES buffer, pH 7.0) promote readily-monitored increases in emission (Figure **2.2**).[2.6]

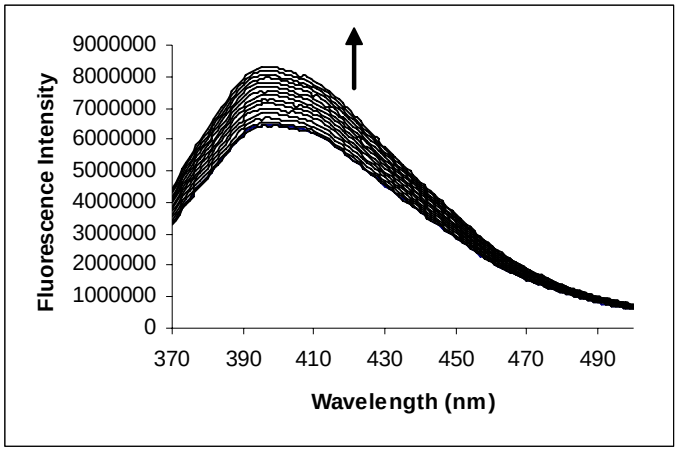

Figure 2.2. Fluorescence changes observed upon titration of 2.1 with D-glucose in 0.1M HEPES buffer, pH 7.0. The concentration of 2.1 is 6×10^{-6} M. The concentration of glucose is increased from 0 to 6×10^{-4} M. Excitation is at 360 nm, emission is monitored at 400 nm.

Lanthanide coordination to salens whereby the ligand conformation is brought into a more rigid cyclic structure, increases ligand-centered fluorescence emission.[2.6] Ternary complex formation upon saccharide addition apparently enhances this latter effect. In the ^{1}H-NMR of a solution of **2.1** and D-glucose in D_2O, the imine protons of **2.1** exhibit a modest up-field shift, in keeping with analogous salophene-metal complexes upon binding analytes[2.3] (Figure **2.3**).

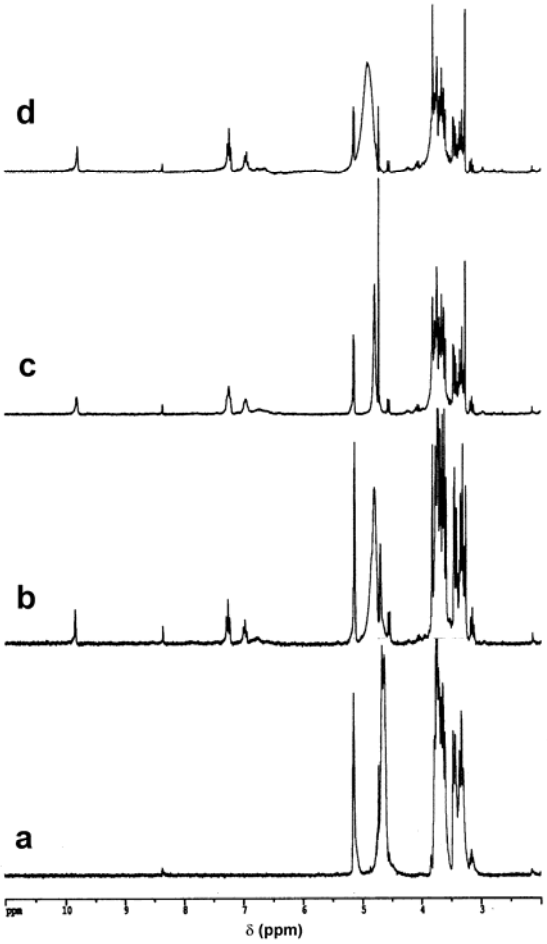

Figure 2.3. ^{1}H-NMR study of glucose titrated with **2.1**: (a) 1.8 mg of glucose in 0.75 ml of D_2O; (b) after addition of 0.2 equiv **2.1**; (c) after the addition of 0.4 equiv 1; (d) after addition of 0.6 equiv **2.1** (1.5 mg of **2.1** in 0.1 ml of D_2O in each addition). The imine protons of **2.1** exhibits a modest up-field shift (from 9.84 ppm to 9.79 ppm) in keeping with analogous salophene-metal complexes upon binding analytes (see reference **2.3** for analogous responses in the NMR of other salophenes upon tertiary complex formation).

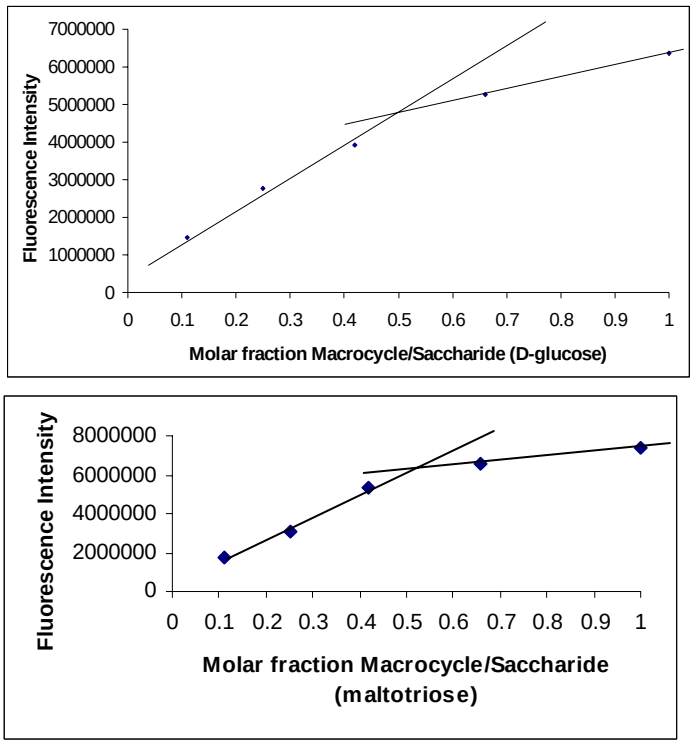

Figure 2.4. (Top) Job's plot of **2.1** and D-glucose in 0.1M HEPES buffer pH 7.0 and (Bottom) Job's plot of **2.1** and maltotriose in 0.1M HEPES buffer pH 7.0 both of which indicate a 1:1 stoichiometry.

The continuous variation indicates a 1:1 stoichiometry between glucose, maltose, maltotriose and **2.1** (Figure **2.4**). Glucose, maltose and maltotriose exhibit binding constants of 500, 1666 and 2500 M^{-1} respectively. These values compare very favorably to those of sugar-boronate complexes.[2.7] This is significant since boronic acid-containing fluorophores are currently reagents of choice for sugar detection in aqueous and mixed-aqueous media. The emission enhancements shown herein in the presence of neutral sugars range from *ca*. 25% – 60% (Figure **2.5**).

Common anions (citrate, phosphate and pyrophosphate) studied under these conditions promote relatively weaker emission responses. Additionally, bovine serum albumin-containing solutions exhibit increased fluorescence only when glucose is present. The concentration of glucose in plasma is typically *ca.* 10^{-3}. The next most

abundant monosaccharides are galactose and fructose, present at concentrations of 2 orders of magnitude less than that of glucose. Investigations towards minimizing potential interferences as well as improving selectivity for specific neutral sugars are in progress.

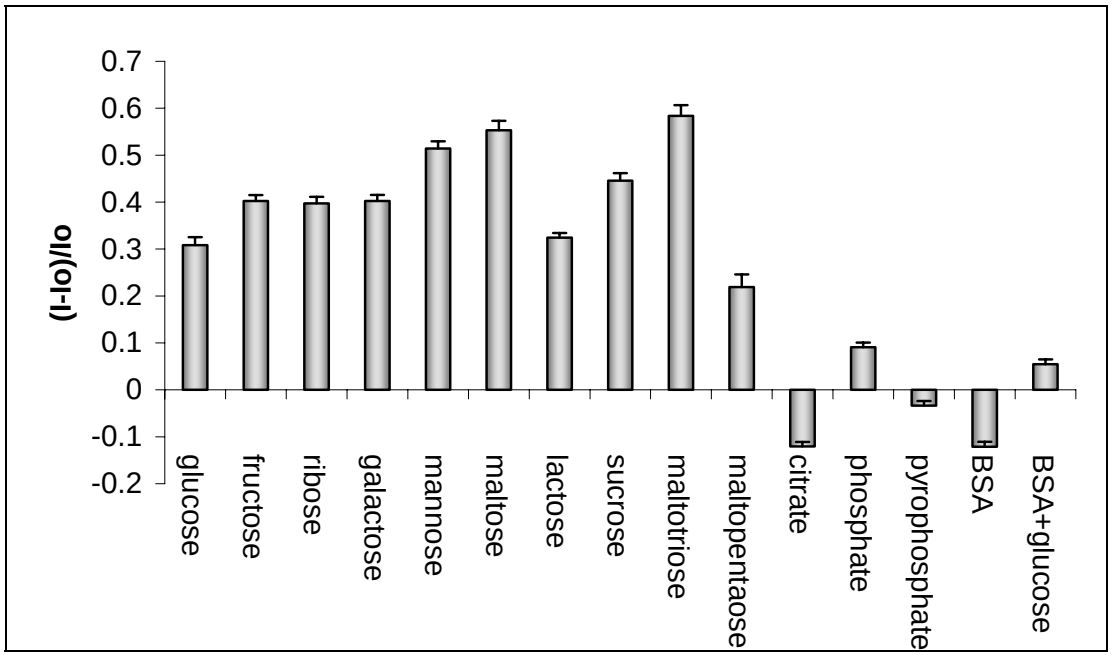

Figure 2.5. Relative fluorescence emission (400 nm) changes observed in solutions of **2.1** (5.53×10^{-6} M) in the presence of mono-, oligosaccharides, anions (1.1×10^{-3} M), BSA (1 mg/mL) and a mixture of BSA and glucose (1 mg/mL and 1.1×10^{-3} M, respectively) in HEPES buffer solution (pH 7.0). The standard deviation (n=3 for each analyte) of the relative fluorescence intensity ranges from 0.01-0.027.

2.2.2. The Selective Detection of Gangliosides under Neutral Conditions

It is well-known that an increase or decrease in total sialic acid levels (conjugated plus freely circulating) in biological fluids can indicate the occurrence of certain cancers. The acid-catalyzed liberation of bound sialic acid residues from gangliosides for assay typically results in destruction of the analyte.[2.8] In the case of enzymatic hydrolysis

incomplete sialic acid liberation is a problem.[2.9] Effective sensing agents for sialic acid-containing gangliosides (Figure **2.6**) are needed.

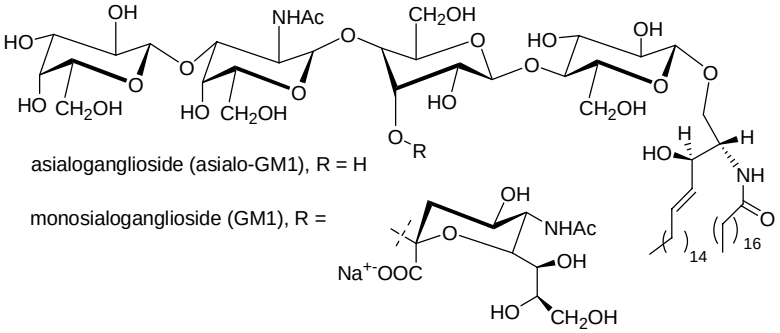

Figure 2.6. The structures of asialo-GM_1 and GM_1.

Selectivity towards various anionic substrates can be tuned via the appropriate choice of lanthanide metal.[2.10] Importantly, Sillerud *et al*. have provided precedent for favorable cooperative binding interactions of the oligosaccharide and sialic acid moieties of micellar gangliosides with Eu^{3+}.[2.11] For example, the higher affinity of Eu^{3+} to GM_1 as compared to sialic acid was attributed not only to an electrostatic interaction with the GM_1 sialic acid carboxylate but also to secondary interactions with the proximal oligosaccharide hydroxyls. This results in a coordination shell (Figure **2.7**).

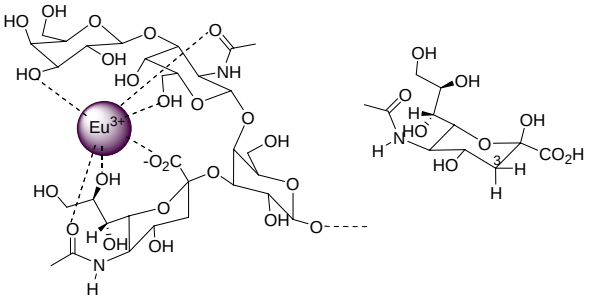

Figure 2.7. Left: Coordination of GM_1 to Eu^{3+}. Right: Free sialic acid

We thus hypothesize that **2.2** may afford enhanced signaling in the presence of charged gangliosides as compared to neutral sugars and sialic acid. Compound **2.2**

promotes the detection of sialic acid-containing gangliosides selectively compared to asialo-GM_1 (Figure **2.8** and Figure **2.9**). In contrast, **2.1** affords greater fluorescence enhancement than **2.2** in the presence of neutral asialo-GM_1 (Figure **2.10**).

The smaller the ionic radius of a lanthanide is, the more significant are the intramolecular interactions between its ligands. The salophene ligands of **2.1** and **2.2** contain both polar and apolar moieties. The combination of these latter structural features along with the smaller ionic radius of Eu^{3+} compared to La^{3+}, apparently renders **2.2** a better substrate for detecting anionic gangliosides compared to **2.1**.

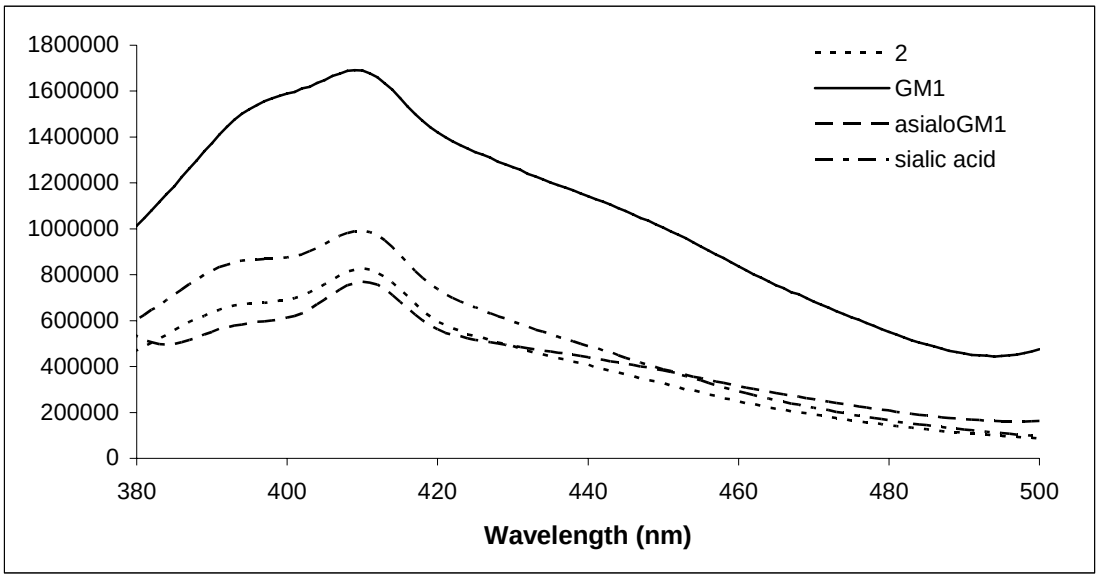

Figure 2.8. Fluorescence intensity change of solutions of **2.2** (5.53×10^{-6} M) in response to added gangliosides (0.5 mg/mL, *ca*. 10^{-4} M each) and sialic acid (1×10^{-3} M) in 0.1 M HEPES buffer solution (pH 7.0). Excitation 360 nm, emission 400 nm.

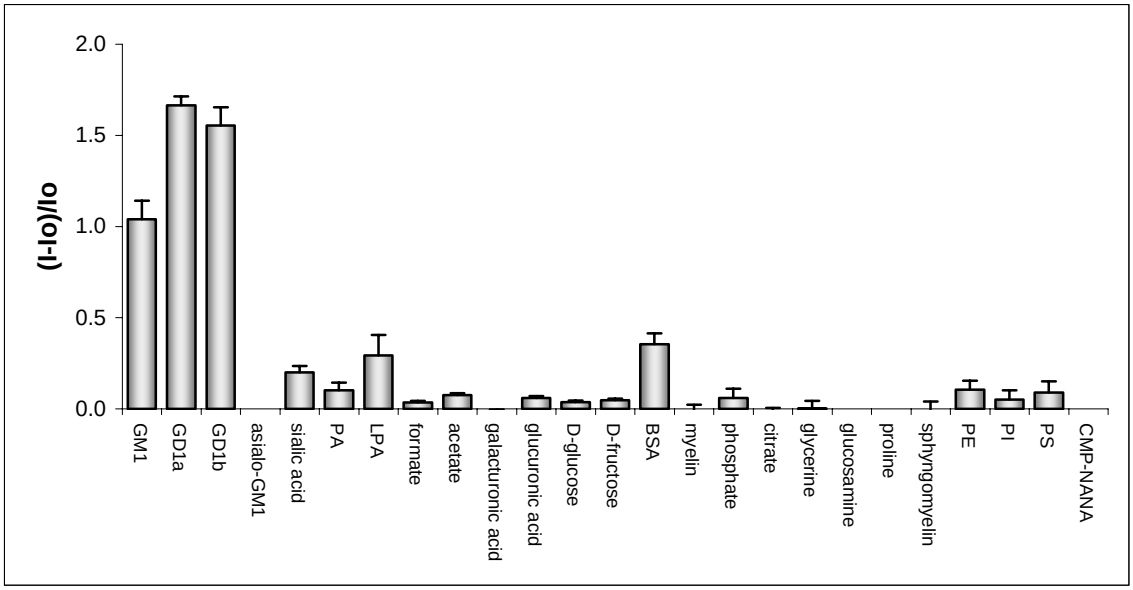

Figure 2.9. Relative fluorescence intensity changes of solutions of **2.2** (5.53×10^{-6} M) in HEPES buffer pH 7.0 in the presence of various gangliosides, phospholipids and other charged and neutral analytes. Ganglioside concentration = 0.5 mg/mL, *ca*. 10^{-4} M each. Concentration of other analytes = 1.1×10^{-3} M. The standard deviation (n=3) of the relative fluorescence intensity for each analyte ranges from 0.01-0.11. Proteins such as myelin and BSA were studied at 1 mg/mL concentrations. Asialoganglioside GM1 = Asialo-GM1; monosialoganglioside GM_1 = GM_1; disialogangliosides = GD_{1a} and GD_{1b}; L-α-phosphatidyl inositol = PI; L-α-phosphatidyl ethanolamine = PE; L-α-phosphatidyl serine = PS; CMP-NANA=Cytidine-5'-mono phospho-*N*-acetylneuraminic acid).

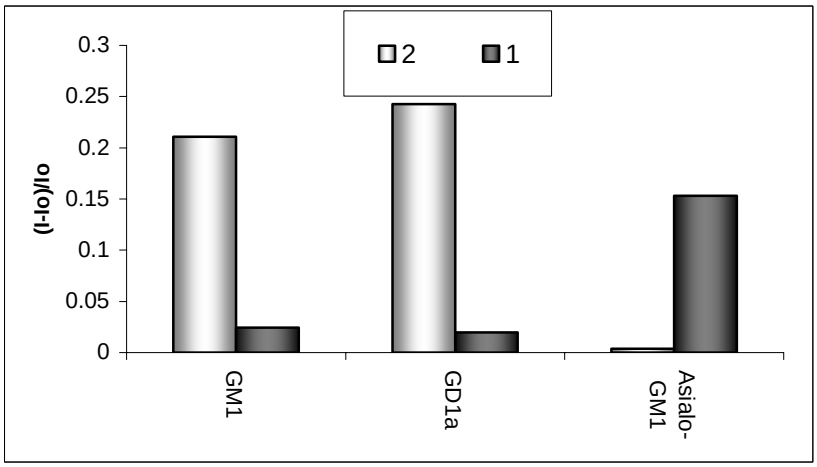

Figure 2.10. Relative fluorescence intensity spectra of compounds **2.1** and **2.2** in the presence of gangliosides in 0.1M HEPES buffer pH 7.0. Gangliosides GM_1 and GD_{1a} contain sialic acid moiety; Ganglioside asialo-GM_1 does not contain the sialic acid moiety.

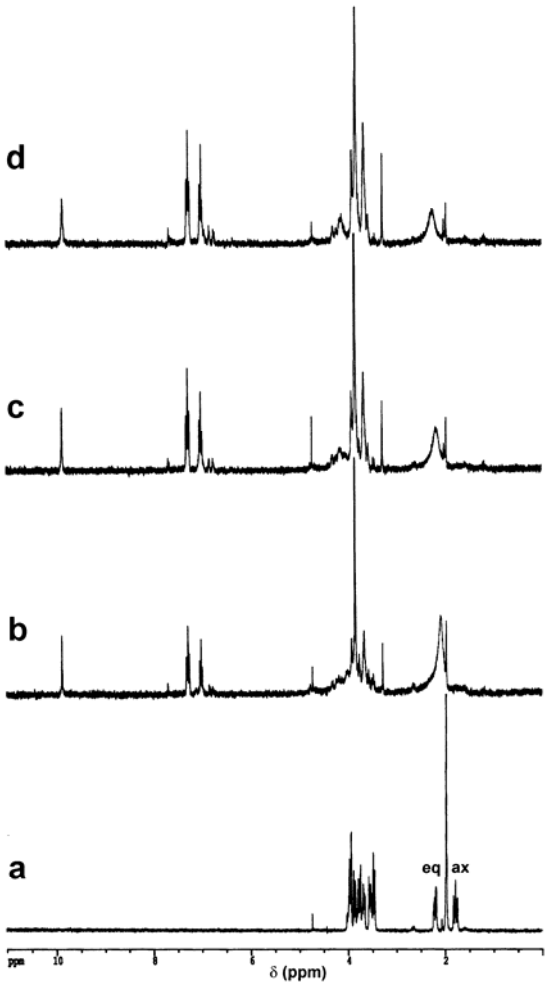

Figure 2.11. ^{1}H-NMR study of a titration of sialic acid with **2.2**: (a) 0.73 mg of sialic acid in 0.75 ml of D_2O; (b) after addition of 0.2 equiv **2.2;** (c) after the addition of 0.4 equiv **2.2;** (d) after the addition of 0.6 equiv **2.2** (0.35 mg of **2.2** in 0.1 ml of D_2O in each addition). When sialic acid is titrated with **2.2**, the NMR signals corresponding to the protons on the glycerol side chain and pyranose ring undergo substantial peak-broadening. The 3-H_{ax} proton, on the same side of the pyranose as the carboxylate moiety, is relatively closer to the metal site than 3-H_{eq}. The axial proton resonance of carbon 3 broadens to a greater extent than that of 3-$H_{eq.}$

The sialic acid residue of GM_1 binds Eu^{+3} via multiple coordination sites (Figure **2.7**). Free sialic acid binding (as predominantly the β-pyranose form) to metals has also been reported.[2.12] The carboxylate, pyranose ring and glycerol side-chain oxygens of sialic acid directly participate in coordination. When sialic acid is titrated with

2.**2** in D_2O, the ^{1}H-NMR signals corresponding to the protons on the glycerol side chain and pyranose ring undergo substantial peak-broadening. The $3H_{ax}$ proton, on the same side of the pyranose as the carboxylate moiety, is relatively closer to the metal site than $3\text{-}H_{eq}$. The axial proton resonance of carbon 3 broadens to a greater extent than that of $3\text{-}H_{eq}$ (Figure **2.11**).

Many compounds are present in typical ganglioside extracts (Figure **2.7**-**2.9**).[2.13] Major components include free sialic acids, phospholipids, myelins, proline and glucosamine. These and many structurally-related compounds do not interfere with ganglioside detection in neutral buffer solution (Figure **2.7**). Interestingly, the disiaiogangliosides (GD_{1a} and GD_{1b}, Figure **2.9**)-**2.2** complexes show stronger emission than the corresponding complex of monosialo GM_1-**2.2**.

Based on these results, we conclude, in agreement with Sillerud *et al.*, that a sialic acid moiety appended to an oligosaccharide sequence leads to enhanced affinity. Comparison of the fluorescence spectra of **2.2** in the presence of GM_1 with neutral asialo GM_1 as well as several other analytes suggests that proximal oligosaccharide-sialic acid sequences are important factors leading to signal transduction (Figure **2.7**).

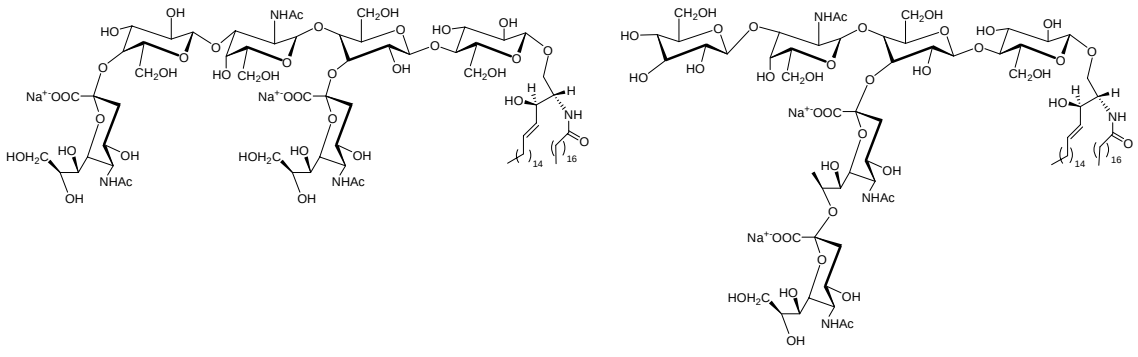

Disialoganglioside (GD_{1a}) Disialoganglioside (GD_{1b})

Figure 2.12. The structure of disialigangliosides GD_{1a} and GD_{1b}.

Gangliosides and neutral sugars can also be monitored using the well-known fluorescent europium(III)-tetracycline (Eu-Tc) complex. The Eu-Tc complex exhibits efficient ligand to metal energy transfer (LMCT).[2.14] This allows for fluorescence monitoring at the common europium emission wavelength of 615 nm, rather than at the ligand emission, as in the case of **2.1** or **2.2** (Figure **2.13**). The Eu-Tc complex is well-known to exhibit fluorescence emission enhancement upon complexation via displacement of bound water.[2.14] However, the Eu-Tc complex is not as selective as **2.1** and **2.2**. It exhibits fluorescence emission enhancement in the presence of several neutral sugars and anions.

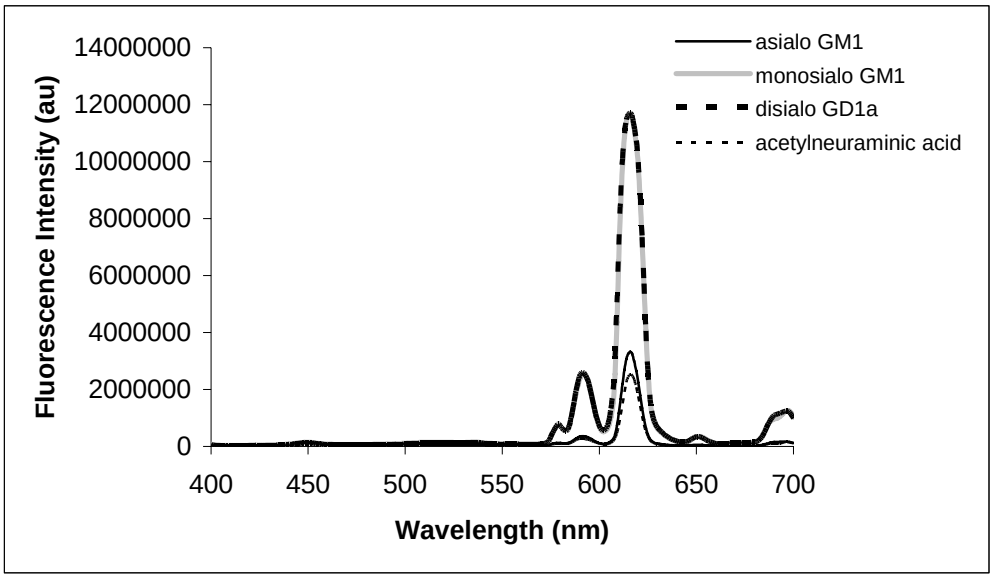

Figure 2.13. Fluorescence intensity change of solutions of Eu-Tc complex (5.53×10^{-6} M) in response to added gangliosides (1.1×10^{-4} M) and sialic acid (1×10^{-3} M) in 0.1 M HEPES buffer solution (pH 7.0). Excitation is at 390 nm, emission at 615 nm.

2.2.3. The Selective Detection of Lysophosphatidic Acid

MeOH solutions containing **2.2** exhibit increased emission in the presence of commercially available lysophosphatidic acid LPA (oleoyl-L-α-lysophosphatidic acid Na salt, 5.53×10^{-6} M λ_{ex} 360 nm λ_{em} 403 nm). Solutions containing commercial

phosphatidic acid PA (3-*sn*-phosphatidic acid Na salt) exhibit minor fluorescence changes at 400 nm (Figure **2.14** and **2.15**), even at millimolar PA levels.

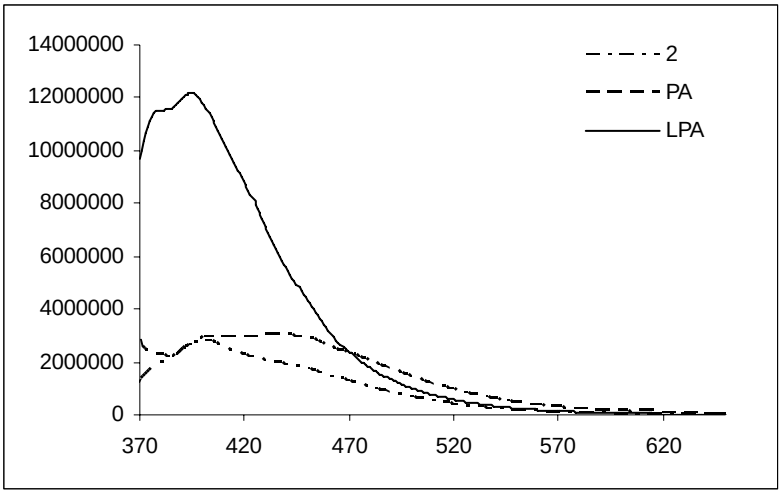

Figure 2.14. Fluorescence intensity change of solutions of **2.2** (5.53×10^{-6} M) in response to added LPA or PA (1.1×10^{-4} M) in MeOH. Emission is at 360 nm, excitation at 400 nm.

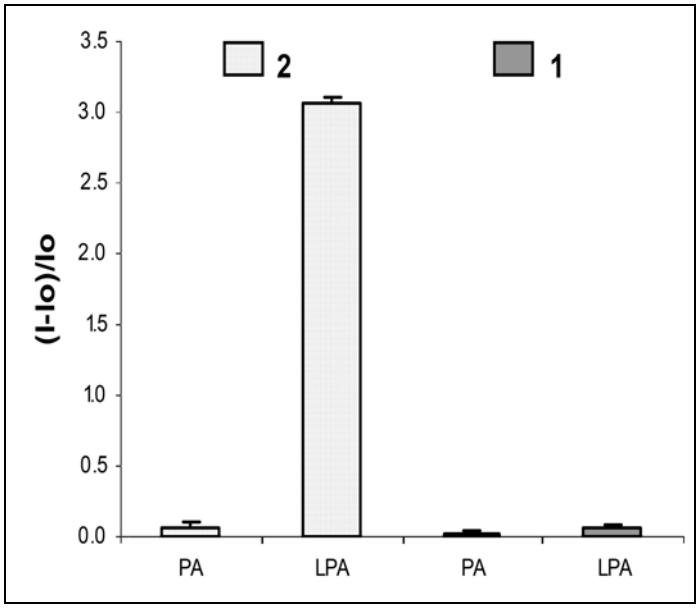

Figure 2.15. Relative fluorescence intensity changes of solutions of **2.1** or **2.2** (5.53×10^{-6} M) in response to added LPA or PA (1.1×10^{-4} M) in MeOH. Emission is at 360 nm, excitation at 400 nm. The standard deviation (n=3) of the relative fluorescence intensity for each analyte ranges from 0.01-0.03.

Distinct affinities of LPA and PA for **2.2** can be interpreted in terms of the magnitude of their corresponding negative charges.[2.15] Intramolecular hydrogen bonding between the phosphate and the 2-*sn*-OH moieties is observed in the crystal structure of LPA, and is known to persist at physiological pH (Figure **2.16**).[2.16] The phosphate hydroxyl of LPA is thus more prone to ionization as compared to the phosphate proton of PA. This generates a higher negative charge on the LPA phosphate, facilitating proposed binding to **2.2** dominated by ionic interactions.

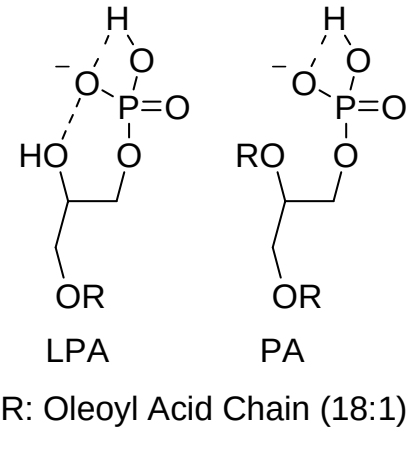

Figure 2.16. Intramolecular hydrogen bonding patterns of LPA and PA explain the lower pK_a of LPA (see reference **2.16**).

The free hydroxyl oxygen of LPA may also serve as a cooperative binding site to the lanthanide. It is known that a second coordinating site, especially one containing a hard atom such as oxygen or nitrogen, enhances lanthanide affinity (see also Figure 5).[2.17] Indeed, we observe significant broadening of the ^{1}H-NMR resonances corresponding to protons on carbons 1-3 (Figure **2.15**) of LPA compared to the other peaks. We propose that this latter feature, in combination with the relatively higher negative charge of LPA compared to PA, should allow selective detection of LPA compared to PA, using **2.2**.

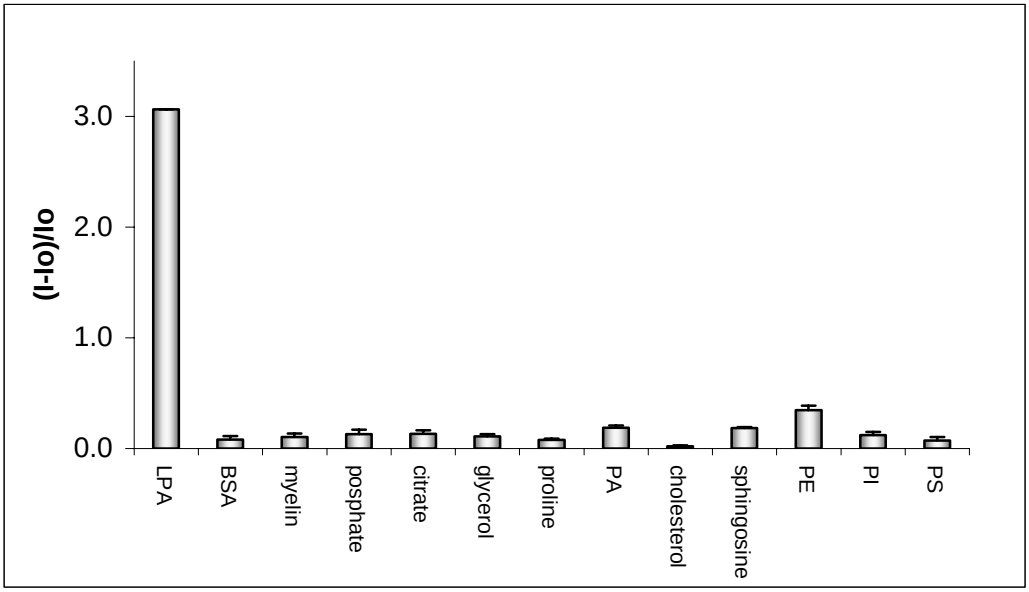

Figure 2.17. Relative fluorescence intensity changes of solutions of **2.2** in MeOH (5.53×10^{-6} M) in the presence of various phospholipids (LPA and PA *ca*. 10^{-3} M) and other charged and neutral analytes. Concentration of other analytes = 1.1×10^{-3} M. The standard deviation (n=3) of the relative fluorescence intensity for each analyte ranges from 0.01-0.11.

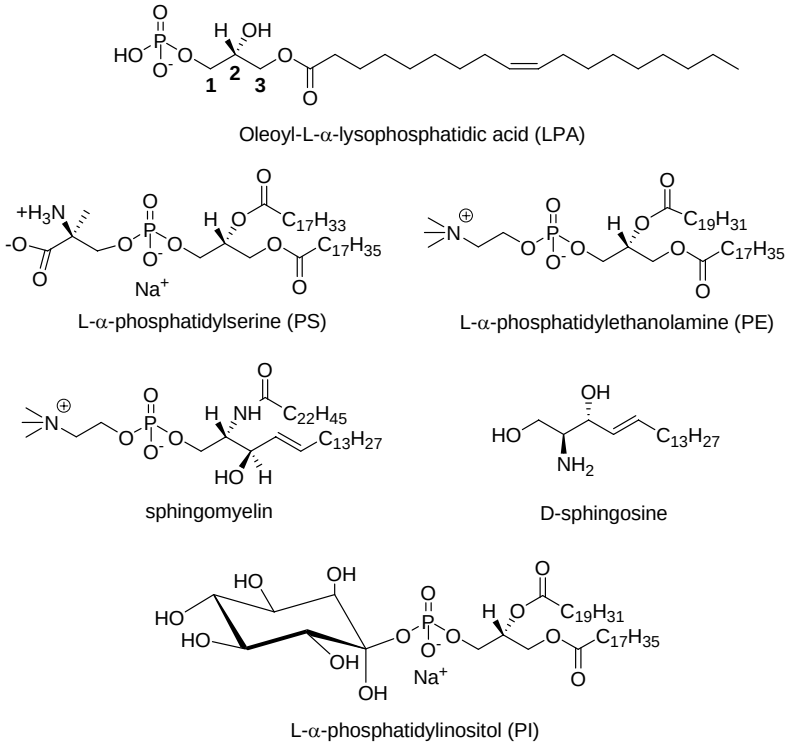

Figure 2.18. Structure of LPA and other phospholipids investigated.

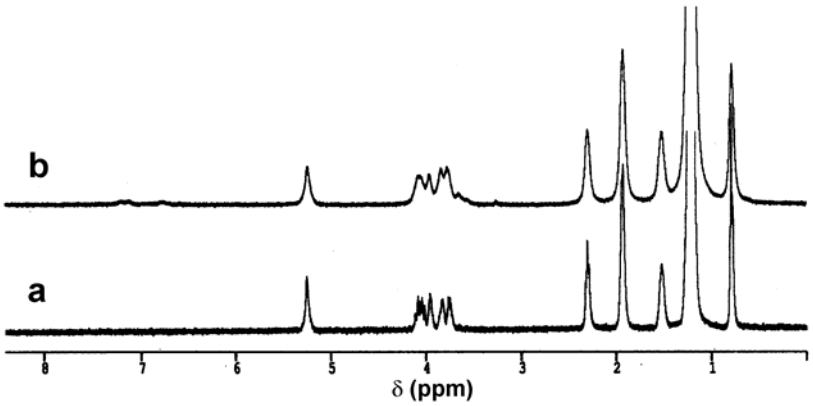

Figure 2.19. ^{1}H NMR study of the titration of LPA with **2.2**: (a) 1 mg of LPA in 0.75 ml D_2O; (b) after addition of 0.2 equiv **2.2**. Significant broadenings of the ^{1}H-NMR resonances corresponding to protons on carbons 1-3 (3.7 ppm to 4.1 ppm on Figure **2.14**) of LPA are observed.

Ovarian cancer is a global problem. A main reason for the low survival rate of ovarian cancer is the fact there is no method for early detection. There is evidence that lysophosphatidic acids (1-acyl-glycerol-3-phosphates), the simplest phospholipids, are promising markers for the early detection of ovarian cancer.[2.18] Current assays for LPA are unsuitable for routine diagnostic and point-of-care use. LPA is relatively difficult to detect in nonpolar lipid extracts. LPA is detected selectively by **2.2** via an increase in fluorescence in MeOH. Figure **2.13** shows that well-known components of phospholipid extracts [2.19,2.20] do not afford fluorescent emission signals comparable to that of LPA in solutions of **2.2** in MeOH**.**

We observe a correlation between fluorescence intensity and LPA concentration in MeOH extracts of lyophilized human plasma previously spiked with LPA (as well as $LaCl_3$ to remove neutral interferents, Figure **2.15**). LPA is detected in the concentration range 1.83×10^{-5} M to 9.15×10^{-5} M (Figure 11). Physiological concentrations of LPA in plasma are *ca.* < 0.1 to 6.3 μM. Danger levels for ovarian cancer are *ca.* ≤ 43.1 μM.[2.18]

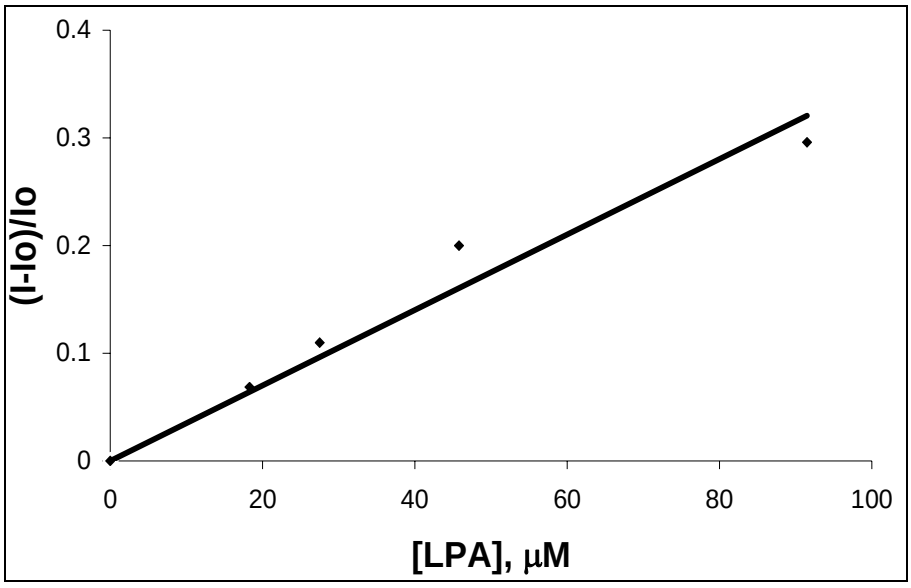

Figure 2.20. Relative fluorescence emission vs. concentration at 437 nm of methanolic extracts of blood plasma samples containing **2.2** and various concentrations of LPA. When carried out in triplicate the standard deviation of the relative fluorescence intensity does not exceed 0.03.

2.3. Conclusion

To date, the lack of receptors that effectively mimic lectin binding is largely due to the inability to achieve sugar-metal coordination under neutral conditions. The design of compound **2.1** is inspired by calcium-saccharide interactions found in C-type lectins. It allows for the successful detection of neutral mono- and oligosaccharides in neutral buffer solution. Analogs of **2.1** that promote high selectivity for specific sugars in the visible and near-IR spectral regions will be reported in due course. Our initial studies to date show that complex **2.2** exhibits enhanced fluorescence emission with anionic lipid analytes that possess proximal hard atom (oxygen) coordination sites, such as the alpha hydroxyl of LPA and the oligosaccharide hydroxyls of gangliosides. This is in excellent accord with prior studies of related systems.[2.17] Compound **2.2** can be used to selectively

detect **(i)** sialic acid-containing gangliosides in buffer solution and (**ii**) LPA in MeOH. These latter results are steps towards developing non-hydrolytic assays for sialic acid and facilitating the detection of LPA, respectively. Our initial focus has been on the selectivity and the signal transduction mechanisms. The complexity of the biomolecules and the nature of the emission (i.e., ligand emission rather than lanthanide emission) render the structural study of the tertiary complexes highly challenging. X-ray crystallographic analysis and further extensive NMR investigations to reveal the precise nature of the tertiary complexes will be reported in due course.

2.4. Materials and Methods.

2.4.1. Materials and Instrumentation

All chemicals were purchased for Sigma-Aldrich and used without further purification. Gangliosides were purchased from Calbiochem. Phospholipids were purchased from Avanti Polar Lipids. Fluorescence spectra were recorded using a spectrofluorimeter SPEX Fluorolog-3 equipped with double excitation and emission monochromators and a 400W Xe lamp. ^{1}H and ^{13}C NMR spectra were acquired on a Bruker DPX-250 or DPX-300 spectrometer. All δ values were reported in ppm. Coupling constants are reported in Hz. Fourier-Transform Infrared Spectra were acquired on a Tensor 27 Infrared Spectrophotometer (Bruker Optics Inc.). MS were performed on a Bruker ProFLEX III MALDI-TOF mass spectrometer.

2.4.2. Synthesis of compounds 2.1 and 2.2

The scheme describing the synthesis of **2.1** and **2.2** follows:

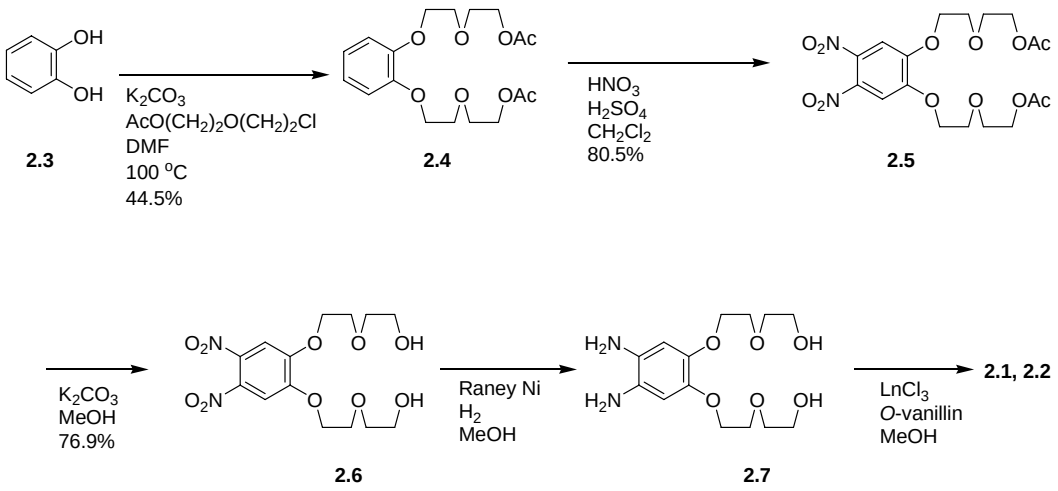

Scheme 2.1. Synthesis of compounds **2.1** and **2.2. 2.1,** Ln = $LaCl_3$**, 2.2**, Ln=$EuCl_3$.

2.4.3. Synthesis of 2.4

To a suspension of K_2CO_3 (3.76 g, 27.24 mmol) in DMF (60 mL) under N_2, catechol **2.3** (1 g, 9.80 mmol) in DMF (20 mL) and O-acetyl-2-(2-chloro-ethoxy)-ethanol (2.1 g, 18.16 mmol) in DMF (10 mL) are added. The final mixture is heated overnight at 100 ˚C. K_2CO_3 is filtered. After the reaction mixture is diluted with EtOAc (60 mL), it is washed with H_2O (4 × 30 mL). The organic phase is dried over Na_2SO_4 and concentrated under reduced pressure. The product is obtained as yellow oil (1.5 g, 44.5%). ^{1}H NMR (250 MHz, DMSO-d_6) δ (ppm): 1.99 (6H, s, CH_3) 3.69 (8H, m, CH_2) 4.09 (8H, m, CH_2) 6.92 (4H, m, ArH). ^{13}C NMR (62.5 MHz, DMSO-d6) δ (ppm): 21.6, 65.0, 69.1, 69.3, 69.8, 115.2, 122.1, 149.2, 171.2.

2.4.4. Synthesis of 2.5[2.21]

2.4 (1.6 g, 4.32 mmol) is dissolved in DCM (50 ml). The solution is cooled on an ice bath and fuming HNO_3 (12 mL) is added. The ice-bath is removed and the solution is stirred overnight at room temperature. The reaction mixture is poured onto a mixture of ice and water (80 mL). The organic phase is collected, neutralized with 10% $NaHCO_3$ and washed with H_2O. The organic layer is dried over anhydrous Na_2SO_4. The solvent is

removed under reduced pressure. The product is chromatographed on silica gel to give compound **2.5** (1.6 g, 80.5%). ^{1}H NMR (250MHz, DMSO-d_6) δ (ppm): 1.97 (6H, s, CH_3) 3.68 (2H, t, CH_2) 3.80 (2H, t, CH_2) 4.10 (2H, t, CH_2) 4.33 (2H, t, CH_2) 7.79 (2H, s, ArH). ^{13}C NMR (62.5 MHz, DMSO-d_6) δ (ppm): 21.4, 55.7, 64.0, 69.3, 70.4, 110.1, 136.7, 152.0, 171.2.

2.4.5. Synthesis of 2.6

To a solution of **2.5** (0.52 g, 1.13 mmol) in MeOH (30 mL), KOH (0.13 g, 2.26 mmol) is added. The mixture is stirred at room temperature for 4 hours. The reaction mixture is neutralized with 2N HCl. MeOH is removed under reduced pressure. The product is extracted with DCM. After washing with H_2O, the organic layer is dried over anhydrous Na_2SO_4. After removing DCM under reduced pressure, **2.5** is obtained (0.33 g, 76.9%) and is used without further purification in the subsequent steps.

2.4.6. Synthesis of 2.1

Compound **2.6** (0.2 g, 0.53 mmol) is dissolved in MeOH (15 mL). Raney Ni is added. Hydrogenation is carried out at 50 psi and monitored via H_2 consumption. Raney Ni is removed by filtration through celite. The filtrate containing **2.7** is immediately used in the next step to prevent any unwanted oxidation. To a refluxing solution of $LaCl_3$ (0.13 g, 0.53 mmol) in 10 mL MeOH, o-vanillin (0.16 g, 1.1 mmol) in 10 mL MeOH and the solution containing **2.7** are simultaneously added over 20 min. The final solution is refluxed for 2 h. The reaction mixture is concentrated under reduced pressure and the residue washed with EtOAc (3x 5 mL). The product is obtained as a dark-red solid (0.37 g). ^{13}C-NMR (62.5 MHz, DMSO-d6) δ (ppm): 49.4, 56.5, 56.9, 61.1, 69.7, 69.8, 73.1, 73.3, 113.8, 114.0, 118.4, 120.0, 120.9, 123.4, 149.2, 151.4, 192.8. MALDI-Tof

(m/z): calcd. $C_{30}H_{34}LaN_2O_{10}$, 721.13; found, 721.48. IR (cm^{-1}) 3206.20, 1614.33, 1439.22, 1209.10, 1036.87.

2.4.7. Synthesis of 2.2

This compound is synthesized as described above for 2.1 except $EuCl_3$ is used instead of $LaCl_3$. The product is obtained as a dark-red solid (0.35 g). ^{13}C-NMR (62.5 MHz, DMSO-d_6) δ (ppm): 49.4, 56.6, 57.0, 61.1, 69.7, 69.8, 73.1, 73.4, 118.4, 119.3, 120.1, 120.9, 123.4, 147.3, 149.0, 149.3, 151.6, 192.8. MALDI-Tof (m/z): calcd. $C_{30}H_{34}EuN_2O_{10}$, 735.14; found, 735.34. IR (cm^{-1}) 3104.00, 1638.44, 1444.54, 1214.76, 1018.07.

2.5. References.

2.1. For example: Weis, W. I.; Drickamer, K.; Hendrickson, W. A. *Nature*, **1992**, 360, 127.

2.2. Horrocks, W. DeW., Jr.; Sudnick, D. R. *Acc. Chem. Res.* **1981**, 14, 384**.**

2.3. Review of salophenes and related compounds: vanVeggel, F. C. J. M.; Verboom, W.; Reinhoudt, D. N. *Chem. Rev*. **1994**, 94, 279.

2.4. (a) Striegler, S.; Dittel, M. *J. Am. Chem. Soc.* **2003**, 125, 11518. (b) Review: Davis, A. P.; Wareham, R. S. *Angew. Chem. Int. Ed.* **1999**, 38, 2978.

2.5. (a) Angyal, S. J. *Aust. J. Chem.* **1972**, 25, 1957. (b) Angyal, S. J., Greeves, D.; Mills, J. A. *Aust. J. Chem.* **1979**, 32, 1993.

2.6. Liu, G.-D.; Yang, X.; Chen, Z.-P.; Shen, G.-L.; Yu, R.-Q. *Anal. Sci*. **2000**, 16, 1255 and references cited therein.

2.7. Reviews: (a) James, T. D.; Shinkai, S. *Top. Curr. Chem*. **2002**, 218, 159. (b) Wang, W.; Gao, X.; Wang, B. Curr. *Org. Chem*. **2002**, 6, 1285.

2.8. (a) Svennerholm, L. *Biochem. Biophys. Acta* **1957**, 24, 604. (b) Warren, L. *J. Biol. Chem*. **1959**, 234, 1971. (c) Schauer, R.; Kelm, S.; Rerter, G.; Roggentin, P.; Shaw, L. in *Biology of the Sialic Acids,* ed. Rosenburg, A. (Plenum, New York) **1995**, pp. 7. (d) Nagai, Y.; Iwamori, M.; Iwamori, M. *Biology of the Sialic Acids,* ed. Rosenburg, A. (Plenum, New York) **1995**, pp. 197. (e) Mattoo, R. L.; Roseman,S. *Anal. Biochem*. **1997**, 246, 3

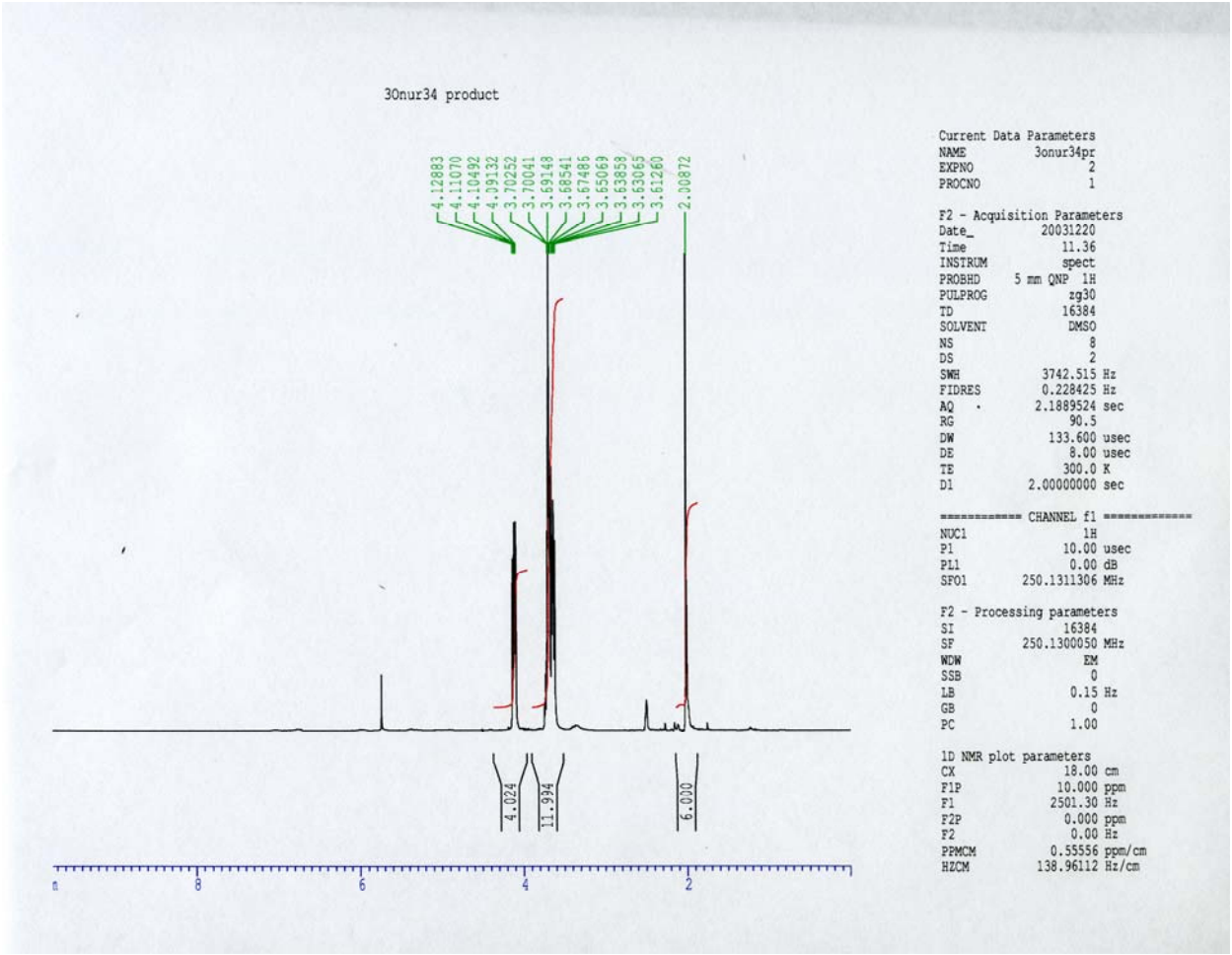

Figure 2.21. ^{1}H-NMR Spectrum of 2-(2-chloroethoxy)ethyl acetate in DMSO-d_6

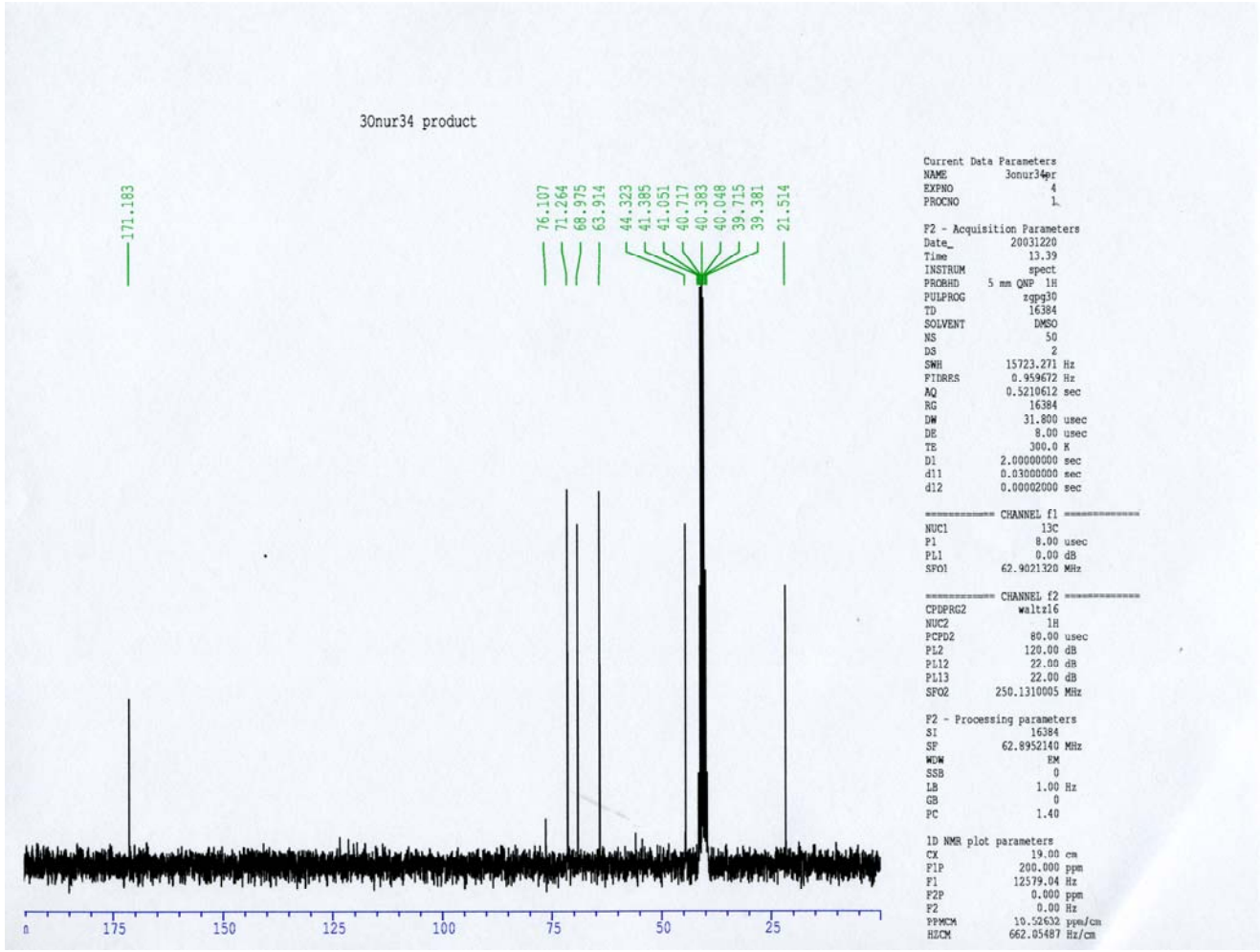

Figure 2.22. ^{13}C-NMR Spectrum of 2-(2-chloroethoxy)ethyl acetate in DMSO-d_6

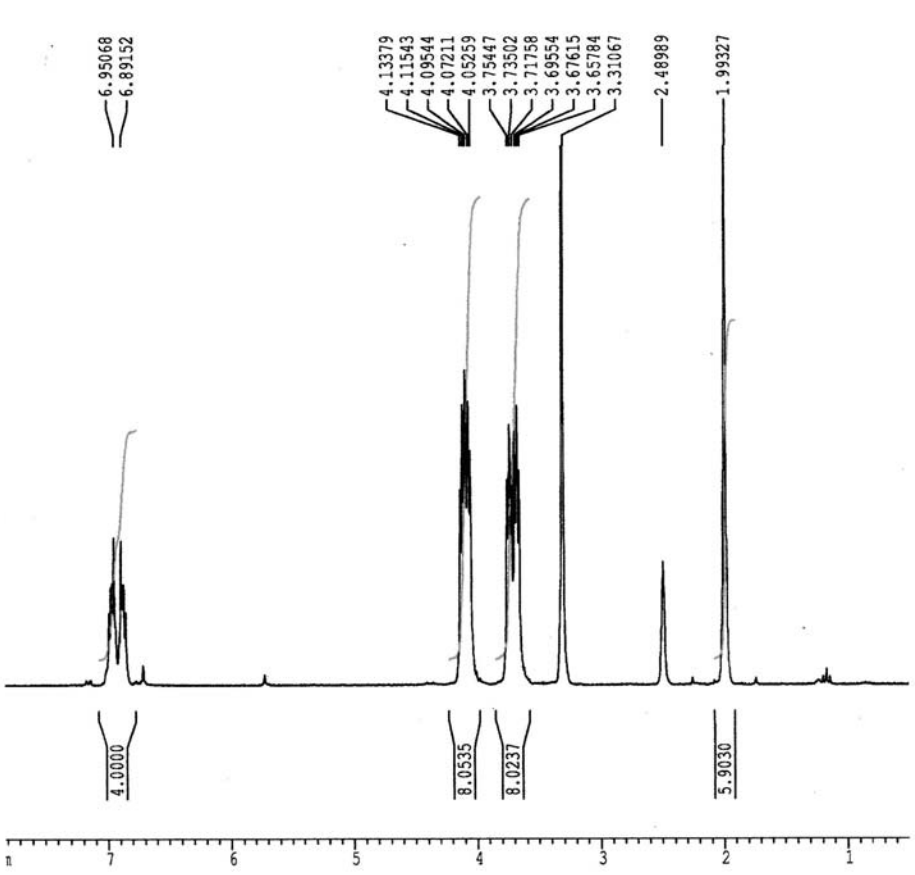


```
Current Data Parameters
NAME            2Wang-81
EXPNO                  1
PROCNO                 1

F2 - Acquisition Parameters
Date_           20050719
Time               18.07
INSTRUM            spect
PROBHD     5 mm QNP  1H
PULPROG             zg30
TD                 16384
SOLVENT             DMSO
NS                     8
DS                     2
SWH             3742.515 Hz
FIDRES          0.228425 Hz
AQ              2.1889524 sec
RG                   362
DW               133.600 usec
DE                 8.00 usec
TE                300.0 K
D1             2.00000000 sec

============ CHANNEL f1 ============
NUC1                  1H
P1                 10.00 usec
PL1                 0.00 dB
SFO1          250.1311306 MHz

F2 - Processing parameters
SI                 16384
SF            250.1300050 MHz
WDW                   EM
SSB                    0
LB                  0.15 Hz
GB                     0
PC                  1.00

1D NMR plot parameters
CX                 18.00 cm
F1P                 8.000 ppm
F1               2001.04 Hz
F2P                 0.500 ppm
F2                125.07 Hz
PPMCM           0.41667 ppm/cm
HZCM          104.22083 Hz/cm
```

Figure 2.23. ^{1}H-NMR Spectrum of **2.4** in DMSO-d_6

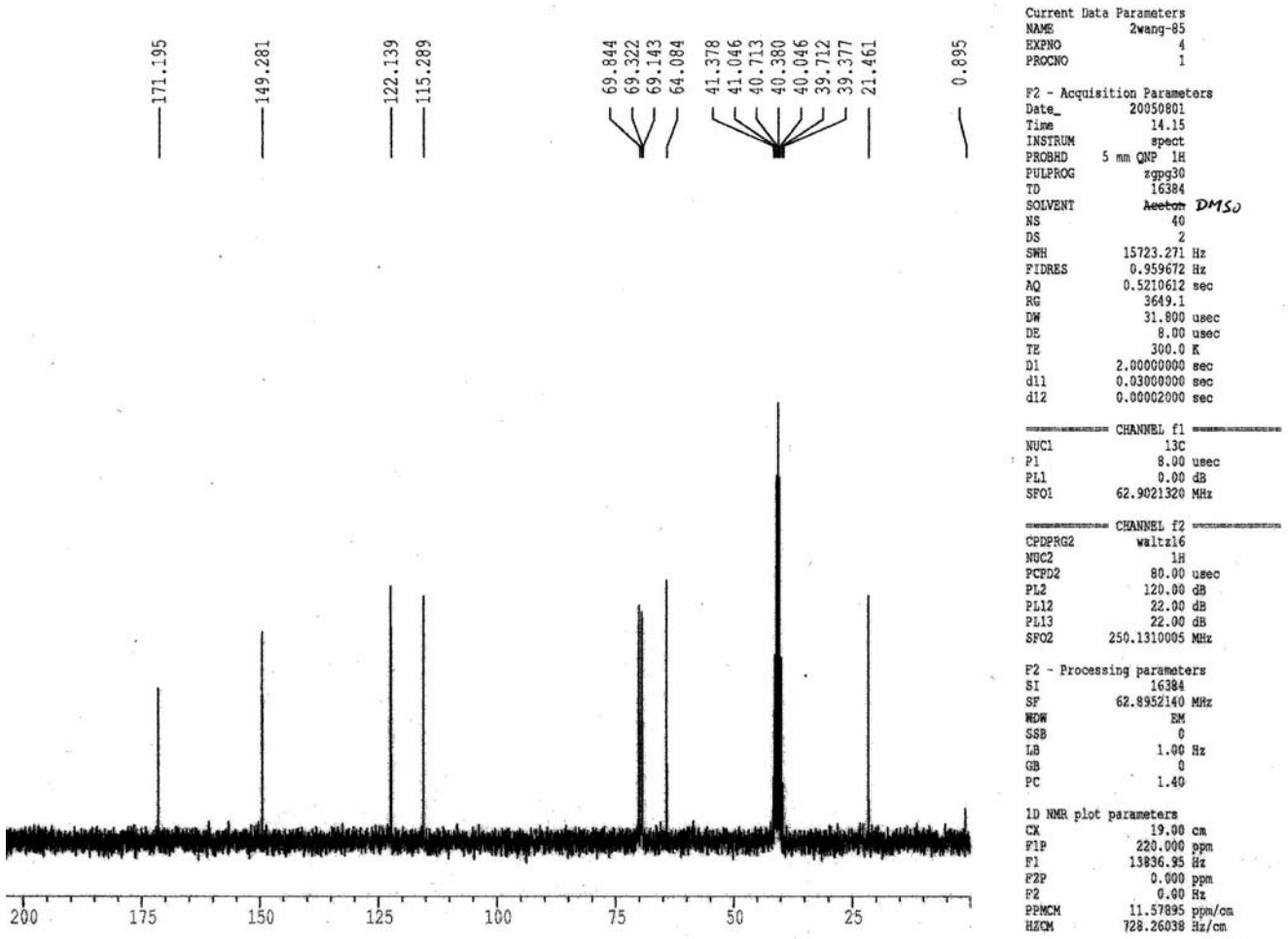

Figure 2.24. ^{13}C-NMR Spectrum of **2.4** in DMSO-d_6

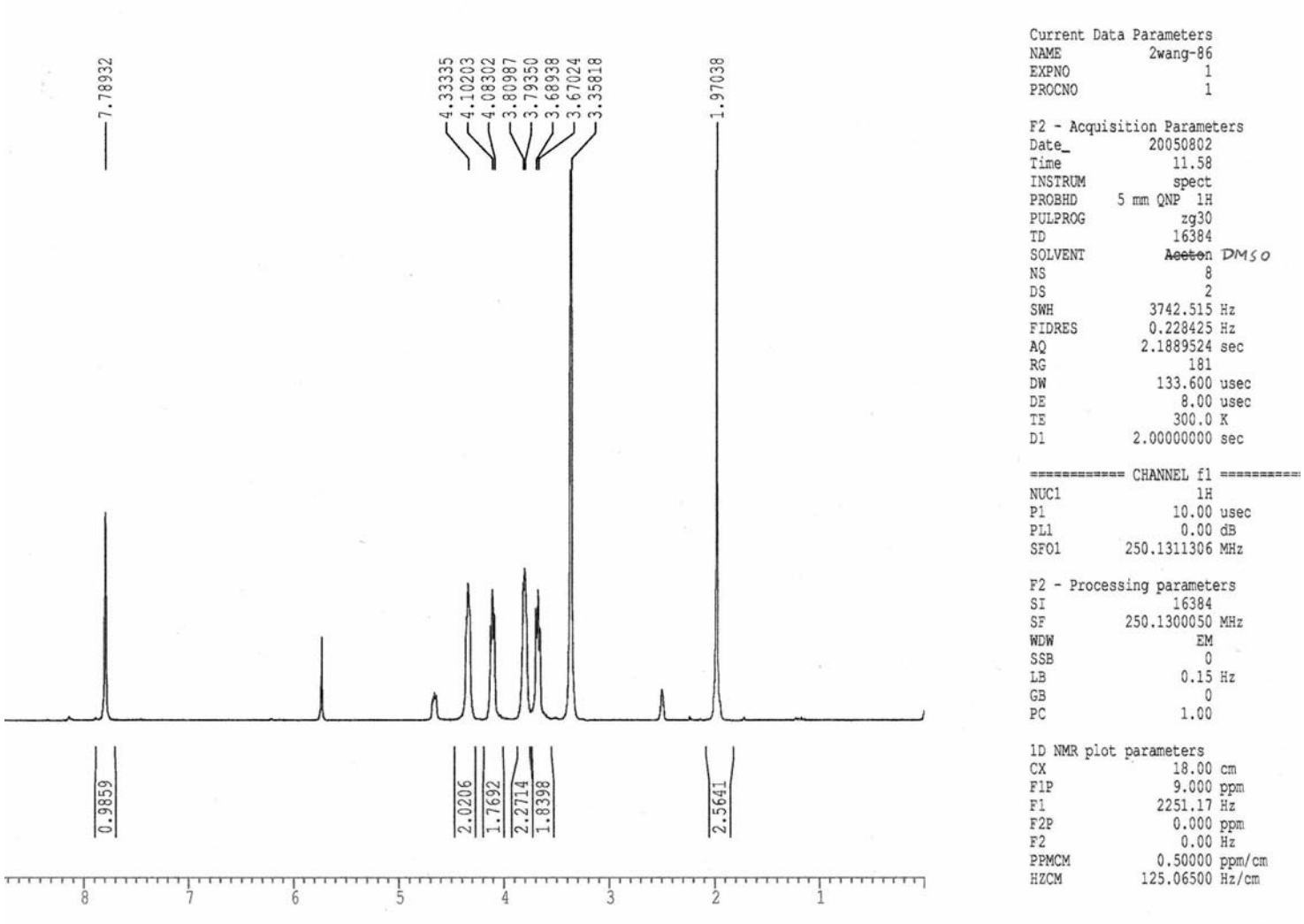


```
Current Data Parameters
NAME            2wang-86
EXPNO                  1
PROCNO                 1

F2 - Acquisition Parameters
Date_           20050802
Time               11.58
INSTRUM            spect
PROBHD     5 mm QNP  1H
PULPROG             zg30
TD                 16384
SOLVENT          Aceton DMSO
NS                     8
DS                     2
SWH             3742.515 Hz
FIDRES          0.228425 Hz
AQ             2.1889524 sec
RG                   181
DW               133.600 usec
DE                 8.00 usec
TE                300.0 K
D1             2.00000000 sec

============ CHANNEL f1 ==========
NUC1                  1H
P1                10.00 usec
PL1                0.00 dB
SFO1         250.1311306 MHz

F2 - Processing parameters
SI                 16384
SF           250.1300050 MHz
WDW                   EM
SSB                    0
LB                  0.15 Hz
GB                     0
PC                  1.00

1D NMR plot parameters
CX                18.00 cm
F1P               9.000 ppm
F1              2251.17 Hz
F2P               0.000 ppm
F2                 0.00 Hz
PPMCM          0.50000 ppm/cm
HZCM         125.06500 Hz/cm
```

Figure 2.25. ^{1}H-NMR Spectrum of **2.5** in DMSO-d_6

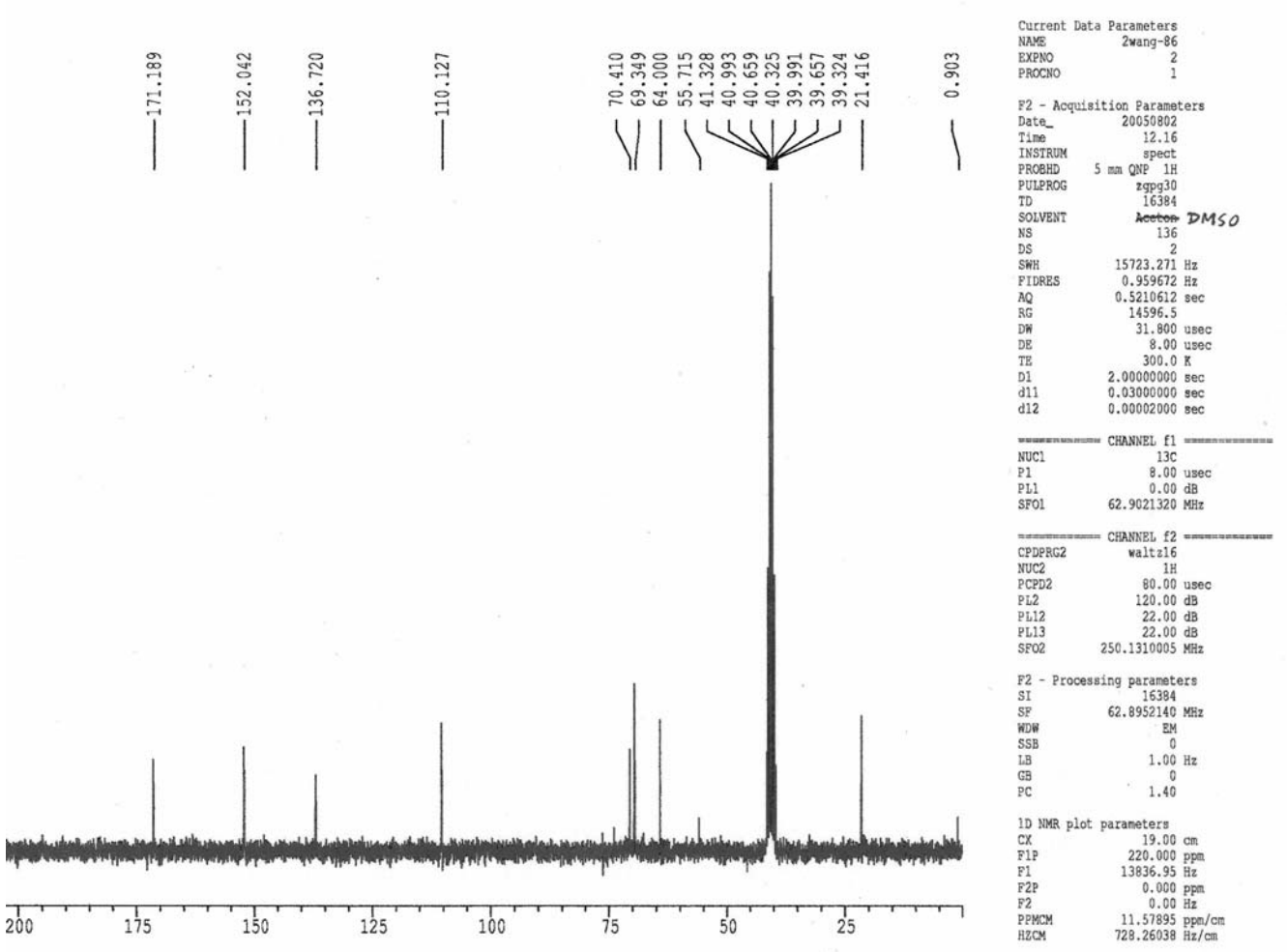

Figure 2.26. ^{13}C-NMR Spectrum of **2.5** in DMSO-d_6

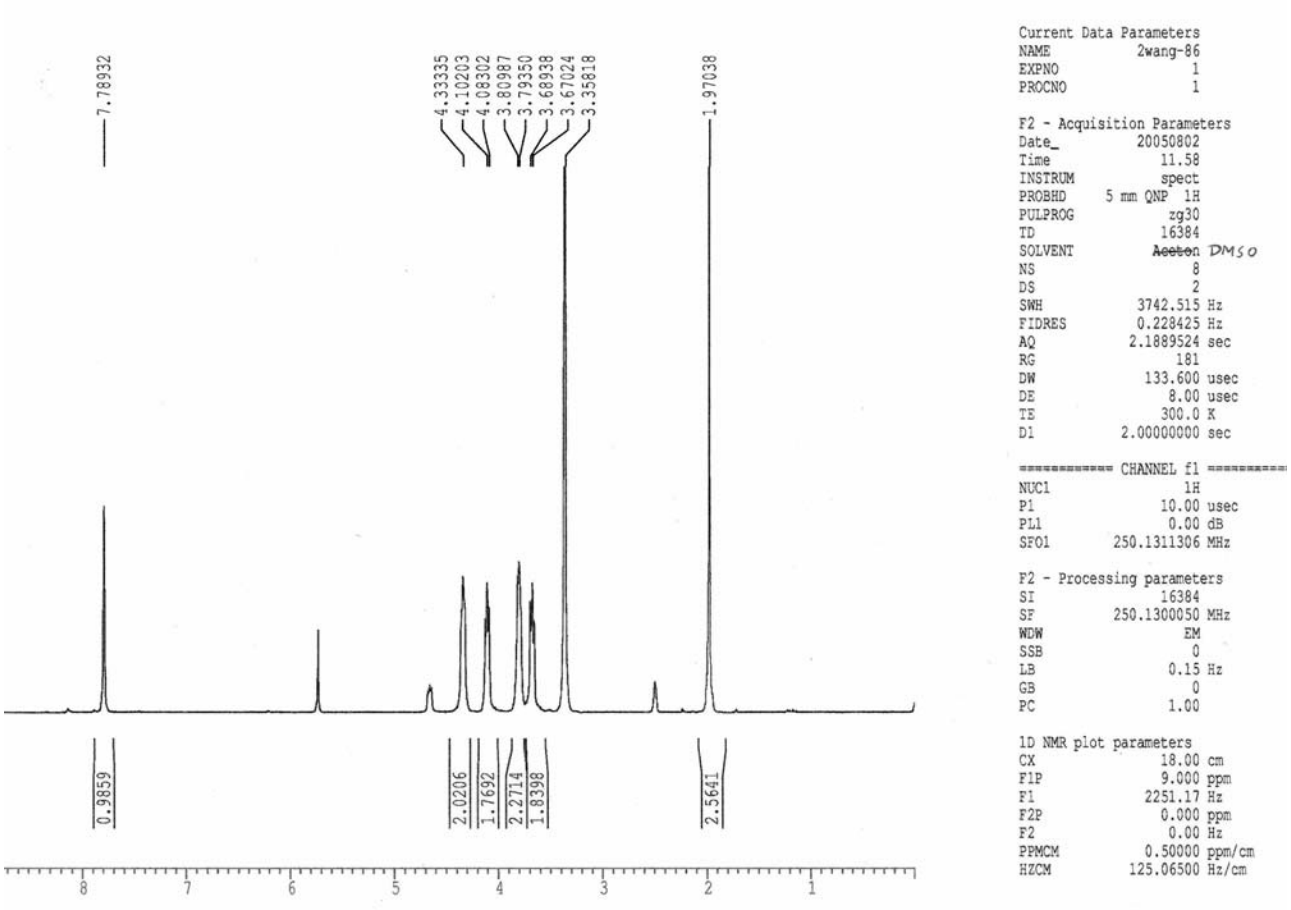


```
Current Data Parameters
NAME            2wang-86
EXPNO                  1
PROCNO                 1

F2 - Acquisition Parameters
Date_           20050802
Time               11.58
INSTRUM            spect
PROBHD     5 mm QNP  1H
PULPROG             zg30
TD                 16384
SOLVENT          Acetn DMSO
NS                     8
DS                     2
SWH             3742.515 Hz
FIDRES          0.228425 Hz
AQ              2.1889524 sec
RG                   181
DW                133.600 usec
DE                  8.00 usec
TE                 300.0 K
D1             2.00000000 sec

========== CHANNEL f1 ==========
NUC1                  1H
P1                 10.00 usec
PL1                 0.00 dB
SF01         250.1311306 MHz

F2 - Processing parameters
SI                 16384
SF           250.1300050 MHz
WDW                   EM
SSB                    0
LB                  0.15 Hz
GB                     0
PC                  1.00

1D NMR plot parameters
CX                 18.00 cm
F1P                9.000 ppm
F1              2251.17 Hz
F2P                0.000 ppm
F2                 0.00 Hz
PPMCM           0.50000 ppm/cm
HZCM          125.06500 Hz/cm
```

Figure 2.27. ^{1}H-NMR Spectrum of **2.6** in DMSO-d_6

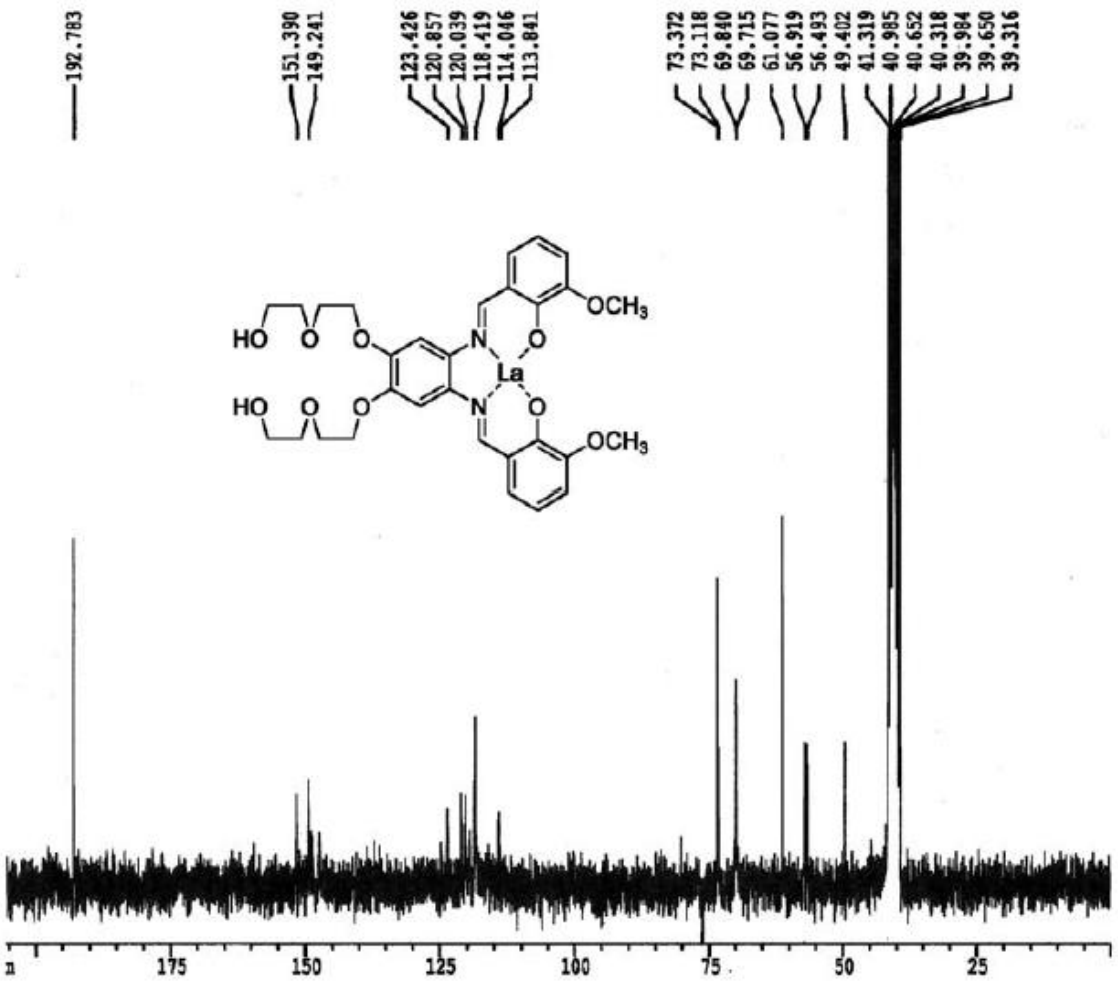


```
Current Data Parameters
NAME                  salen3
EXPNO                      2
PROCNO                     1

F2 - Acquisition Parameters
Date_              20050910
Time                  14.20
INSTRUM                spect
PROBHD     5 mm QNP  1H
PULPROG               zgpg30
TD                     16384
SOLVENT
NS                      2960
DS                         2
SWH               15723.271 Hz
FIDRES            0.959672 Hz
AQ                0.5210612 sec
RG                   14596.5
DW                   31.800 usec
DE                    8.00 usec
TE                   300.0 K
D1                2.00000000 sec
d11               0.03000000 sec
d12               0.00002000 sec

========== CHANNEL f1 ==========
NUC1                      13C
P1                       8.00 usec
PL1                      0.00 dB
SFO1             62.9021320 MHz

========== CHANNEL f2 ==========
CPDPRG2                waltz16
NUC2                       1H
PCPD2                   80.00 usec
PL2                    120.00 dB
PL12                    22.00 dB
PL13                    22.00 dB
SFO2             250.1310005 MHz

F2 - Processing parameters
SI                        16384
SF               62.8952140 MHz
WDW                          EM
SSB                           0
LB                         1.00 Hz
GB                            0
PC                         1.40

1D NMR plot parameters
CX                        19.00 cm
F1P                      210.000 ppm
F1                     13208.00 Hz
F2P                      0.000 ppm
F2                        0.00 Hz
PPMCM                 11.05263 ppm/cm
HZCM                695.15765 Hz/cm
```

Figure 2.28. ^{13}C-NMR Spectrum of **2.1** in DMSO-d_6.

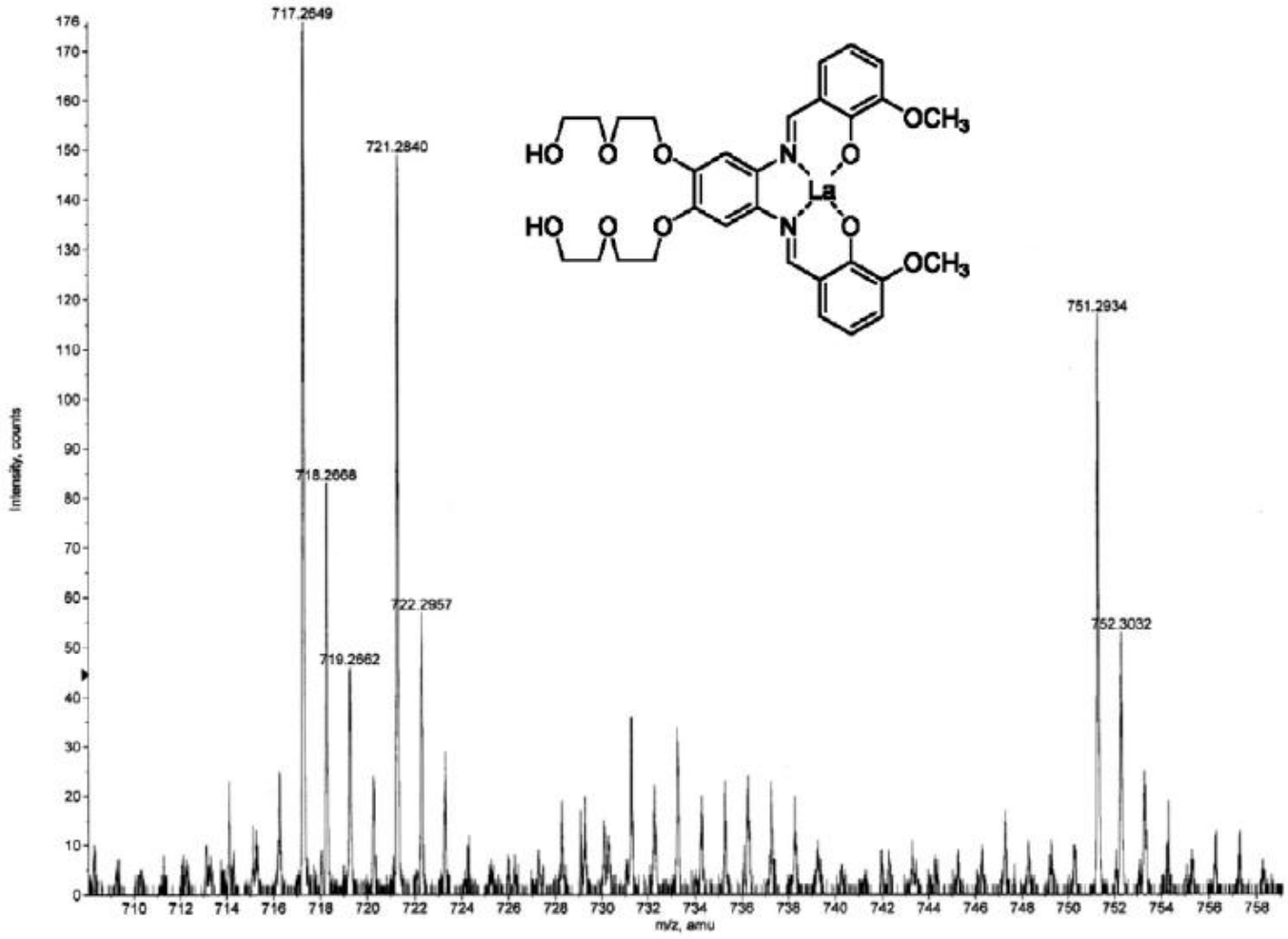

Figure 2.29. MALDI TOF Spectrum of **2.1.**

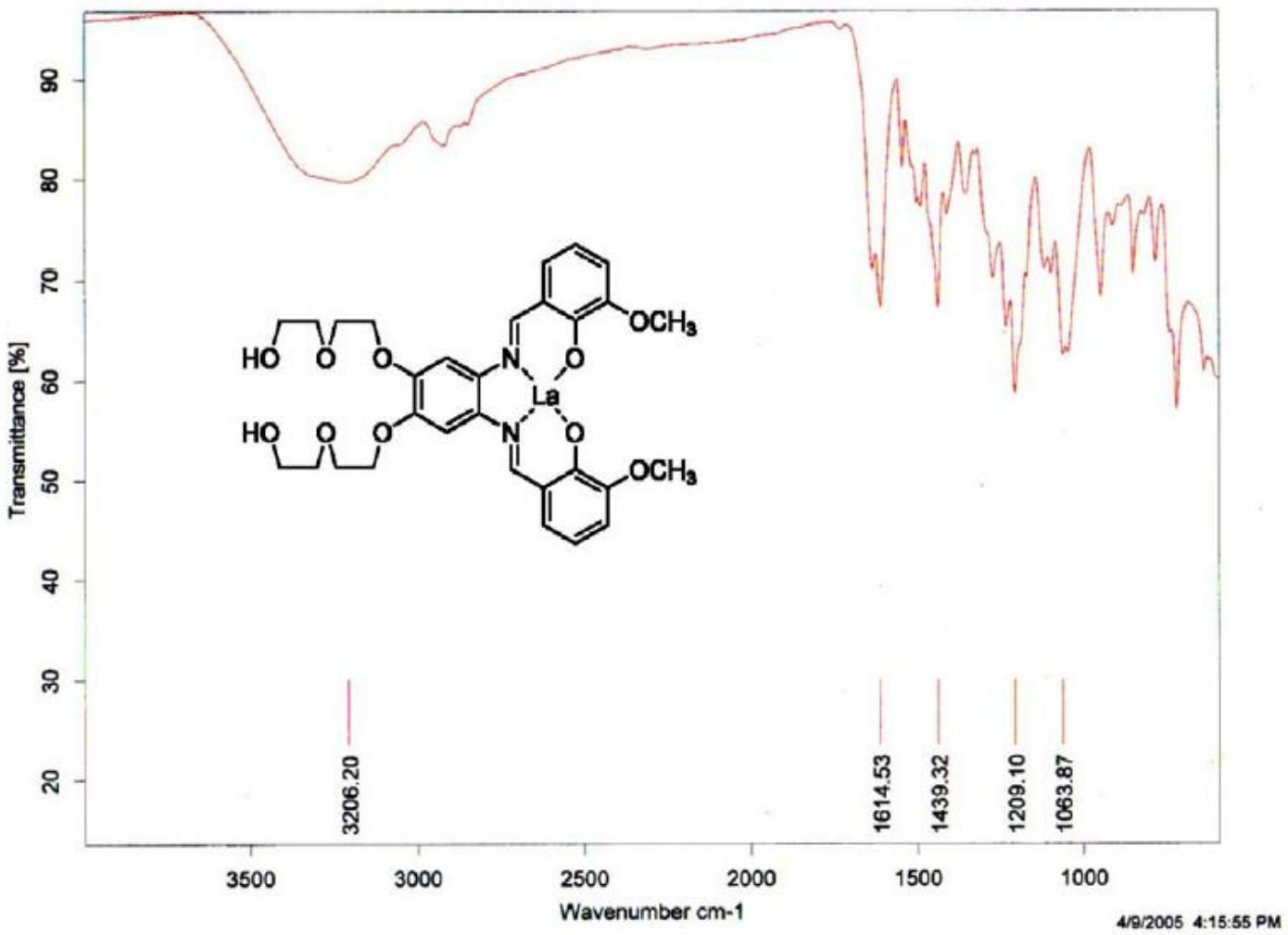

Figure 2.30. FTIR Spectrum of **2.1**.

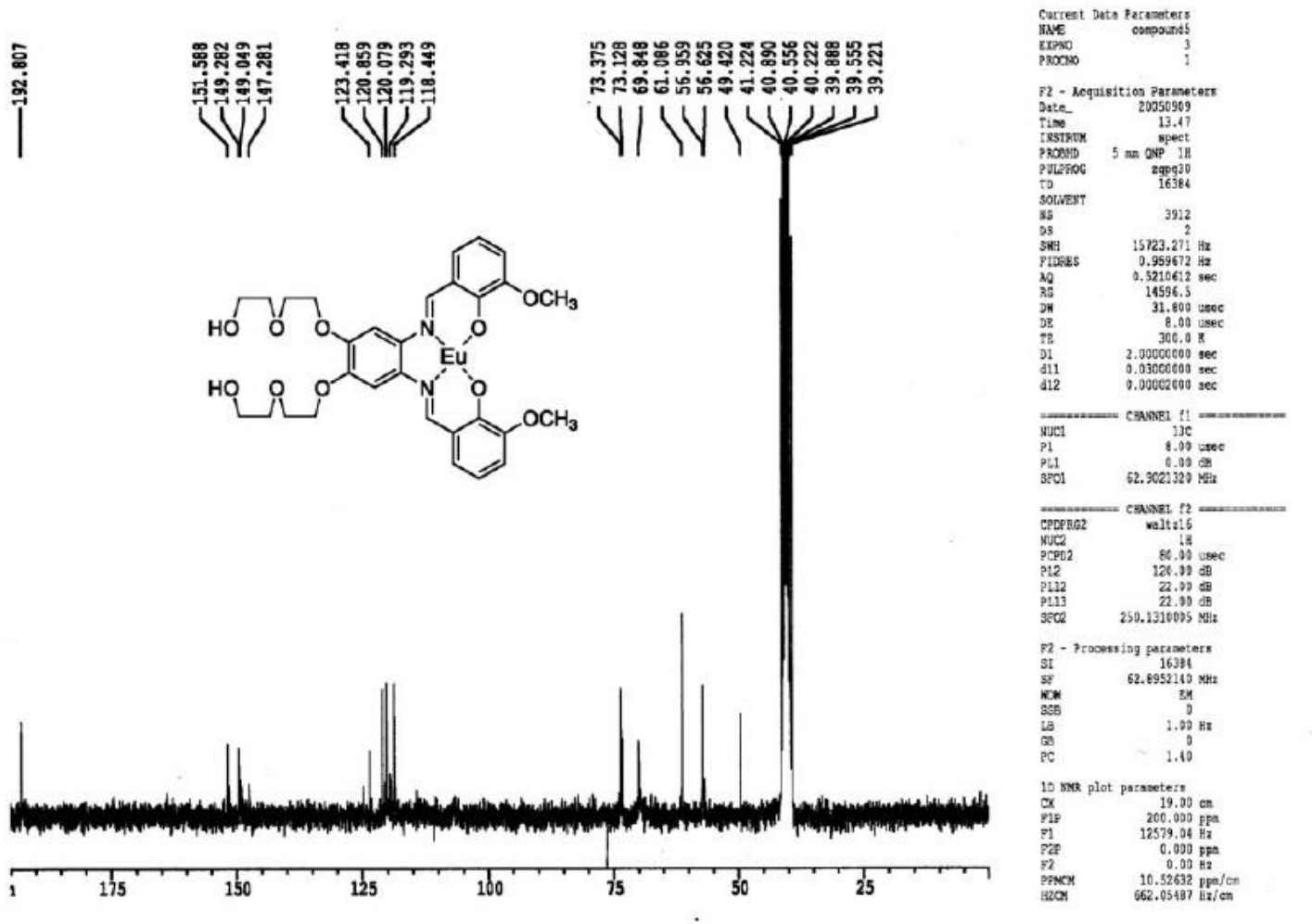

Current Data Parameters
NAME compound5
EXPNO 3
PROCNO 1

F2 - Acquisition Parameters
Date_ 20050909
Time 13.47
INSTRUM spect
PROBHD 5 mm QNP 1H
PULPROG zgpg30
TD 16384
SOLVENT
NS 3912
DS 2
SWH 15723.271 Hz
FIDRES 0.959672 Hz
AQ 0.5210612 sec
RG 14596.5
DW 31.800 usec
DE 8.00 usec
TE 300.0 K
D1 2.00000000 sec
d11 0.03000000 sec
d12 0.00002000 sec

========== CHANNEL f1 ==========
NUC1 13C
P1 8.00 usec
PL1 0.00 dB
SFO1 62.9021329 MHz

========== CHANNEL f2 ==========
CPDPRG2 waltz16
NUC2 1H
PCPD2 80.00 usec
PL2 120.00 dB
PL12 22.00 dB
PL13 22.00 dB
SFO2 250.1310005 MHz

F2 - Processing parameters
SI 16384
SF 62.8952140 MHz
WDW EM
SSB 0
LB 1.00 Hz
GB 0
PC 1.40

1D NMR plot parameters
CX 19.00 cm
F1P 200.000 ppm
F1 12579.04 Hz
F2P 0.000 ppm
F2 0.00 Hz
PPMCM 10.52632 ppm/cm
HZCM 662.05487 Hz/cm

Figure 2.31. ^{13}C-NMR Spectrum of **2.2** in DMSO-d_6.

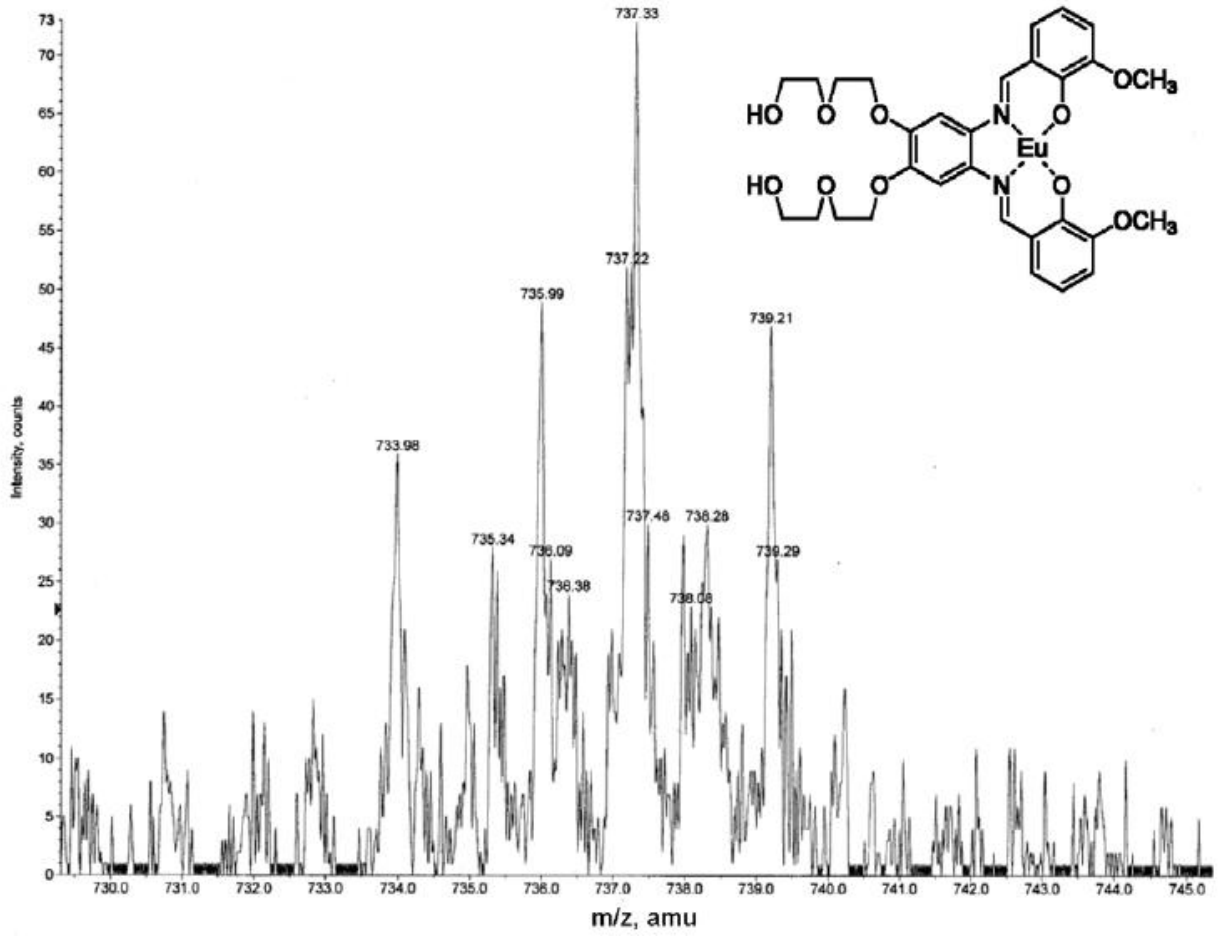

Figure 2.32. MALDI.TOF of Spectrum of **2.2**.

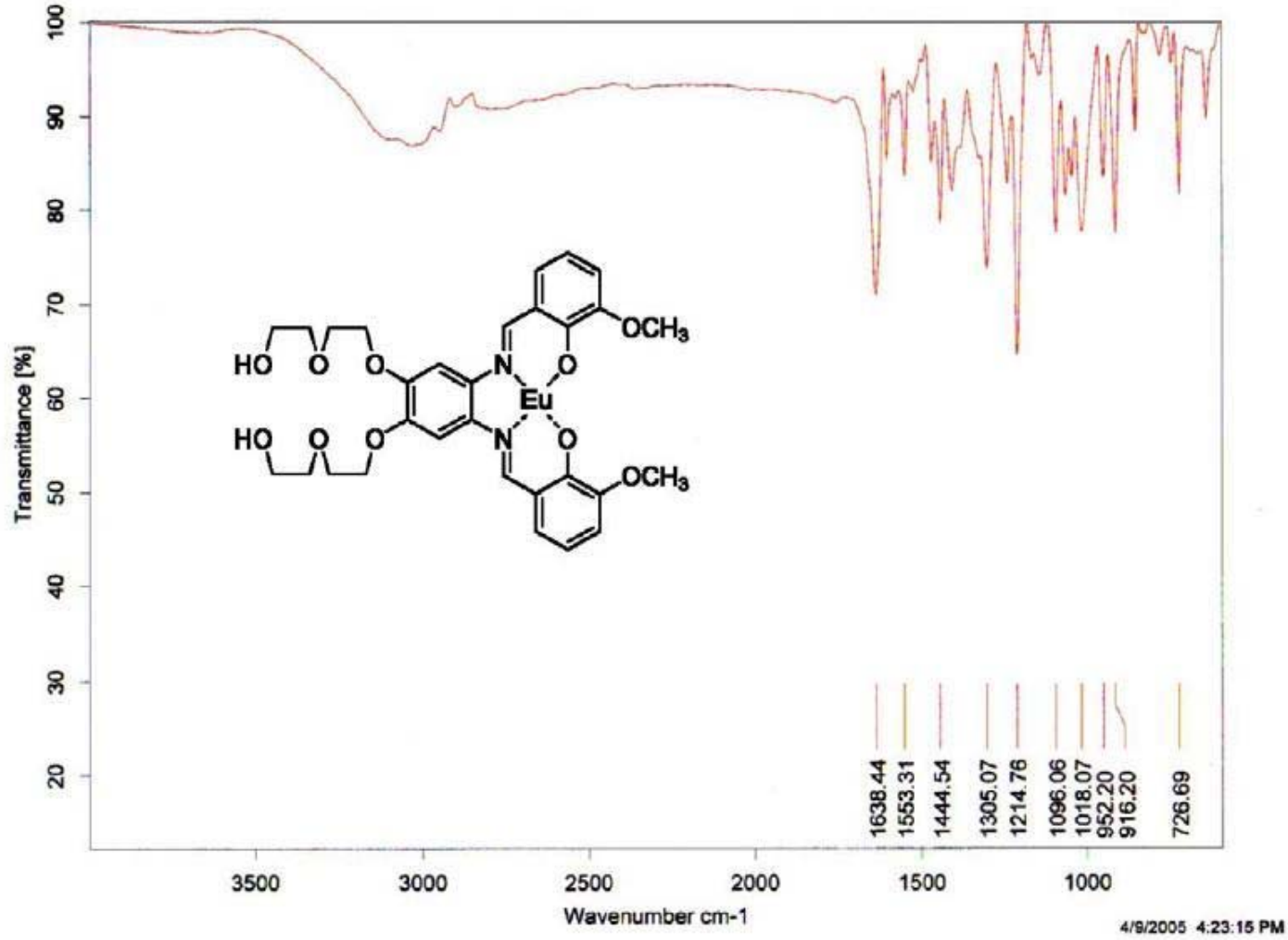

Figure 2.33. FTIR Spectrum of **2.2**.

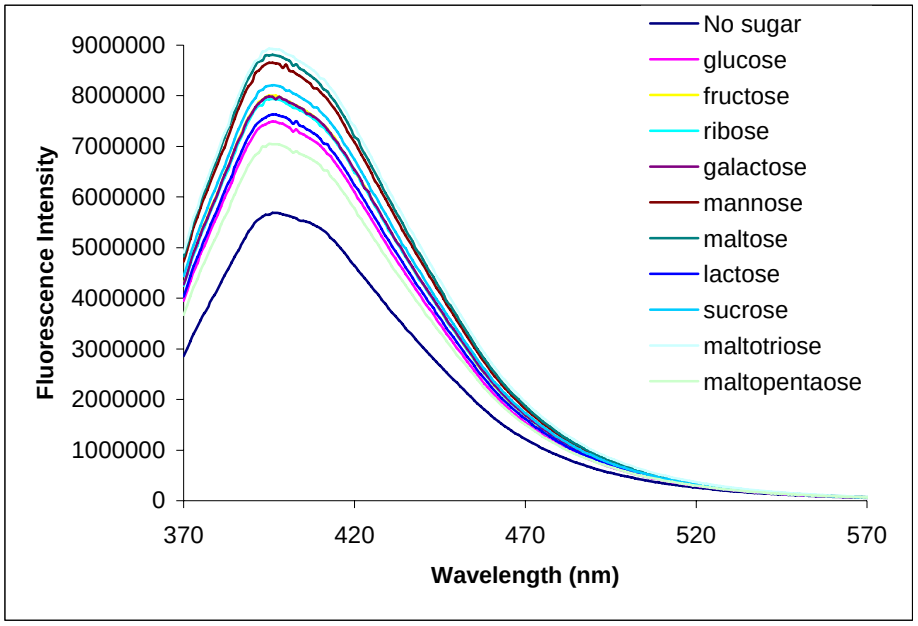

Figure 2.34. Fluorescence intensity changes of **2.1** (5.53 × 10-6 M) in the presence of mono- and oligosaccharides (1.1 × 10-3 M) in buffer solution (pH 7.0).

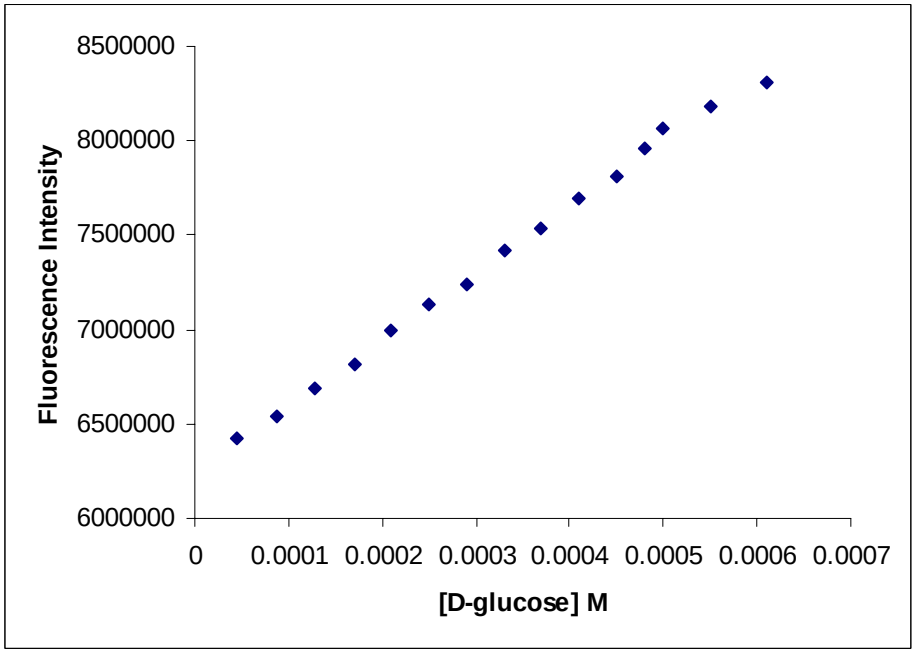

Figure 2.35. Binding isotherm observed upon titration of **2.1** with D-glucose in 0.1 M HEPES buffer, pH 7.0. The concentration of **2.1** is 6×10^{-6} M. The concentration of saccharide is increased to 6×10^{-4} M. Excitation is at 360 nm, emission is monitored at 400 nm.

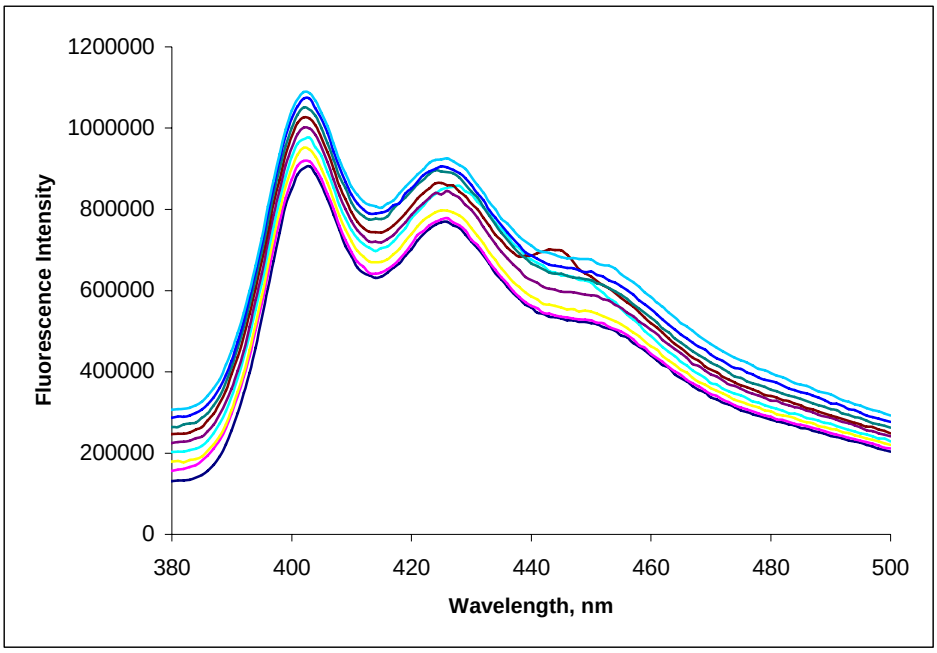

Figure 2.36. Fluorescence intensity spectra of **2.2** in the presence of various concentrations of LPA in MeOH.

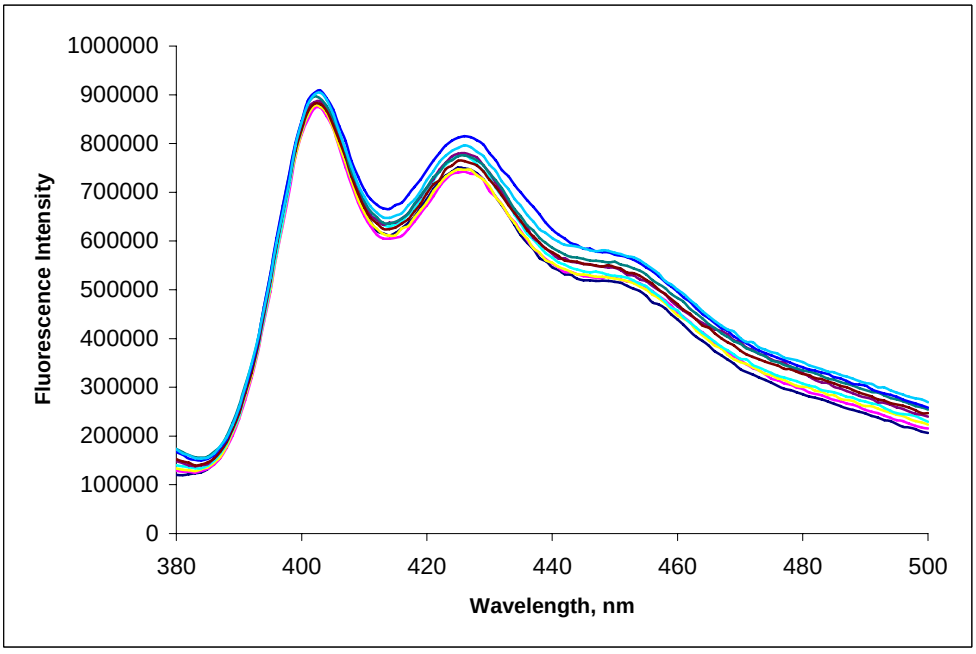

Figure 2.37. Fluorescence intensity spectra of **2.2** in the presence of various concentrations of PA in MeOH.

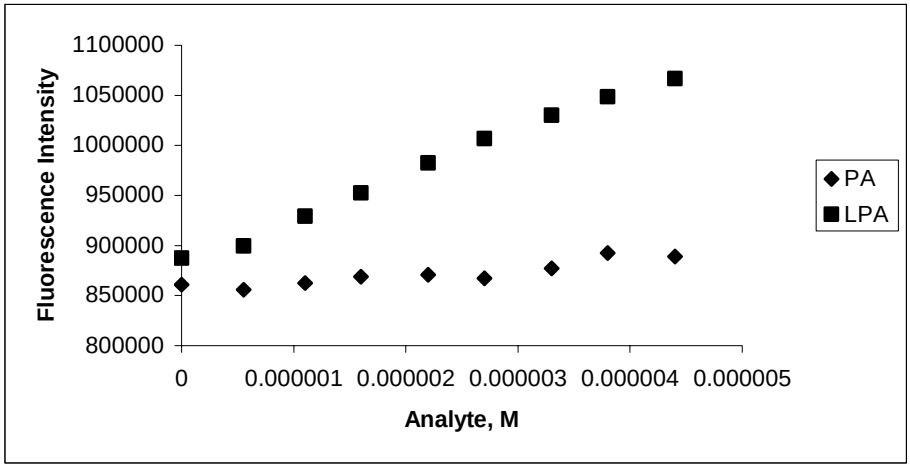

Figure 2.38. Fluorescence intensity at 400 nm of solutions containing **2.2** in the presence of various concentrations of PA and LPA.

2.9. Hikita, T.; Tadano-Aritomi, K.; Iida-Tanaka, N.; Toyoda, H.; Suzuki, A.; Toida, T.; Imanari, T.; Abe, T.; Yanagawa, Y.; Ishizuka, I. *Anal. Biochem.* **2000**, 281, 193.

2.10. Bruce, J. I.; Dickins, R. S.; Govenlock, L. J.; Gunnlaugsson, T.; Lopinski, S.; Lowe, M. P.; Parker, D.; Peacock, R. D.; Perry, J. J. B.; Aime, S.; Botta, M. *J. Am. Chem. Soc.* **2000**, 122, 9674.

2.11. Sillerud, L. O.; Prestégard, J. H.; Yu, R. K.; Schafer D. R.; Konigsberg, W. H. *Biochemistry,* **1978**, 17, 2619.

2.12. Saladini, M.; Menabue, L.; Ferrari, E. *J. Inorg. Biochem.* **2002**, 88, 61.

2.13. Byrne, M. C.; Sbaschnig-Agler, M.; Aquino, D. A.; Sclafani, J. R.; Ledeen, R. W. *Anal. Biochem.* **1985**, 148, 163.

2.14. Ci, Y.-X.; Li, Y.-Z.; Liu, X.-J. *Anal. Chem*. **1995**, 67, 1785.

2.15. Kooijman, E. E.; Carter, K. M.; van Laar, E. G.; Chupin, V.; Burger, K. N. J.; Kruijff, B. D. *Biochemistry*, **2005**, 44, 17007.

2.16. Pascher, I.; Sundell, S. *Chem. Phys. Lipids*, **1985**, 37, 241.

2.17. Fu, P. K.-L.; Turro, C. *J. Am. Chem. Soc.* **1999**, 121, 1.

2.18. For example: Xu, Y.; Shen, Z.; Wiper, D. W.; Wu, M.; Morton, R. E.; Elson, P.; Kennedy, A. W.; Belinson, J.; Markman, M.; Casey, G. *J. Am. Med. Assoc.* **1998**, 280, 719.

2.19. Holland, W. L.; Stauter, E. C.; Stith, B. J. *J. Lipid Res.* **2003**, 44, 854.

2.20. Eryomin, V. A.; Poznyakov, S. P. *Anal. Biochem.* **1989**, 180, 186.

2.21. Duggan, S. A.; Fallon, G.; Langford, S. J.; Lau, V. L.; Satchell, J. F.; Paddon-Row, M. N. *J. Org. Chem.* **2001**, 66, 4419.

CHAPTER 3

MACROCYCLE-DERIVED FUNCTIONAL XANTHENES AND PROGRESS TOWARDS CONCURRENT DETECION OF GLUCOSE AND FRUCTOSE*

3.1. Introduction

There has been great progress made towards the design, synthesis and evaluation of organic dyes functionalized with boronic acids for sugar detection.[3.1] There are relatively few studies, however, addressing the simultaneous detection of common sugars, such as glucose and fructose, in mixtures.[3.1,3.2] It has been known for decades that boronic acids exhibit relatively high affinity for fructose compared to other saccharides.[3.3] More recently several glucose-selective chemosensors have been synthesized.[3.1] Nearly all are based on the key discovery by Shinkai and co-workers that scaffolds containing appropriately spaced bis-boronic acid moieties may selectively chelate glucose.[3.1] Herein we describe novel methodology which shows promise for the detection of both glucose and fructose via a combination of UV-Vis and fluorescence spectroscopy.

Previously we reported the facile synthesis and isolation of **3.1** on multi-gram scale via the acid-catalyzed condensation of resorcinol and 4-formylphenylboronic acid.[3.4] Compound **3.1** is soluble in aqueous polar aprotic solvents such as DMSO. We observed that colorless DMSO solutions containing **3.1** (Figure **3.1**), upon standing or heating at 90 °C for 1 min, turned pinkish-purple. These color changes were monitored

*Reprinted in part with permission from *Journal of Fluorescence*, 2004, Volume 14, pages 609-613; Oleksandr Rusin, Onur Alptürk, Ming He, Jorge O. Escobedo, Shan Jiang, Fareed Dawan, Kun Lian, Matthew E. McCarroll, Isiah M. Warner, Robert M. Strongin. "Macrocycle-Derived Functional Xanthenes and Progress Towards Concurrent Detection of Glucose and Fructose".

with UV-Vis spectroscopy via the appearance of new absorptions at 465 nm, 500 nm and 536 nm.[3.5]

We found that upon heating eleven aqueous DMSO solutions each containing boronic acid resorcinarene macrocycles and eleven respective saccharides, a different solution color could be observed by visual inspection corresponding to each sugar.[3.5] The colorimetric responses were rapid, quantifiable and reproducible. More recently, we applied similar methodology towards the colorimetric detection of neutral oligosaccharides.[3.6]

Mechanistic investigations, based on extensive spectroscopic, chromatographic and crystallographic studies, revealed that the color formation in the macrocycle-containing solutions was due to the formation of ring-opened acyclic oligomers possessing xanthene chromophores (**3.2** in Figure **3.1**).[3.6] Our studies were greatly facilitated by the pioneering work of Weinelt and Schneider who had earlier described the reversible mechanism of resorcinarene macrocycle genesis in homogeneous solutions.[3.7]

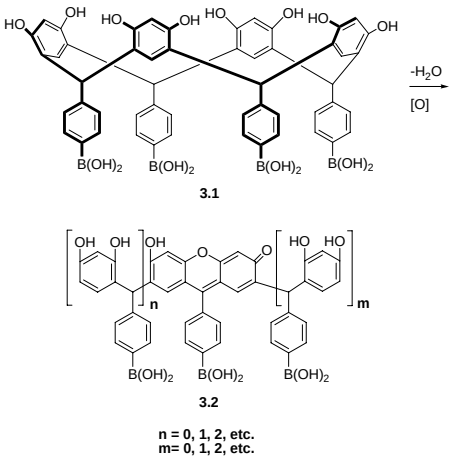

Figure 3.1. Ring opening of resorcinarene boronic acid macrocycle 3.**1** affords acyclic oligomers containing xanthene moieties.

We determined that the sugar-promoted signal transduction arose via the formation of anionic sugar-boronate esters,[3.6] in keeping with the well-known properties of boronic acid-functionalized dyes.[3.1] This was confirmed by ^{13}C-NMR using isotopically labeled sugars.[3.6] Our results were consistent with the important and useful NMR-based characterizations of related sugar-aryl boronates performed by Norrild and co-workers.[3.8]

3.2. Experimental Section

Reagents, solvents and human blood plasma were purchased from Sigma-Aldrich. Lyophilized blood plasma (5.0 mL) was reconstituted with H_2O (2.0 mL) and deproteinized by addition of MeCN (3.0 mL). Clear filtrate was used for the glucose detection experiments.

All spectroscopic data was acquired at room temperature. Colored solutions of **1** were produced via preheating DMSO solutions and cooling to room temperature prior to adding water or plasma and analytes. UV-Vis data was obtained using a Spectramax Plus 384 spectrophotometer (Molecular Devices). Fluorescence spectra were recorded with a HR2000 fiber optic spectrometer (Ocean Optics). The excitation wavelength was 470 nm (Ocean Optics LS-450, blue LED) directed into a fluorescence cuvette via a 600 μm entrance fiber, and emission gathered by a 1000 μm optical fiber at λ_{max} 579 nm. Configured for fluorescence, the setup used two mirrored screw plugs positioned at 90° within the cuvette holder for signal enhancement.

3.3. Results and Discussion.

Selective detection of fructose and the ratiometric monitoring of fructose and glucose via UV-Vis spectroscopy. We find that fructose promotes a striking solution

color change in the presence of preheated, colored arylboronic acid resorcinarene **3.1** (from pink-purple) instantly at room temperature. Colorless chemosensor **3.1** (5.2 mM) is heated at a gentle reflux for 3 min in DMSO (0.9 mL) in air to afford a colored solution containing **3.1**. After cooling to room temperature, fructose (1 equiv) in 0.1 mL H_2O is added. A color change from pink-purple to orange-yellow is observed. Glucose**,** sucrose, maltose, lactose, xylose, and glucose, 3 equiv each, exhibit no color change within 2 h at room temperature (Figure **3.2**).

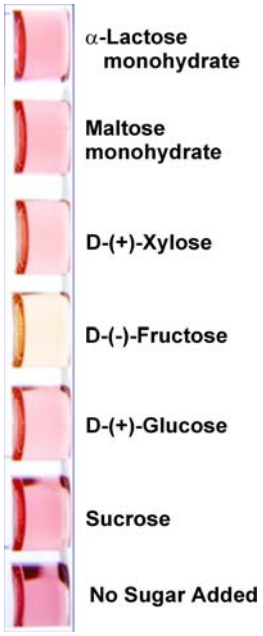

Figure 3.2. A selective color change promoted by fructose is observed at room temperature upon addition to a colored solution containing **3.1**.

The color change is monitored by observing the ratiometric absorbance intensity decrease at 536 nm and increase at 464 nm (Figure **3.3**). The absorbance changes exhibit a linear dependence with fructose concentration (R = 0.9079 and 0.9419 at each of the two wavelengths, respectively)**.** The ratio of glucose to fructose in blood plasma is *ca.* 100:1. Addition of 1 equivalent of fructose to a colored solution containing **3.1** at room temperature results in an 8.6 % increase in the absorbance at 464 nm. Addition of 100

equivalents of glucose to the fructose/**3.1** solution results in no detectable change in the fructose/**3.1** absorbance at 464 nm. Addition of a second equivalent of fructose to this latter solution results in a readily observable absorbance increase of 3.3 %.

At 536 nm, the absorbance of solutions of **3.1** is lowered by 20 % upon addition of 1 equiv fructose. Subsequent addition of 100 equivalents of glucose lowers the absorbance further by 12 %. Addition of another equivalent of fructose again lowers the absorbance by 24 % (Figure **3.3**).

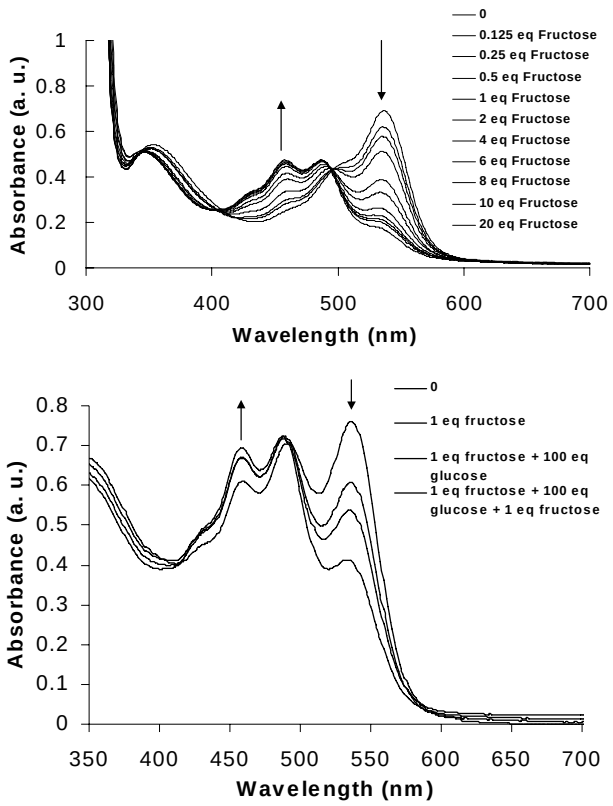

Figure. 3.3. Upper: Addition of fructose to a preheated (3.0 min at reflux) solution of **3.1** (5.2 x 10^{-3} *M*) in DMSO at room temperature affords concentration-dependent absorbance changes at 464 nm and 536 nm. **Lower:** UV-Vis spectra of a 9:1 DMSO:H_2O solution containing **3.1** (5.2 x 10^{-3} *M*) pre-heated (1.5 min at reflux) (i) alone, (ii) upon addition of 1 equiv fructose at room temperature which produces an absorbance increase at 464 nm and a corresponding decrease at 536 nm, (iii) upon addition of 100 equiv glucose which produces no absorbance change at 464 nm but a decrease at 536 nm and (iv) upon addition of a second equivalent of fructose which affords a further absorbance increase at 464 nm and decrease at 536 nm.

This result indicates the potential feasibility of determining fructose, in the presence of excess of glucose, by monitoring fructose concentrations at 464 nm, where an absorbance change is not produced in response to glucose. In addition, one should be able to concurrently determine the glucose present in a sample via analysis of the ratio of the absorbance at 536 nm (at which wavelength both glucose and fructose promote signal changes) to the absorbance at 464 nm, for instance, after the fructose concentration is determined at 464 nm.

The selectivity for fructose appears consistent with our previous binding constant studies of neutral sugars.[3.6] Additionally, we determined that anionic fructose-boronate formation lowers the pK_a of the colored xanthenes (**3.2**), resulting in absorbance changes.[3.6] It is well-known that xanthene dyes show an increase in absorbance at their shorter visible wavelength and a decrease in absorbance at their longer visible wavelength in response to a lowering of solution pH. Thus, we can ascribe the ratiometric responses observed at 464 nm and 536 nm in the current studies as due, in large part, to a lowering of xanthene pK_a upon sugar binding.

The UV-Vis studies described above would require higher concentrations of sugars than typically found in most naturally-occurring biological samples in order to generate useful signals. We are investigating the synthesis and study of new functional xanthene dyes with enhanced sensitivity in order to avoid concentration steps in sample monitoring. Since the xanthenes (**3.2**) are present in colored solutions only at micromolar levels,[3.6] their synthesis and/or isolation as discreet compounds should afford materials with higher colorimetric sensitivity, since a significant amount of sugar binds to excess colorless boronic acid **3.1**. We meantime find, however, that colored solutions containing

3.1 show promise for monitoring glucose levels in the range of physiological levels via fluorescence spectroscopy.

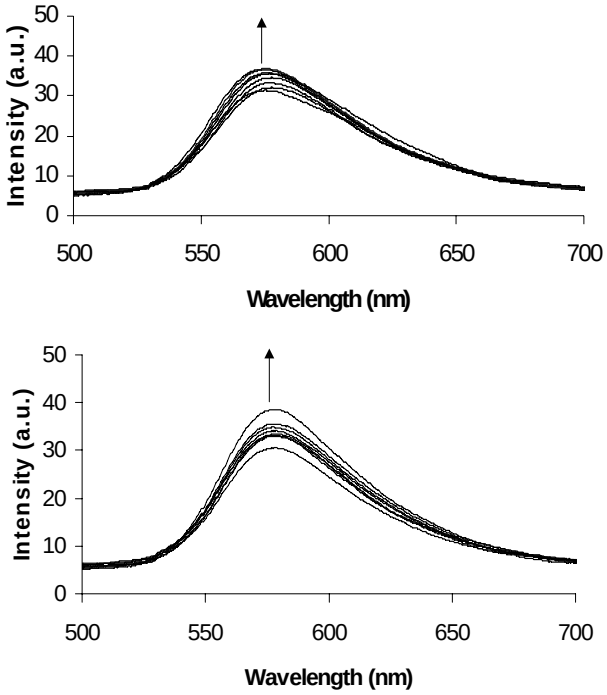

Figure 3.4. Upper: Fluorescence emission changes produced upon addition of D-glucose to a colored solution (DMSO:H_2O 9:1) containing **3.1** (5.0 x 10^{-3} *M*) at room temperature. The glucose concentration was increased from 0 to 7.4 x 10^{-4} *M*. **Lower:** Fluorescence emission changes produced upon addition of D-fructose to a colored solution (DMSO:H_2O 9:1) containing **3.1** (5.0 x 10^{-3} *M*) at room temperature. The fructose concentration was increased from 0 to 1.8 x 10^{-3} *M*.

Enhanced glucose selectivity via fluorescence detection in the range of physiological concentrations and in human blood plasma. The fluorescence emission spectra of colored solutions containing **3.1** and added glucose or fructose are shown in Figure **3.4**. As the sugar concentration is increased we observe concomitant emission increases promoted by fructose and glucose. The significant signaling generated by glucose is in contrast to the UV-Vis studies (*vide supra*) in which relatively much weaker absorbance responses were promoted by glucose as compared to fructose.

The normal level of D-fructose in human blood plasma is *ca*. 50 μM. Fluorescence emission spectra of colored solutions containing **3.1** and added fructose, obtained over the fructose concentration range of 20 μM to 100 μM, exhibit no detectable fructose-promoted emission. Healthy levels of D-glucose are *ca*. 5 mM. The emission spectra of glucose (5.5 x 10^{-3} *M*) and **3.1** (1.0 x 10^{-3} *M*) in DMSO:H_2O, 9:1, as well as in a 9:1 DMSO:plasma solution, are shown in Figure **3.5**. Emission increases due to the presence of glucose are observed in both cases. A dependence of fluorescence emission intensity on increased glucose levels in plasma is observed (Figure **3.5**).

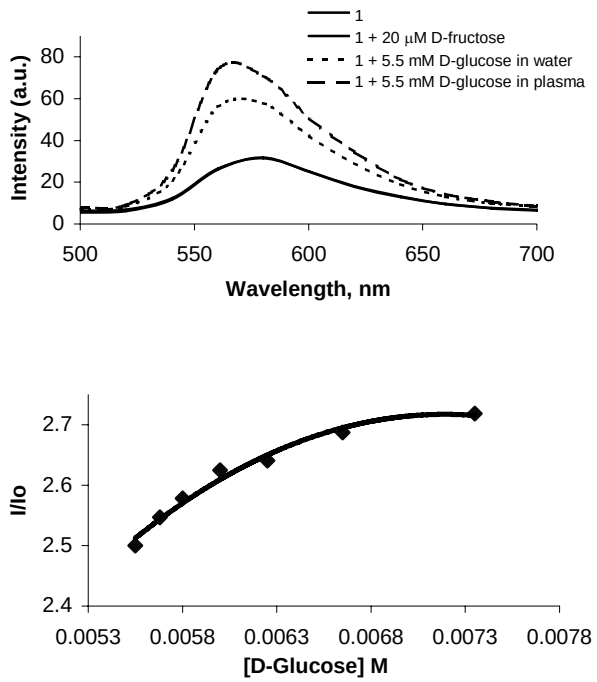

Figure. 3.5. Upper: Fluorescence emission spectra produced by (i) a preheated (3 min at reflux) colored solution (DMSO:H_2O 9:1) containing 3.**1** (5.0 x 10^{-3} *M*) at room temperature, (ii) the same conditions but in the presence of 20 μM D-fructose, added at room temperature, which affords no observable change in emission, (iii) the same conditions as (i) but with added D-glucose (5.3 μM) which promotes an emission increase and (iv) same conditions as (iii) but in deproteinized human blood plasma instead of H_2O, which exhibits an emission increase in response to added glucose. **Lower:** Concentration-dependent emission changes produced via room temperature additions of D-glucose to a 9:1 DMSO:plasma solution containing **1**.

The results of the fluorescence studies show that the boronic acid-functionalized xanthenes (**3.2**) may promote the detection of glucose in blood plasma with negligible interference from fructose. New UV-Vis and near-IR absorbing congeners of **3.2**, possessing functionality for greater potential glucose signaling ability, are currently being designed in our lab to address potential fluorescence interference issues in blood plasma.

The enhanced fluorescence emission promoted by glucose, as compared to its relatively weaker UV-Vis responses (e.g., relative to fructose), may be attributed to chelation by neighboring boronic acids of **3.2**. It is well-known that glucose can be chelated by bis-boronic acids. This results in chemosensor scaffold rigidification effects, which have been previously demonstrated to afford fluorescence emission enhancement.[1,9] An excess of boronic acid binding sites relative to glucose should promote chelation. The large excess of non-absorbing **3.1** compared to responsive fluorophores **(3.2)** should thus facilitate glucose-promoted emission by competing for glucose binding to **3.2**.

3.4. Conclusion

We have presented evidence that oligomeric xanthene dye-functionalized boronic acids, which form *in situ* from tetraaryl boronic acid resorcinarene macrocycles, show promise for the selective detection of glucose and fructose. The fluorescence studies indicate that selectivity for glucose over fructose at physiological levels in plasma may be achieved. Via UV-Vis spectroscopy, we observe high fructose selectivity. Additionally, ratiometry may also be used to simultaneously measure fructose and glucose levels, at proportionally higher concentrations. The mechanistic insights gained from these results will aid us in designing improved xanthene-derived chemosensors with tuneable

properties. The synthesis of water soluble and surface-bound congeners of the molecules described herein is also in progress.

3.5. References

3.1. James, T. D.; Shinkai, S. *Top. Curr. Chem*. **2002**, 218, 159. (b) Wang, W.; Gao, X.; Wang, B.; *Curr. Org. Chem*. **2002**, 6, 1285.

3.2. Arimori, S.; Bell, M. L.; Oh, C. S.; Farimat, K. A.; James, T. D. *Chem. Commun.* **2001**, 1836.

3.3. Lorand, J. P.; Edwards, J. D. *J. Org. Chem.* **1959**, 24, 769.

3.4. Lewis, P. T.; Davis, C. J.; Saraiva, M.; Treleaven, W. D.; McCarley, T.; Strongin, R. M. *J. Org. Chem.* **1997**, 62, 6110.

3.5. Davis, C. J.; Lewis, P. T.; McCarroll, M. E.; Read, M. W.; Cueto, R.; Strongin, R. M. *Org. Lett.* **1999**, 1, 331.

3.6 He, M.; Johnson, R. J.; Escobedo, J. O.; Beck, P. A.; Kim, K. K.; St. Luce, N. N.; Davis, C. J.; Lewis, P. T.; Fronczek, F. R.; Melancon, B. J.; Mrse, A. A.; Treleaven, W. D.; Strongin, R. M. *J. Am. Chem. Soc.* **2002**, 124, 5000.

3.7. Weinelt, F.; Schneider, H.-J. *J. Org. Chem.* **1991**, 56, 5527.

3.8. Norrild, J. C.; Eggert, H. *J. Chem. Soc., Perkin Trans.* 2, **1996**, 12, 2583.

3.9. (a) M. Takeuchi, S. Yoda, T. Imada and Shinkai, S. *Tetrahedron*, **1997**, 53, 8335. (b) Takeuchi, M.; Mizuno, T.; Shinmori, H.; Nakashima, M.; Shinkai, S. *Tetrahedron*, **1996**, 52, 1195.

CHAPTER 4

ORGONAMETALLIC COMPLEXES AS THERAPEUTIC AGENTS

4.1. Introduction

This chapter describes the synthesis and applications of synthetic organometallic complexes herein called metallosalophenes (MSPs). Included are metal-chelating analogs. The animal studies described herein were performed at Brown University Medical School under the direction of Dr. Laurent Brard.

MSPs are currently employed in the protection of tissues and/or cell types during cancer chemotherapy[4.1], as de-novo drugs and or analogs possessing such therapeutic applications as anti-neoplastic, anti-angiogenic and anticancer activity[4.2]. More importantly, they function as free radical scavengers[4.3] in the case of the some other diseases such as Alzheimer's[4.4].

It has now been discovered that a number of MSPs display anticancer activity. This has been demonstrated *in vitro* in various cultured solid tumor cancer cells such as neuroblastoma, breast, ovarian, prostate, pancreatic, vulvar, and liver and in other non-solid human tumors too. Furthermore, MSP anticancer activity is present *in vivo*.

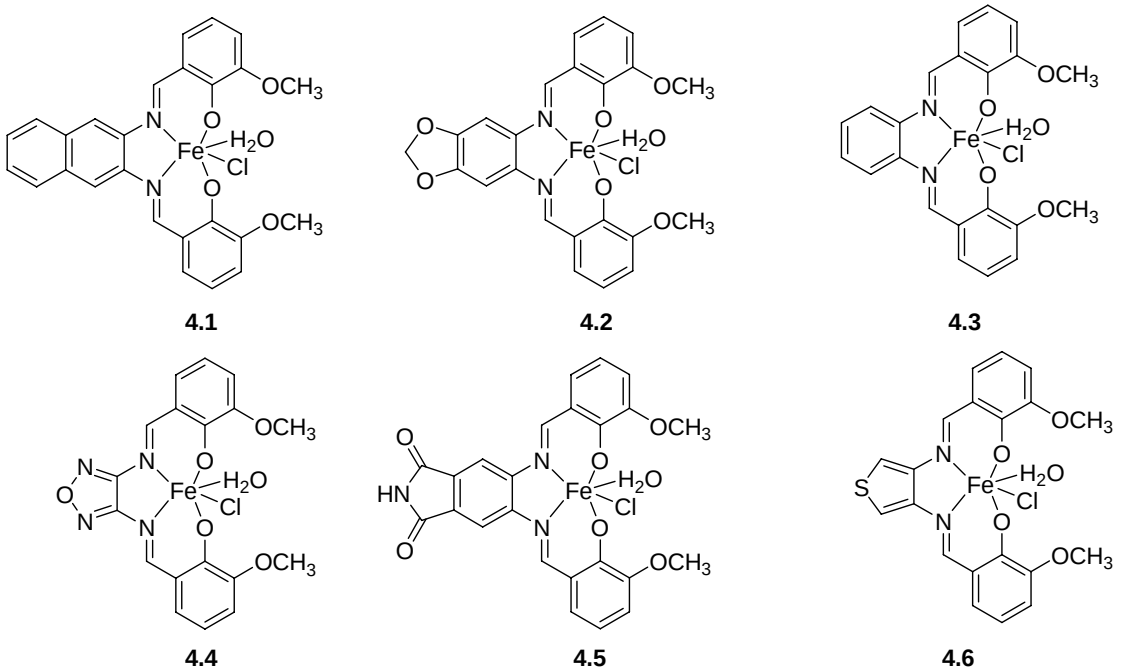

Figure 4.1. The structures of metallosalophenes

The preparation of the salophene-based metal complexes involve a condensation reaction of a substituted salicylaldehyde and a substituted diamine.[4.5] In general, the quantities of these compounds are reacted in a 2:1 molar ratio in absolute ethanol. The solutions are refluxed for 1 h. The salophene ligand is either precipitated in analytically pure form by the addition of water, or the metal complex is generated directly by addition of the corresponding metal as its acetate, halide, or triflate salt.

Another method of preparing the complexes is as follows: the starting diamine is R,R- or S,S-1,2-diamino-1,2-diphenylethane and the starting salicylaldehyde is 3-tert-butylsalicylaldehyde. A solution of 2.0 mmol of 3-tert-butylsalicylaldehyde in 3 ml of absolute ethanol is added dropwise to a solution of 1.0 mmol of (R,R)-1,2-diamino-1,2-diphenylethane in 5 ml of ethanol. The reaction mixture is heated to reflux for 1 h and then 1.0 mmol of $Mn(OAc)_2$. 4 H_2O is added in one portion to the hot (60° C.) solution. The color of the solution immediately turns from yellow to brown upon addition. It is refluxed for an additional 30 min and then cooled to room temperature. A solution of 10% NaCl (5 ml) is then added dropwise and the mixture stirred for 0.5 h. The solvents are then removed *in vacuo* and the residue is triturated with 50 ml of CH_2Cl_2 and 50 ml of H_2O. The organic layer is separated and the brown solution is washed with saturated NaCl. Separation of the organic phase and removal of solvent resulted in a crude material which can be recrystallized from C_6H_6/C_6H_{14} to give a (R,R)-salophene-Mn complex.

Salophenes **4.3** and **4.6** are synthesized as per the scheme described below (Scheme **4.1.** and Scheme **4.2**).

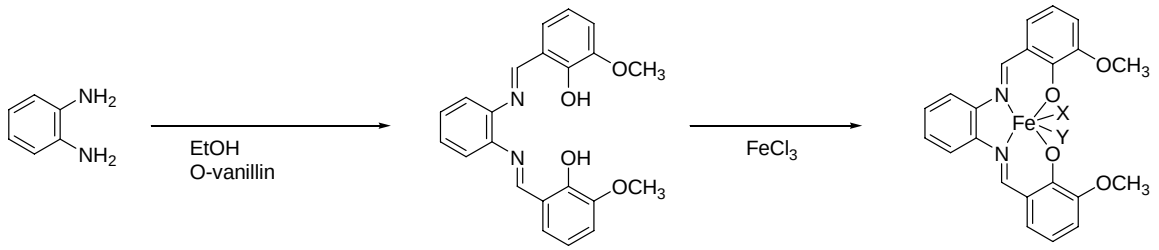

4.7 **4.8** **4.3**

Scheme. 4.1. The synthesis of **4.3**.

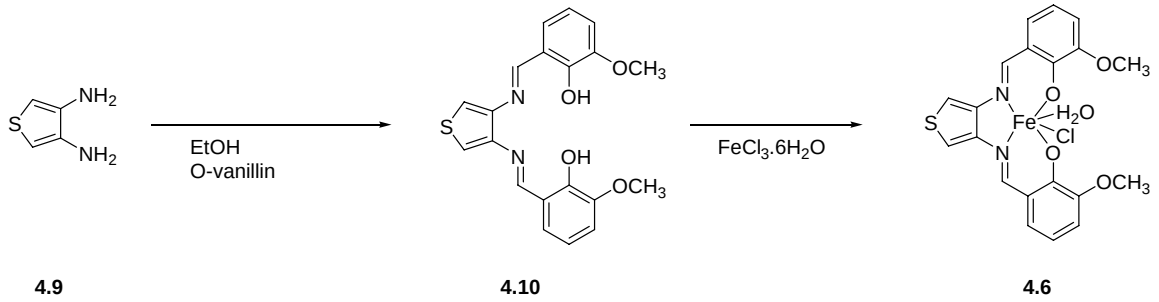

4.9 **4.10** **4.6**

Scheme. 4.2. The synthesis of **4.6**

4.2. Results and Discussion

4.2.1. Iron-Salen Complex Inhibits Proliferation of Epithelial Ovarian Cancer Cells

Given the exciting activity of iron-salen on platinum-resistant SKOV-3 epithelial ovarian cancer cells, we re-assessed viability via the MTS assay using a narrow dose range (0-5 μM). These additional experiments have re-confirmed the previous conclusions (IC50 = 630 nM, Figure **4.2**) and added additional insight regarding the potency of this iron-salen complex.

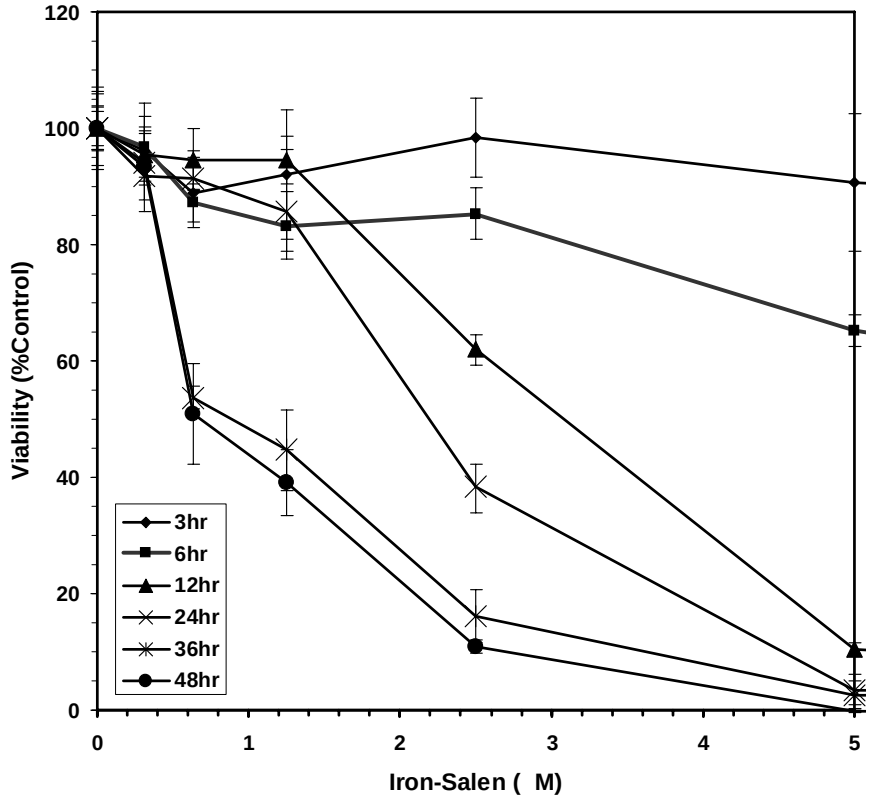

Figure 4.2. Iron-salen significantly inhibits the viability of SKOV-3 ovarian cancer cells.

4.2.2. Acute Toxicity Studies

Iron-salen was administered orally and intra-peritoneally to two groups of 7 animals and acute toxicity was evaluated by the up-and-down method. The estimated LD50 was >2000 mg/kg body weight (PO) and > 5.5mg/kg, body weight (IP) (Figure **4.9**).

Animal #	Dose (mg/kg)	Outcome	LD_{50} (IP)
1	55	X	
2	17.5	X	
3	5.5	O	
4	17.5	X	>5.5mg/Kg
5	5.5	O	
6	17.5	X	
7	5.5	O	

Animal #	Dose (mg/kg)	Outcome	LD_{50} (PO)
1	55	O	
2	175	O	
3	550	O	
4	2000	O	>2000mg/Kg
5	2000	O	
6	2000	O	
7	2000	O	

Figure 4.3. Acute Toxicity (PO); O = No Response, X = Death within 2-14 days (right)

4.2.3. Caspase Activation *in vivo*

The possible role of caspase-3 in iron-salen induced apoptosis *in vivo* was evaluated by Western blotting wherein the full-length and activated from of caspase-3 are probed by the use of specific antibodies. Following treatment, tumor tissue was harvested and this tissue was sonicated for 5 minutes. After this material re-suspended in lysis buffer, it is separated on 12% SDS PAGE. Subsequently, it is blotted on to PVDF membrane and treated with antibodies specific for monitoring both pro- and activated caspase-3 (Figure **4.4**). Treatment of 344 Fischer rats injected NUTU-19 ovarian cancer cells by iron-salen resulted in cleavage of pro-caspase-3 in a dose-dependent manner, as evidenced by the appearance of 19 and 17 kDa intermediates. PARP-1 cleavage was measured by employing antibodies specific to cleaved PARP-1. Treatment of 344 Fischer rats injected NUTU-19 ovarian cancer cells resulted in PARP-1 cleavage in a dose-dependent fashion, as shown by the increase of the 85 kDa inactive intermediate band. Increased PARP-1 cleavage coincided with increased caspase-3 activation. The caspase-3 and PARP-1 results suggest that iron-salen affects ovarian cancer cells in a similar fashion both *in vitro* and *in vivo.*

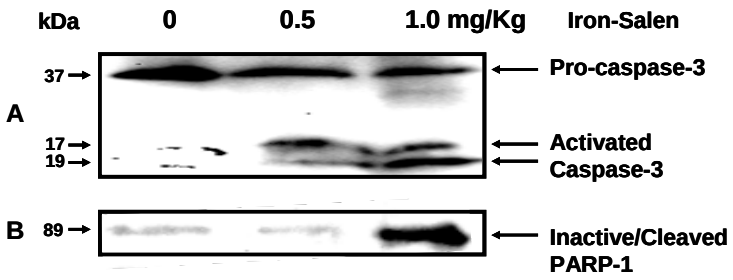

Figure 4.4. Caspase-3 activation and PARP-1 inactivation by Iron-Salen

4.2.4. Preliminary Therapeutic Trial

In this preliminary trial, twenty rats, divided into two treatment groups of five animals each (0.5 mg/kg and 1.0 mg/kg) and one control group (12 animals) were used. The rat ovarian cancer model has been described elsewhere.[4.6] NUTU-19 cells were cultured to 80% confluence, harvested, counted for cell number and viability, and injected intra-peritoneal (IP). Iron-salen was applied to two treatment groups in the form of daily IP injections (the stock solution of iron-salen in DMSO/water (20/80 v/v) mixture were diluted 100-fold prior to injection) and vehicle (DMSO/water 20/80 v/v) was injected to the untreated control group. Two different concentrations of iron-salen are determined based on previous *in vitro* work and acute toxicity results.

The treatment of experimental animals began in week 3 to mimic the conditions following cytoreductive surgery. According to this model, 100% of animals develop disease after three weeks and are euthanized secondary to overwhelming tumor burden by 8-12 weeks (post-injection). Duration of treatment was 12 days and was based on tumor burden in the control animals. Animals were monitored for any discomfort and pain per IACUC protocols. All twenty animals were euthanized at week 5 and tumor tissue was harvested. While control animals showed a constantly elevated amount of hemorrhagic ascites, those treated with the iron-salen treated displayed substantially less hemorrhagic ascites volume (Figure **4.5**). More importantly, decrease in ascitic volume appeared to be dose-dependent. The difference was especially substantial in the 1mg/Kg treatment group.

Parallel results were afforded with omental weight between control and treatment groups. As previously depicted, it was found to be consistently higher in control animal than in treatment groups. Furthermore, 7 (70%) animals afforded response to treatment

with iron salen during this preliminary treatment trial. As 40% of treated animals displayed a complete response (Figure **4.6** and **4.7**), 30% had partial response.

Consequently, these preliminary in vivo experiments have provided a firm evidence that iron-salen is a potent anti-ovarian cancer drug with high potential in the treatment of this devastating disease.

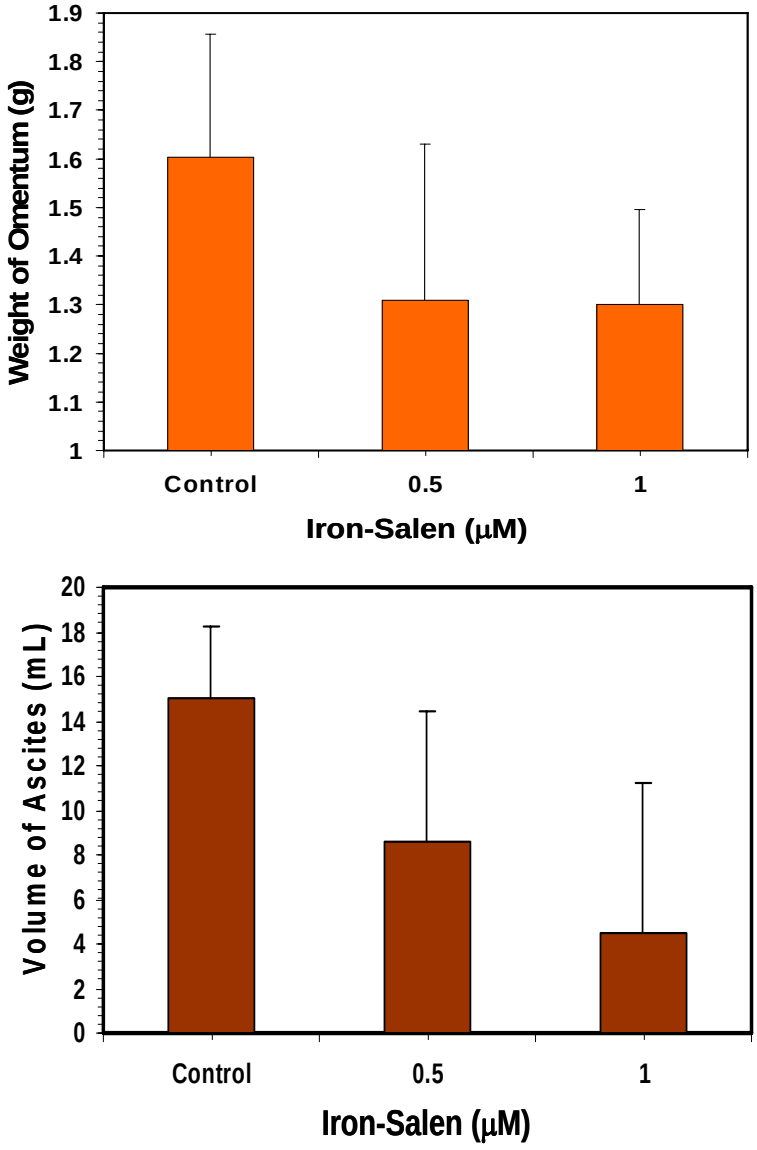

Figure 4.5. (Top) Effect of Iron-Salen on Tumor Burden: Weight of Omentum **(bottom)** Effect of Iron-Salen on Hemorrhagic ascites.

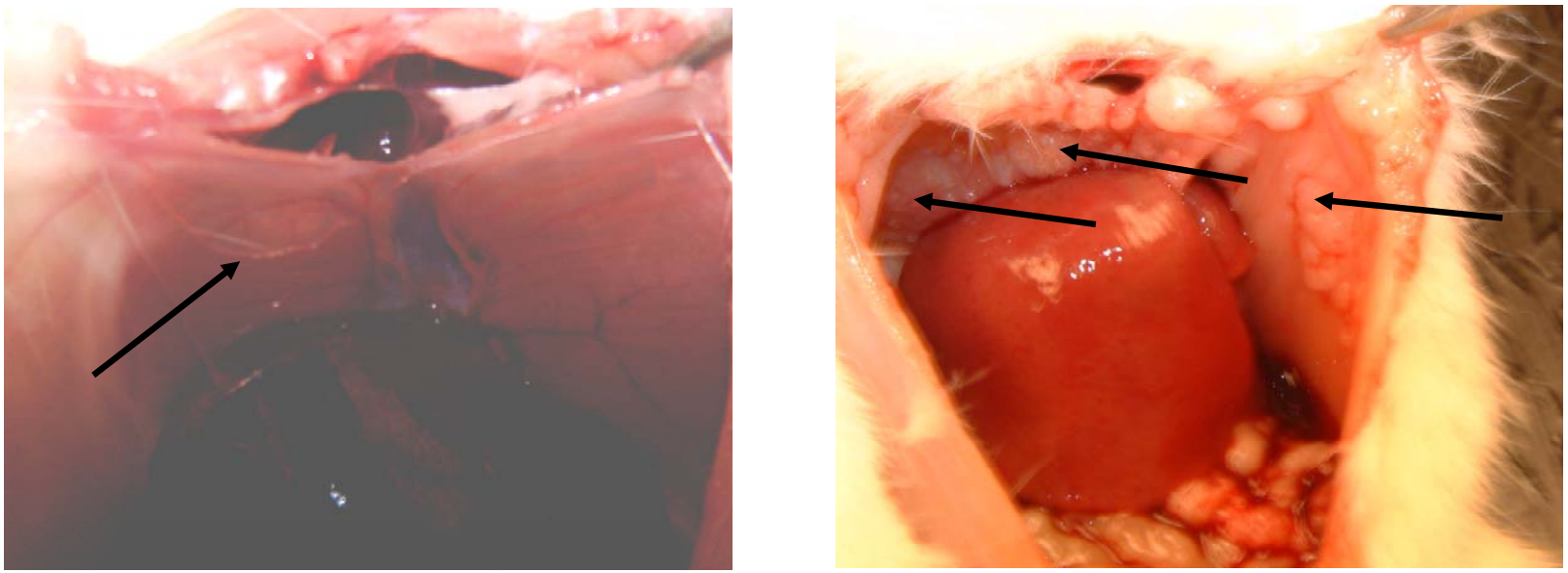

Figure 4.6. (Left) Photograph of diaphragm in treated rat (1 mg/Kg). Arrow: Normal diaphragm, (**right**) Photograph of diaphragm in control rat. Arrows represent tumor nodules

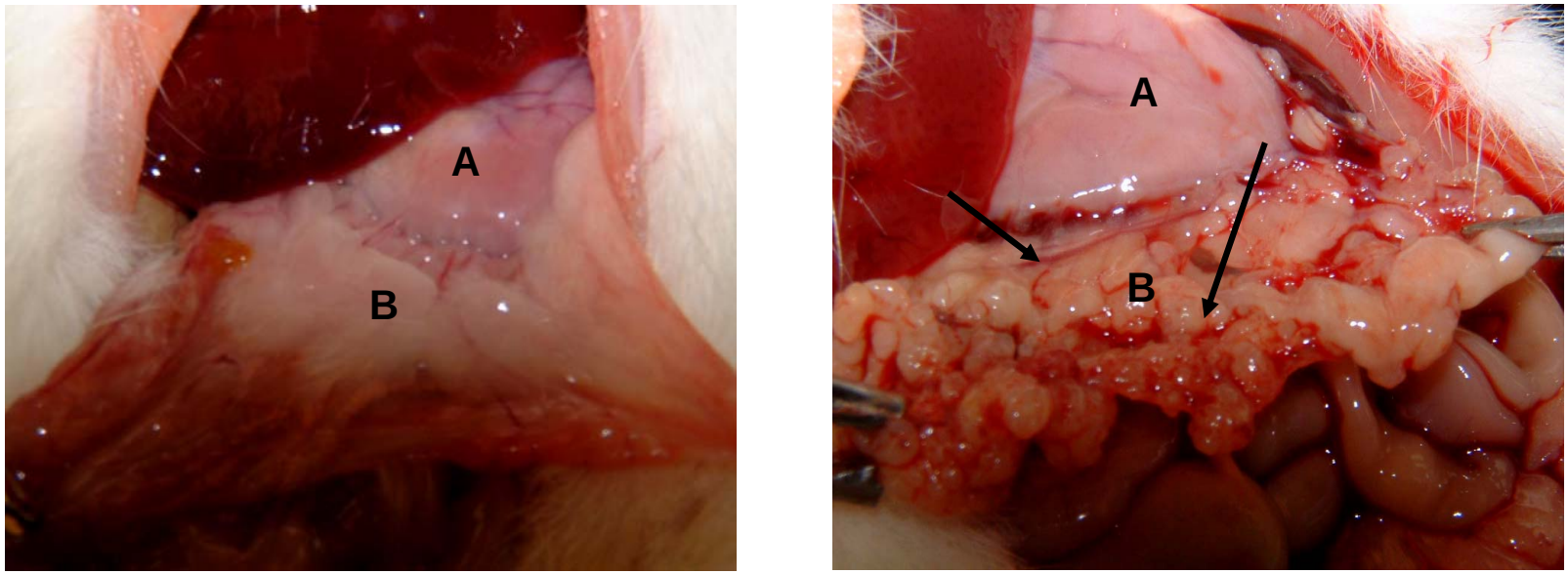

Figure 4.7. (**Left**) Photograph of omentum in treated rat (1 mg/Kg). A = Stomach, B = Omentum), (**right**) Photograph of omentum in control rat. Arrows represent tumor nodules.

4.3. Experimental Section.

4.3.1. Synthesis of 4.8

To a suspension of o-vanillin (1.52 g, 9.99 mmol) in of anhydrous ethanol (15 ml), 1,2-diaminobenzene (0.54 g, 4.99 mmol) is added. Upon reflux for 2 hours, an orange precipitate is afforded. The final compound **4.8** is isolated via suction and washed with cold ethanol (1.5 g, 80.2%).[4.7] ^{1}H-NMR (300 MHz, DMSO-d_6) δ (ppm): 3.82 (s, 6H), 6.9 (t, *J* = 7.87 Hz, 2H), 7.14 (d, *J* = 7.34 Hz, 2H), 7.27 (d, *J* = 7.65 Hz, 2H), 7.41-7.48 (m, 4H), 8.93 (s, 2H).^{13}C-NMR (62.5 MHz, DMSO-d_6) δ (ppm): 57.6, 117.3, 120.5, 121.3, 121.8, 125.8, 125.8, 129.8, 144.1, 149.9, 152.6, 166.3.

4.8.2. Synthesis of 4.3

To a suspension of **4.8** (0.4 g, 1.06 mmol) in anhydrous ethanol (15 ml), $FeCl_3.6H_2O$ (0.286 g, 1.06) is added. Upon reflux for 1 hour, a grey-black precipitate is afforded.[4.8] The final compound **4.3** is isolated via suction and washed with cold ethanol (0.11 g, 21.5%).

4.8.3. Synthesis of 4.6

The compound **4.6** is prepared *in situ* upon from the condensation reaction of 3,4-diaminothiophene **4.9** and o-vanillin in the presence of $FeCl_3.6H_2O$. To a solution of o-vanillin (057 g, 3.74 mmol) in of anhydrous ethanol (7 ml), 3,4-diaminothiophene.2HCl (0.35 g, 1.87 mmol) and $FeCl_3.6H_2O$ (0.5 g, 1.87 mmol) are added. Upon reflux for 1 hour, a dark-blue precipitate is afforded. The final compound **4.6** is isolated via suction and washed with cold ethanol (0.52 g, 56.7%).

4.4. References

4.1. a) Malfroy-Camine, B.; Baudry, M. Synthetic catalytic free radical scavengers useful as antioxidants for prevention and therapy of disease. US 5,403,834 (b) Malfroy-Camine; B.; Doctrow, S. R. Synthetic catalytic free radical scavengers useful as antioxidants for prevention and therapy of disease. US 5834509, US 5,696,109, US 5,827,880.

4.2. a) Kasugai, N.; Murase, T.; Ohse, T.; Nagaoka, S.; Kawakami, H.; Kubota, S. *J. Inorg. Biochem*., **2002**, 91, 349. b) Kariya, K.; Nakamura, K.; Nomoto, K.; Kobayashi, Y.; Namiki, M. *Cancer Biotherapy*, **1995**, 10, 139. c) Jerome, A.; Carole, N.; Christiane, C.; Alexis, L.; Bernard, W.; Francois, G.; Frederic, B. *J. Natl. Cancer I*., **2006**, 98, 236.

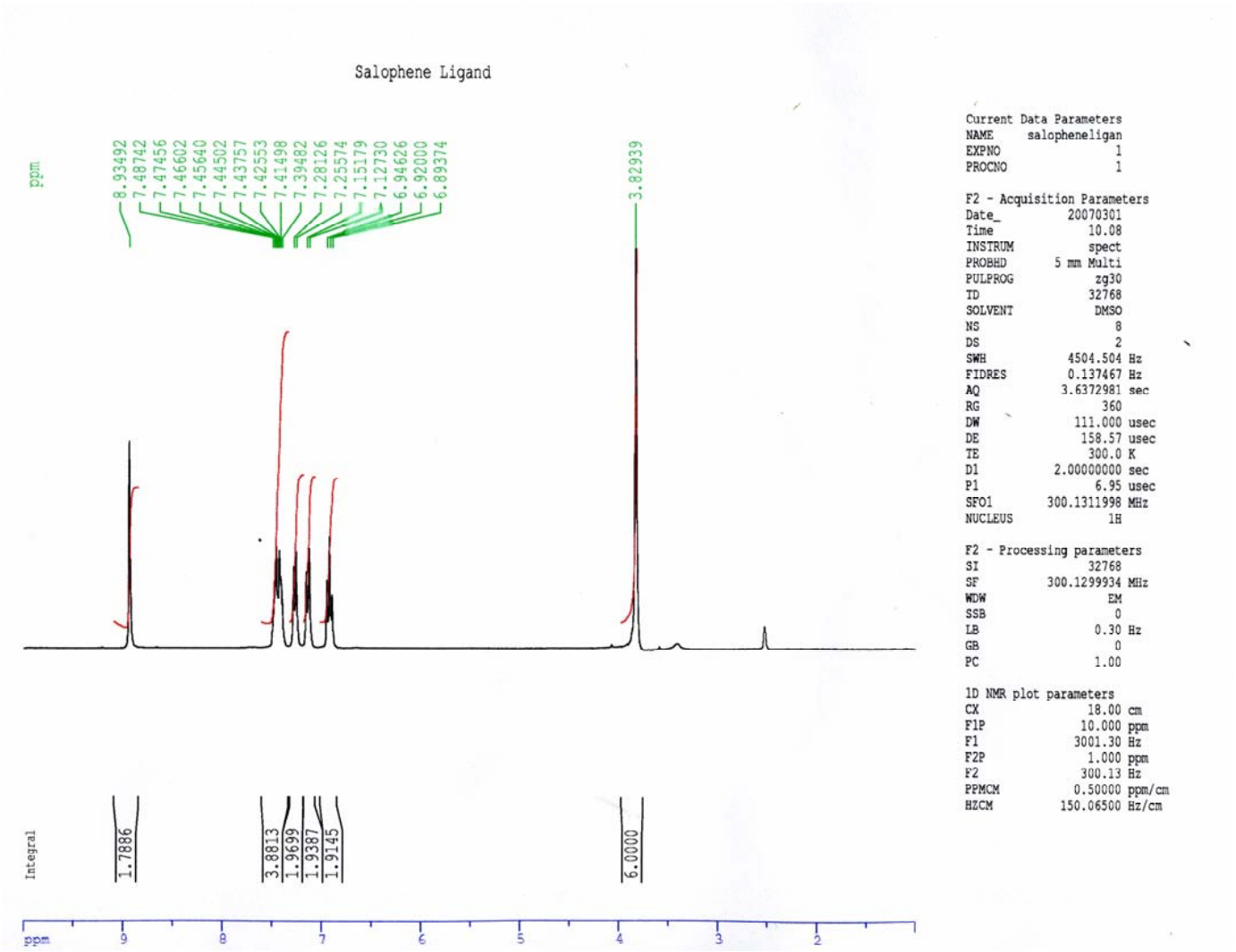

Figure 4.8. ^{1}H-NMR of **4.8**

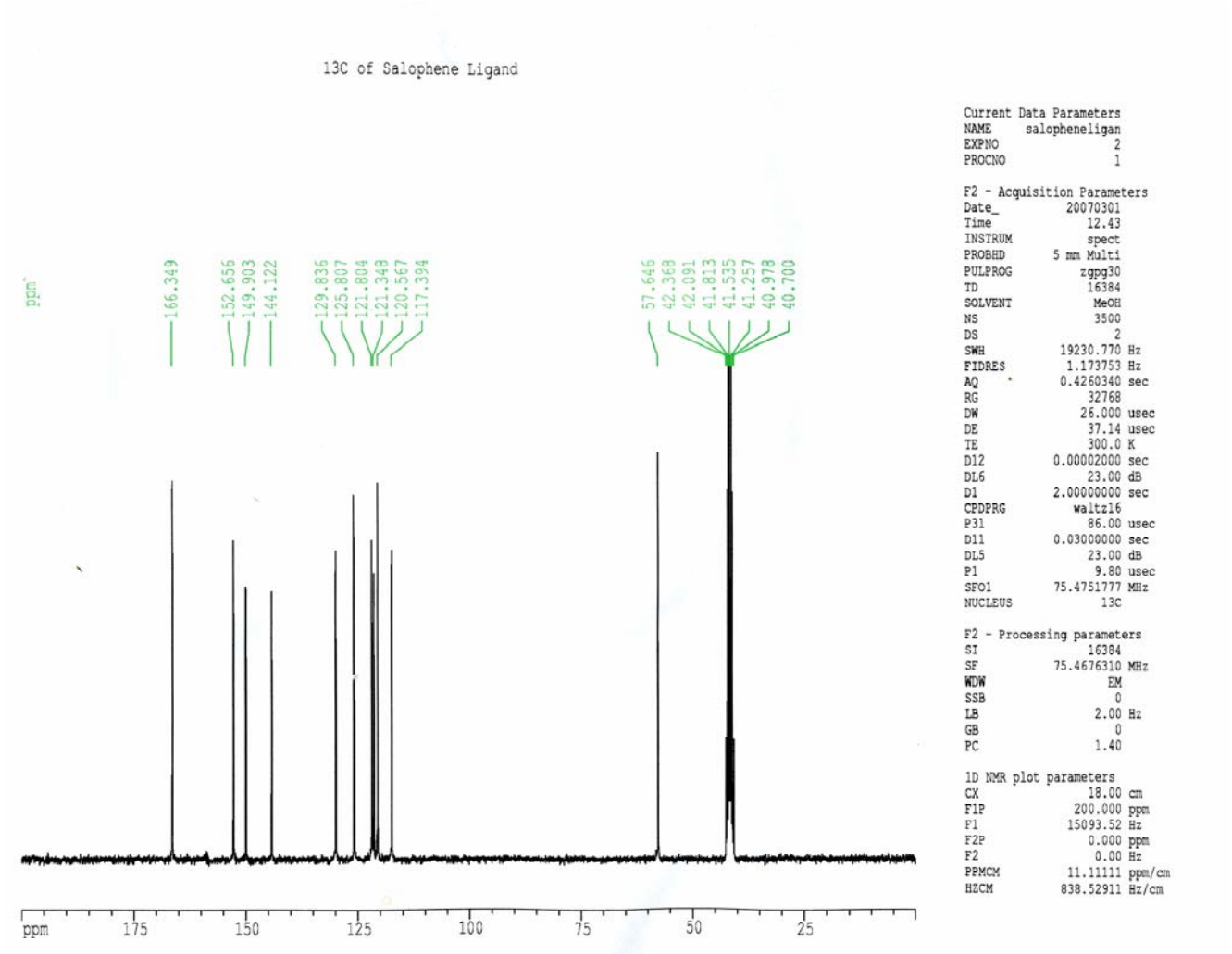

Figure 4.9. ^{13}C-NMR of **4.8.**

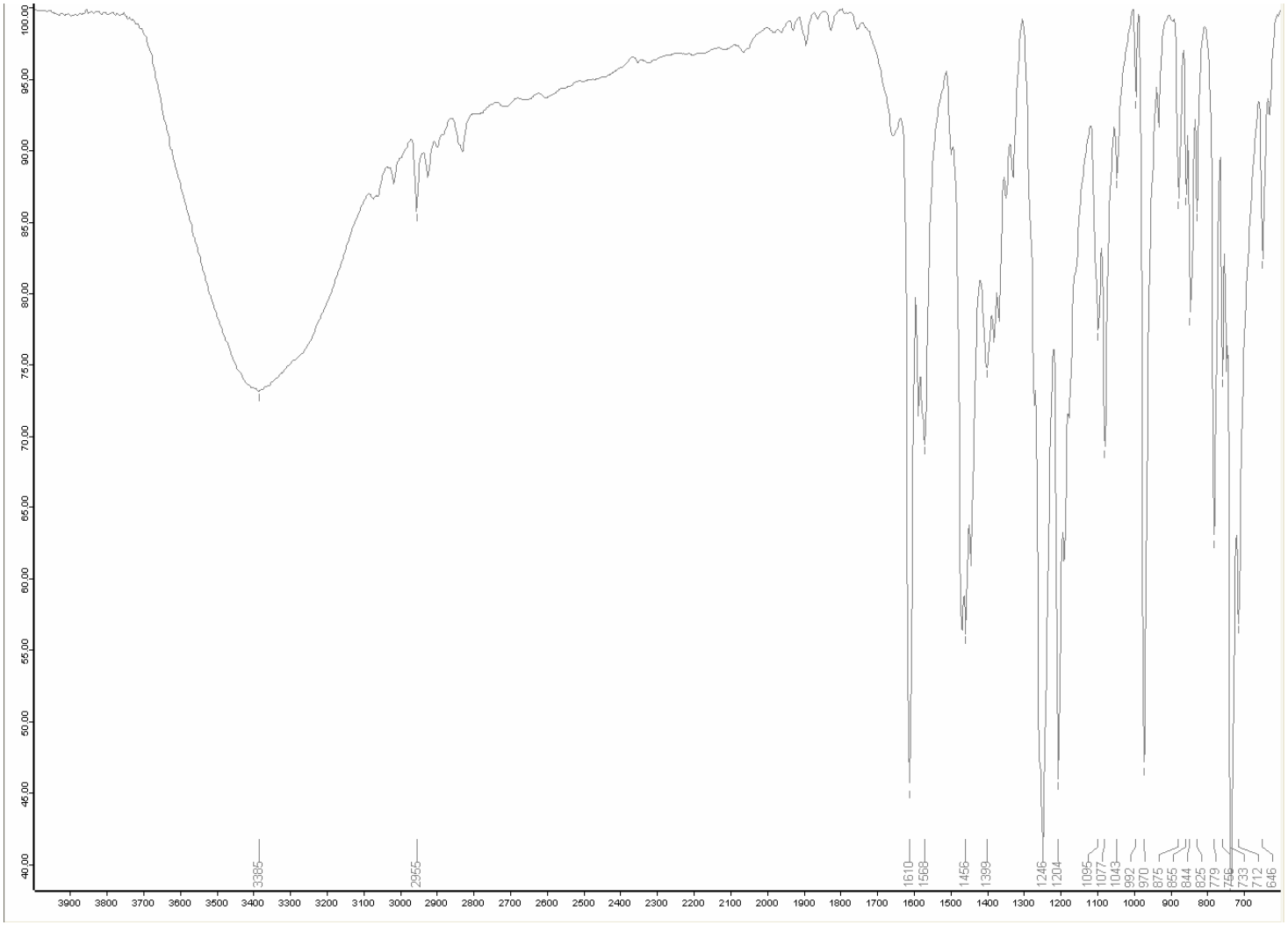

Figure 4.10. FTIR of **4.8**.

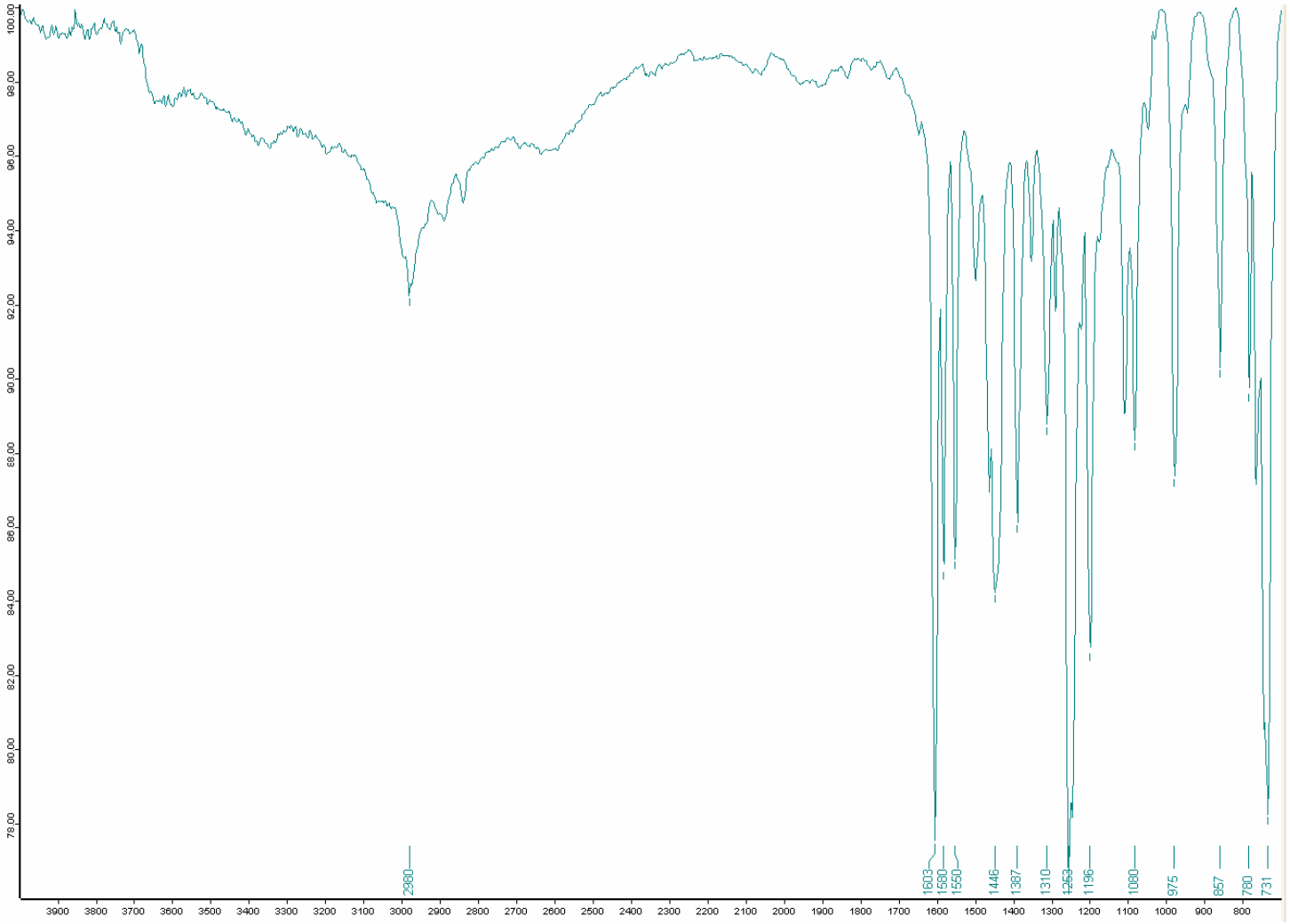

Figure 4.11. FTIR of **4.3**.

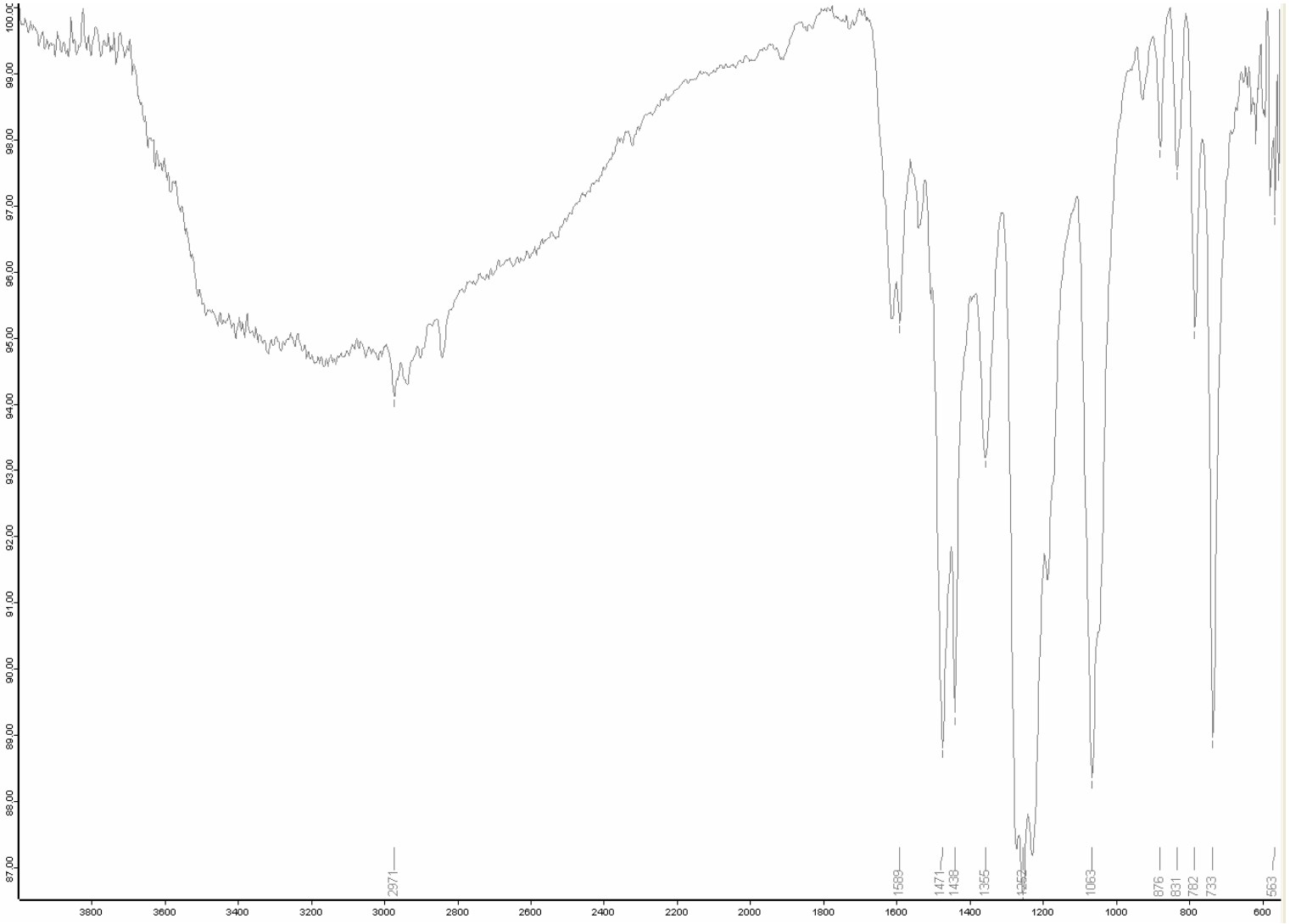

Figure 4.12. FTIR of **4.6**.

4.3. For an extensive review, see: Riley, D. P. *Chem. Rev*., **1999**, 99, 2573

4.4. Henke, S. L. Expert. *Opin. Ther. Pat*. **1999**, 9, 169.

4.5. Hennessy, E. J.; Buchwald, S. L. J. *Org. Chem*., **2005**, 70, 7371.

4.6. Robison, K.; Steinhoff, M. M.; Granai, C. O.; Brard, L.; Gajewski, W.; Moore, R. G. *Gynecol. Oncol.* **2006**, 101, 24.

4.7. Caifeng, B.; Yuhua, F.; Guoxin, S.; Gengxiu, Z.; Guangyou. Z. *Syn. React. Inorg. Met*. **2001**, 31, 219.

4.8. Zanello, P.; Cini, R.; Cinquantini, A. *Polyhedron*, **1985**, 4, 1383.

APPENDIX A. LETTER OF PERMISSION FROM PNAS

PNAS Author Rights and Permission FAQs

1. **If I transfer copyright to PNAS, what rights do I have?**

As a PNAS author, you and your employing institution or company retain extensive rights for use of your materials and intellectual property. You retain these rights and permissions without having to obtain explicit permission from PNAS, provided that you cite the original source and copyright notice:

- The right to post a PDF of your article on your web site or that of your employer's institution (provided that the institution is nonprofit).
- The right to make electronic or hard copies of articles for your personal use, including classroom use, or for the personal use of colleagues, provided those copies are not for sale and are not distributed in a systematic way outside of your employing institution.
- The right to post and update a preprint version of your article on a public electronic server such as the World Wide Web. See the information on electronic preprints below.
- The right to permit others to use your original figures or tables published in PNAS for noncommercial and educational use (i.e., in a review article, in a book that is not for sale), provided that the original source and copyright notice are cited. Third parties need not ask PNAS for permission to use figures and tables for such use
- The right, after publication in PNAS, to use all or part of your article in a printed compilation of your own works, such as collected writings or lecture notes.
- If your article is a "work for hire" made within the scope of your employment, your employer may use all or part of the information in your article for intracompany use.
- **The right to include your article in your thesis or dissertation.**
- The right to present all or part of your paper at a meeting or conference, including ones that are webcast, and to give copies of your paper to meeting attendees before or after publication in PNAS. For interactions with the media prior to publication, see the PNAS Policy on Media Coverage.
- The right to publish a new or extended version of your paper provided that it is sufficiently different to be considered a new work.
    - The right to expand your article into book-length form for publication.
    - The right to reuse your original figures and tables in your future works.
    - Patent and trademark rights or rights to any process or procedure described in your article

APPENDIX B. LETTER OF PERMISSION FROM SPRINGER

Dear Onur Alpturk,

This letter is to inform you that Springer gives permission to Onur Alpturk, 2nd author of article entitled "Macrocycle-Derived Functional Xanthenes and Progress Towards Concurrent Detection of Glucose and Fructose" published in Journal of Fluorescence (J. Fluoresc., 2004, 14(5), 609-613 to use the article mentioned in his thesis for educational purposes as stated in your request dated April 5th, 2007. The fee associated with this permission is waived based on the fact that
the article will only be used in thesis for educational reasons; and will not be reproduced. If the article is reproduced; please contact me directly at 212-620-8495 for additional permission and at which point a fee will be imposed.

All the best,
Evelisa Rosario
Springer
Corporate Reprint Sales Assistant
233 Spring Street | 7th floor | New York
NY 10013 | USA
Office +1 (212) 620-8495
New Fax +1 (212) 620-8442
evelisa.rosario@springer.com
www.springer.com

-----Original Message-----
From: Onur Alpturk [mailto:oalptu1@lsu.edu]
Sent: Thursday, April 05, 2007 4:40 PM
To: Rosario, Evelisa, Springer US
Subject: Request for Permission
Importance: High

To whom this may concern,

My name is Onur Alpturk and I am 2nd author of the paper titled as "Macrocycle-Derived Functional Xanthenes and Progress Towards Concurrent
Detection of Glucose and Fructose" published in Journal of Fluorescence (J. Fluoresc., 2004, 14(5), 609-613). I would like to ask for permission
to include this paper into my thesis.

Best Regards,

Onur Alpturk

VITA

Onur Alptürk was born in Ankara, Turkey, on April, 17th of 1975. After graduation from high-school, he enrolled in the chemistry department of Middle East Technical University. While at METU, he carried out his undergraduate research under the supervision of Prof. Engin U. Akkaya on the synthesis of low-molecular weight phosphodiesterase mimics. In 1998, he enrolled in the biochemistry program of the same university. Under the supervision of Prof. Ayhan S. Demir and Prof. Mesude Iscan, he has worked on the synthesis of camptothecin prodrugs and some biologically active compounds and their effects on glutathione S-transferase. Additionally, he contributed to the project on a novel methodology to convert chiral amines into their corresponding pyrrole derivatives without racemization.

In 2001, he entered the graduate program in the Department of Chemistry at Louisiana State University (LSU) in Baton Rouge, Louisiana. Under the guidance of Prof. Robert M. Strongin, he has developed the synthesis of novel lanthanide based chemosensors for the quantification of carbohydrates and certain cancer biomarkers. In collaboration with Prof. Laurent Brard from Brown University, Medical School, he worked on the synthesis and applications of metallosalophenes for treatment of the ovarian cancer. His research gathered him LSU Research Award in chemistry. The degree of Doctor of Philosophy will be awarded to him at the May 2007 commencement.